ANALYSIS OF PRESSURE RECOVERY COEFFICIENT IN PARALLEL HUB ANNULAR DIFFUSER

A major thesis submitted
In partial fulfillment of the requirements for the award of the degree of

Master of Engineering
In
Thermal Engineering

By
Pratap Singh Chauhan
Roll No. 3203

Under the Guidance of
Prof. B. B. Arora

Department of Mechanical Engineering,
Delhi College of Engineering, University of Delhi
Session 2003-05

Candidate's Declaration

I hereby declare that the work which is being present in the thesis entitled ***" Analysis of Pressure Recovery Coefficient in Parallel Hub Annular Diffuser "*** in partial fulfillment for the award of degree of **Master of Engineering** with specialization in **"Thermal Engineering"** submitted to **Delhi College of Engineering, University of Delhi**, is authentic record of my own work carried out under the supervision of **Prof. B. B. Arora,** Department of Mechanical Engineering, Delhi College of Engineering, University of Delhi. I have not submitted the matter in this dissertation for the award of any other Degree or Diploma or any other purpose whatever.

(Pratap Singh Chauhan)
Univ. Roll No. – 3203
Date – July 27, 2005. College Roll No. – 03/ME(Th)/03

Certificate

This is to certify that above statement made by the candidate is true to the best of my knowledge and belief.

(B. B. Arora)
Asstt. Professor
Department of Mechanical Engg.,
Delhi College of Engg., Delhi.

Acknowledgement

It is distinct pleasure to express my deep sense of gratitude and indebtedness to my learned supervisor **Mr. B B. Arora**, Asst. Professor in the Department of Mechanical Engineering, Delhi College of Engineering, for his invaluable guidance, encouragement and patient review. His continuous inspiration only has made me complete this major dissertation.

It is a great pleasure to have the opportunity to extent my heartiest felt gratitude to everybody who helped me throughout the course of this dissertation.

I would also like to take this opportunity to present my sincere regards to my teachers for their kind support and encouragement.

I am thankful to my friends and classmates for their unconditional support and motivation during this project.

(Pratap Singh Chauhan)
Roll No . 03/Mech(Thermal)/03
University Roll No. 3203

ABSTRACT

Annular diffusers are often used in conjunction with turbo machines to increase the static pressure and reduce the velocity of the discharge flow.

The present investigation involves a systematic analysis of parallel hub and diverging outer wall annular diffusers configurations with varied AR and diverging angle for pressure recovery coefficient and static pressure at casing wall and hub wall, reverse flow prone zone in diffuser with help of FLOTRAN ANSYS 9.0 CFD tool.

Each diffuser is tested with varying axial inlet flow velocity ranges from M = 0.14 to M= 0.46 and zero inlet swirl angle to provide a comprehensive basis on which generalize the influence of geometry parameter AR, θ on pressure recovery in annular diffusers.

Flow in diffuser is observed and analyzed for changes in pressure recovery coefficient and static pressure at casing wall and hub wall. It observed that pressure recovery coefficient does not change significantly with Mach number for which tested and improve with increase in length of diffuser and decrease with increase in diverging angle. Pressure recovery coefficient at increase sharply at entrance of diffuser than it rate of increase decreases, similar characteristic shown by static pressure.
It is also observed that stable flow at exit give high pressure recovery coefficient.

Content

		i
	Certificate	
	Acknowledgement	ii
	Abstract	iii
	Contents	iv
	List of Tables	vii
	List of Figure	viii
	Abbreviations	xi
1	Introduction	1-7
	1.1 Diffuser performance parameter	2
	1.1.1 Geometric parameters	2
	1.1.2 Aerodynamic blockage	3
	1.1.3 Reynolds number	3
	1.1.4 Inlet Mach number	3
	1.1.5 Inlet Turbulence intensity	4
	1.1.6 Inlet velocity profile	4
	1.1.7 Effect of Compressibility:	4
	1.2 Design Performance Parameters	5
	1.2.1 Pressure Recovery Coefficient, Cp	5
	1.2.2 Ideal Pressure Recovery	5
	1.2.3 Diffuser Effectiveness η	6
	1.2.4 Total Pressure Loss Coefficient	6
	1.3 Motivations	7
2	Literature Survey	8-11
3	CFD Analysis in FLOTRAN	12-21
	3.2 FLOTRAN Features	13
	3.2.1 FLOTRAN Capabilities	13
	3.3 Getting Started Using FLOTRAN	14
	3.3.1 FLOTRAN Processes	14

3.3.2 FLOTRAN Modeling 14
3.3.2.1 Modeling Constraints 15
3.3.2.2 Modeling Guidelines 15
3.3.2.3Boundary Condition Types 15
3.3.2.4 Optimum Order for Setting Boundary conditions 15
3.3.2 FLOTRAN Solution 16
3.3.2.1 Results Evaluation 17
3.3.3 FLOTRAN Post processing 17
3.3.4 Read Results File3.4 Error and Trouble Shooting 18
3.4. Common Causes of Divergence 19
3.5 Trouble Shooting Guide 20
3.6 FLOTRAN Applications 20

4 FLOTRAN Math Model 22-40
4.1 Fluid Flow Fundamentals 22
4.1.1. Continuity Equation 22
4.1.2. Momentum Equation 23
4.1.3. Compressible Energy Equation 25
4.1.4. Incompressible Energy Equation 26
4.1.5. Turbulence 27
4.1.5.1. Standard k-ε Model 30
4.1.5.2. RNG Turbulence Model 32
4.1.5.3. NKE Turbulence Model 32
4.1.5.4. GIR Turbulence Model 33
4.1.5.5. SZL Turbulence Model 34
4.1.5.6. Standard k-ω Model 35
4.1.5.7. SST Turbulence Model 36
4.1.5.8. Near-Wall Treatment 36
4.1.6. Pressure 39

5 Results and discussion 41-43
5.1 Inlet Flow Conditions 41
5.2 Velocity Distribution 41
5.3 Static Pressure 42
5.4 Static Pressure Recovery Coefficient 42
5.5 Mach number 43

6 Conclusion and Future Scope 44-45
6.1 Future Scope 45

References 46-48
Figures 50-94

List Tables

1 Table 1 Basic Equations of fluid ……..12

2 Table 2 Geometric Parameters For Tested Annular Diffuser……95

List of figures

List of color maps of pressure and velocity

1 Annular performance chart B= .02, Sovaran and Klomp……..10

2 Diffuser AR = 2; α = 10 deg.; Re= 5.15×10^5 -7.7×10^5 ……..50

3 Diffuser AR = 2; α = 15 deg.; Re= 5.15×10^5 -7.7×10^5 ……51

4 Diffuser AR = 2; α = 15 deg.; Re= 7.15×10^5 -7.7×10^5 ……..52

5 Diffuser AR = 3; α = 5 deg.; Re= 5.15×10^5 -7.7×10^5 ……...53

6 Diffuser AR = 3; α = 5 deg.; Re= 5.15×-7.7×10_5.....54

7 Diffuser AR = 3; α = 10 deg.; Re= 5.15×10^5 -7.7×10^5 ……..55

8 Diffuser AR = 4; α = 5 deg.; Re= 5.15×10^5 -7.7×10^5 ……56

9 Diffuser AR = 4; α = 10 deg.; Re= 5.15×10^5 -7.7×10^5 ……...57

10 Diffuser AR = 4; α = 10 deg; α =15 deg; Re= 2.5×10^5 ……..58

11 Diffuser AR = 5; α = 5 deg.; Re= 5.15×10^5 ; Re=7.7×10^5 ……..59

12 Diffuser AR = 5; α = 15 deg.; Re= 5.15×10^5 -.7×10^5 ……60

13 Diffuser AR = 5; α = 20deg; Re= 5.15×10^5 -7.7×10^5 ……61

14 Diffuser AR = 6; α = 5 deg.; Re= 5.15×10^5 ; Re=7.7×10^5 ……62

15 Diffuser AR = 5; AR = 6 α = 5 deg.; Re= 2.5×10^5 ……62

16 Diffuser AR = 6; α = 10 deg.; Re= 5.15×10^5 ; Re= 7.7×10^5 ……63

17 Diffuser AR = 6; α = 15 deg.; α = 10deg; Re= 2.5×10^5 ……64

18 Diffuser AR = 6; α = 15 deg.; α = 10deg; Re= 5.5×10^5 ; Re= 7.7×10^5 …….65

List of Static Pressure And Cp Charts

19 Pressure at Hub and Tip for AR= 2; α = 5; Re=2.5×10^5 ……....66

20 Pressure Recovery Coefficient at Hub and Tip for AR= 2; α = 5; Re=2.5×10^5 .....66.

21 Pressure at Hub and Tip for AR= 2; α = 10; Re=2.5×10^5 ……67

22 Pressure Recovery Coefficient at Hub and Tip for AR= 2; α = 10; Re=2.5×10^5 ….67

23 Pressure at Hub and Tip for AR= 2; α = 10; Re=5.5×10^5 ……68

24 Pressure Recovery Coefficient at Hub and Tip for AR= 2; α = 10; Re=5.5×10^5 ….68

25 Pressure at Hub and Tip for AR= 2; α = 10; Re=7.5×10^5 ……69

26 Pressure Recovery Coefficient at Hub and Tip for AR= 2; α = 10; Re=7.5×10^5 …..69
27 26 Pressure at Hub and Tip for AR= 2; α = 15; Re=2.5×10^5 ……...70
28 Pressure Recovery Coefficient at Hub and Tip for AR= 2; α = 15; Re=2.5×10^5 …..70
29 Pressure at Hub and Tip for AR= 2; α = 15; Re=5.5×10^5 ……71
30 Pressure Recovery Coefficient at Hub and Tip for AR= 2; α = 15; Re=5.5×10^5 ….71.
31 Pressure at Hub and Tip for AR=3; α=10; Re=5.5×10^5 ……72
32 Pressure Recovery Coefficient at Hub and Tip for AR= 3; α = 10; Re=5.5×10^5 …..72
33 Pressure at Hub and Tip for AR= 3; α = 10; Re=7.5×10^5 ……73
34 Pressure Recovery Coefficient at Hub and Tip for AR= 3; α = 10; Re=7.5×10^5 …..73
35 Pressure at Hub and Tip for AR= 3; α = 10; Re=2.5×10^5 ……74
36 Pressure Recovery Coefficient at Hub and Tip for AR= 3; α = 10; Re=2.5×10^5 …...74.
37 Pressure at Hub and Tip for AR= 3; α = 5; Re=5.5×10^5 ……75
38 Pressure Recovery Coefficient at Hub and Tip for AR= 3; α = 5; Re=5.5×10^5 …….75
39 Static Pressure at Hub and Tip For AR = 4, Angle =5deg; Re=5.5×10^5 ……76.
40 Static Pressure Recovery at Hub and Tip For AR = 4, Angle =5deg; Re=5.5×10^5 …76
41 Static Pressure at Hub and Tip For AR = 4, Angle =5deg; Re=5.5×10^5 …….77
42 Static Pressure Recovery at Hub and Tip For AR = 4, Angle =5deg; Re=5.5×10^5 …77
43 Static Pressure at Hub and Tip For AR = 4, Angle =10deg; Re=7.5×10^5 ……...78
44 Static Pressure Recovery at Hub and Tip For AR = 4, Angle =10deg; Re=7.5×10^5 ..78
45 Static Pressure at Hub and Tip For AR = 4, Angle =10deg; Re=5.5×10^5 ……...79
46 Static Pressure Recovery at Hub and Tip For AR = 4, Angle =10deg; Re=5.5×10^5 ..79
47 Static Pressure at Hub and Tip For AR = 4, Angle =10deg; Re=2.5×10^5 ……....80
48 Static Pressure Recovery at Hub and Tip For AR = 4, Angle =10deg; Re=2.5×10^5 ..80
49 Static Pressure at Hub and Tip For AR = 4, Angle =15deg; Re=7.5×10^5 ……..81
50 Static Pressure Recovery at Hub and Tip For AR = 4, Angle =15deg; Re=7.5×10^5 ..81
51 Static Pressure at Hub and Tip For AR = 4, Angle =15deg; Vx= Re=5.5×10^5 …….82
52 Static Pressure Recovery at Hub and Tip For AR = 4, Angle =15deg; Re=5.5×10^5 ..82
53 Pressure at Hub and Tip for AR= 5; α = 5; Re=2.5×10^5 ……83
54 Pressure Recovery Coefficient at Hub and Tip for AR= 5; α = 5; Re=2.5×10^5 …….83.
55 Pressure at Hub and Tip for A R= 5; α = 10; Re=7.5×10^5 ……84

56 Pressure Recovery Coefficient at Hub and Tip for AR= 5; α =10; Re=2.5×10^5 ……84

57 Pressure at Hub and Tip for A R= 5; α = 15; Re=5.5×10^5 ……..85

58 Pressure Recovery Coefficient at Hub and Tip for AR= 5; α =15; Re=5.5×10^5 ……85

59 Pressure at Hub and Tip for A R= 5; α = 15; Re=7.5×10^5 ……..86

60 Pressure Recovery Coefficient at Hub and Tip for AR= 5; α =15; Re=7.5×10^5 ……86

61 Pressure at Hub and Tip for A R= 5; α = 20; Re=5.5×10^5 ……..87

62 Pressure Recovery Coefficient at Hub and Tip for AR= 5; α =20; Re=5.5×10^5 ……87

63 Pressure at Hub and Tip for A R= 5; α = 20; Re=7.5×10^5 ……..88

64 Pressure Recovery Coefficient at Hub and Tip for AR= 5; α =20; Re=7.5×10^5 ……88.

65 Pressure at Hub and Tip for A R= 5; α = 25; Re=7.5×10^5 ……..89

66 Pressure Recovery Coefficient at Hub and Tip for AR= 5; α =25; Re=7.5×10^5 ……89

67 Pressure at Hub and Tip for AR= 6; α = 10; Re=5.5×10^5 …….....90

68 Pressure Recovery Coefficient at Hub and Tip for AR= 6; α = 10;Re=5.5×10^5 ……90

69 Pressure at Hub and Tip for AR= 6; α = 10; Re=2.5×10^5 ……..91

70 Pressure Recovery Coefficient at Hub and Tip for AR= 6; α = 10; Re=2.5×10^5 …...91

71 Pressure at Hub and Tip for AR= 6; α = 10; Re=7.5×10^5 …….....92

72 Pressure Recovery Coefficient at Hub and Tip for AR= 6; α = 10; Re=7.5×10^5 …..92

Mach number charts

73 Mach number with varying AR at constant $\alpha = 15^o$, Re = 7.7×10^5 ……...93

74 Mach number with varying AR at constant $\alpha = 15^o$, Re = 7.7×10^5 ……93

75 Mach number with varying AR at constant $\alpha = 10^o$, Re = 7.7×10^5 ……94

76 Mach number with varying AR at constant $\alpha = 10^o$, Re = 5.15×10^5 ……..94

Abbreviations

A	Area
AR	Area Ratio
AS	Aspect Ratio
B	Blockage
b	Dimension
C_d	Disc Arch Coefficient
C_f	Friction Coefficient
C_p	Static Pressure Recovery Coefficient
C_p^*	Line of Maximum C_p for Minimum L/R
C_p^{**}	Line of Maximum C_p for Minimum Ar
C_{po}	Total Pressure Loss Coefficient
C_{pt}	Total Pressure Loss Coefficient
C_{pi}	Ideal Pressure Coefficient
G	Gravitational Acceleration
H	Passage Height, Shape Factor
K	Total Pressure Loss Coefficient
M	Mach Number
L	Length
M	Mass Flow, Momentum Ratio
P	Pressure
P_t	Total Pressure
Pr	Pressure Ratio
P	Static Pressure
Q	Volume Flow Rate
Re	Reynolds Number
R	Radius
T_u	Turbulence Intensity
T	Thickness
U, V, W	Velocity Components

X, Y, Z	Cartesian Coordinates
Vx, Vy, Vz	Components of the Velocity Vector in the x, y and z Directions
ρ	Density
T	Time
R	Gas Constant
T	Temperature
B	Bulk Modulus
T_{ij}	Stress Tensor
U_i	Orthogonal Velocities (U1 = Vx, U2 = Vy, U3 = Vz)
M	Dynamic Viscosity
Λ	Second Coefficient Of Viscosity
G_x, G_y, G_z	Components of Acceleration Due To Gravity
R_x, R_y, R_z	Distributed Resistances
T_x, T_y, T_z	Viscous Loss Terms
Cp	Specific Heat
T_o	Total (Or Stagnation) Temperature
K	Thermal Conductivity
W_v	Viscous Work Term
Q_v	Volumetric Heat Source
Φ	Viscous Heat Generation Term
E_k	Kinetic Energy
V	Magnitude of the Fluid Velocity Vector
$\overline{V}_x$	Mean Component of Velocity In X-Direction
V_x^r	Fluctuating Component of Velocity In X-Direction
Σ^r	Reynolds Stress Terms
M_t	Turbulent Viscosity
Φ	Viscous Dissipation
L_x	Length Scale
L_n	Shortest Distance from the Node to the Closest Wall
L_c	Characteristic Length Scale
C_μ	Turbulence Constant

k	Turbulent kinetic energy (ENKE)
ε	Turbulent kinetic energy dissipation rate (ENDS)
ω	Specific dissipation rate
C_r	Constant depending on turbulence model used
Ω_m	Angular velocity of the coordinate system
ε_{mji}	Alternating tensor operator
v_{tan}	Velocity parallel to the wall
τ	Shear stress
ν	Kinematic viscosity
κ	Slope parameter of law of the wall
E	Law of the wall constant
δ	Distance from the wall
ε_{en}	Near wall dissipation rate
k_{nw}	Near wall kinetic energy
ρ_o	Reference density
P_{ref}	Reference pressure
$\{g\}$	Acceleration vector due to gravity
P_{abs}	Absolute pressure
P_{rel}	Relative pressure
$\{r\}$	Position vector of the fluid particle w. r. to rotating
$\{\omega\}$	Constant angular velocity vector of the coordinate system
$\{V\}$	Vector velocity in the rotating coordinate system
Pr	Prandtl number
μ_e	Effective viscosity
K_e	Effective conductivity
σ_t	Turbulent Prandtl (Schmidt) Number

Chapter 1

Introduction

Annular diffusers are often used in conjunction with turbo machines to increase the static pressure and reduce the velocity of the discharge flow.

The present investigation involves a systematic evaluation of different straight hub and diverging outer wall annular diffusers configurations with varied AR and diverging angle. Each diffuser is tested with varied axial inlet flow velocity and zero inlet swirl angle to provide a comprehensive basis on which generalize the influence of geometry parameter AR, θ on pressure recovery in annular diffusers[4].

Diffusers are ducts that convert flow kinetic energy to pressure by decelerating the flow. Flow decelerations affected by varying the cross sectional area. From mass conservation it follows that diffusers for incompressible fluids, and for subsonic flow as well, are duct with increasing area along the flow direction[8].

The flow in the diffuser is governed by the behavior of the boundary layers at the diffuser walls. The deceleration of the flow through the diffuser produces a pressure rise in the stream wise direction. The wall shear layers are therefore subjected to a positive or adverse pressure gradient. As is well known, adverse pressure gradients cause the boundary layer thicken and possibly separate from the diffuser walls, forming areas of back flow in diffusers. The net result of thickening of the wall boundary layers or the formation of region of backflow, is the blockage of the flow area which reduce s the effective area available to the flow. Reduction the effective flow area in turn results in a reduced pressure rise through the diffuser. The interaction of wall shear layers and / or separated zone with the core flow in diffusers is very complicated; therefore diffuser design and performance estimation is largely based on experimental data and empiricism.

1.1 Diffuser performance parameter

1.1.1 Geometric parameters

Any duct geometry with an increasing area in the stream wise direction constitutes subsonic diffuser geometry. Therefore, the number of different diffusers geometries that can be conceived is infinite. However in practice, adequate design data are available for a limited number of geometries.

1 .Rectangular cross section or planner diffusers

2 .Conical diffusers

3. Straight walled annular diffusers

Other commonly used diffuser geometries include the radial and axiradial diffusers which are used at the exit of radial and axial turbo machines, respectively.

These geometric parameters can be consolidated to a few non dimensional parameters that are found to be important in terms of diffuser performance. The first is the area ratio, AR, the area ratio of diffuser exit to inlet areas. The area ratio is measure of the theoretical diffusion or pressure recovery expected. The second important parameter is the dimensionless diffuser length define as : N/Wi or L/Wi for planar diffusers, N/ Ri or N/Ri for conical diffusers, and L/(Rit - Rih) , for annular diffusers. This dimensionless diffuser length in combination with the area ratio AR is measure of the overall pressure gradient expected across the diffuser. The third geometric parameter commonly used in displaying diffuser performance is the wall divergence angle--2θ for planar and conical diffusers and θ_t and θ_h, for annular diffusers. The divergence angles, length, and area ratio are related as follows[10].

For planar diffusers: $AR = 1 + 2(N / W_i)\tan\theta$

For conical diffusers: $AR = (1 + (N / R_i)\tan\theta)^2$

For annular diffusers:

$$AR = \frac{(R_{it} + L\sin\theta_t)^2 - (R_{ih} - \sin\theta_h)^2}{R_{it}^{\ 2} - R_{ih}^{\ 2}}$$

1.1.2 Aerodynamic blockage

It is clear that thin inlet boundary layers should be beneficial to high diffuser recovery and those longer diffusers necessary to achieve high levels of recovery as the inlet boundary thickness increases[11].

The blockage is the fraction or percentage of the inlet passage area which is occluded the boundary layer displacement thickness on all walls. The displacement thickness is taken as equal on all surfaces and then the following relationships ensue:

B = 2δ*/h for annular diffusers where h is annular height at inlet

B = 2δ*/ D_i for conical diffusers with uniform inlet boundary layers

1.1.3 Reynolds number:

Viscosity is an important parameter in any fluid dynamic process and normally appears in the form of a Reynolds number. Typically, diffusers are characterizes by Reynolds number based on an inlet hydraulic diameter. All studies reported in this field suggest that the Reynolds number is a comparatively weak parameter as long as the flow is fully turbulent regime[25].

1.1.4 Inlet Mach number:

The Mach number at the inlet to the diffuser was thought to be important at values as low as approximately 0.7 and performance to fall off past this point. No significant on Mach number develops at throat Mach numbers of less than 1.0[35].

1.1.5 Inlet Turbulence intensity

The turbulence intensity is most frequently defined as an RMS value:

$$Tu = \frac{\left[1/3(u'^2 + v'^2 + w'^2)\right]^{1/2}}{U}$$

This equation defines the parameter most frequently used to specify the over all level of inlet turbulence intensity [25].

1.1.6 Inlet velocity profile:

No convention has been developed to specify the inlet velocity profile to diffuser. However, various research programs have shown the effect to be significant.

1.1.7 Effect of Compressibility:

With compressible flow both area, A, and density, ρ, increases with passage down the diffuser so that the reduction in velocity, v, will be greater than in the case of incompressible flow where only the cross sectional area increases. It therefore follows that the pressure recovery coefficient should also be greater.

$$v = \frac{m}{\rho.A}$$

A potential detrimental effect arises from this because the corresponding increase in adverse pressure gradient will not be supported by an increasing transverse energy gradient and so G, the ratio of the two gradients, increases. The diffuser than becomes more susceptible to flow separation.

The rate of increase in value of Cp is not rapid until Mach number of 0.6 have been exceeded and than the effect is most pronounced when area ratios are low. These low area ratios correspond to the diffuser inlet vision and flow separation would therefore

occur here as a result of predicted increasing adverse pressure gradient caused by the higher subsonic inlet mach number.

Furthermore, this onset of flow separation at diffuser inlet would cause the flow stream to accelerate and so deepen the level of depression at the aerodynamic throat.

From the above argument it follows that two modifications should be made to diffusers if they are to operate at high subsonic mach numbers. First, for a given geometric area ratio, they must be made longer than the lengths suggested by diffuser charts derived from tests using incompressible flow. This modification is necessary because of enhancement in overall static pressure recovery. It can be implemented by the derivation of an equivalent area ration that would have been necessary to produce an identical value of Cpi if the flow had been incompressible.

Second, the wall divergence angle must be reduced in order to counteract the effect of compressibility in increasing the adverse pressure gradient.

Effect of Compressibility on Wall Design: the design of diffuser walls is achieved by using a step by step or " marching" method where small element of diffuser are considered in sequence it was recommended the length of each element, s, should be on the order of to percent of the hydraulic diameter when assessed diffuser inlet

1.2 Design Performance Parameters

1.2.1 Pressure Recovery Coefficient, Cp

The performance of diffusers is generally cast in the form of a pressure recovery coefficient, Cp

$$C_p = \frac{p_2 - p_1}{\frac{1}{2}\rho v^2_{av1}}$$

where p_e and p_i are the diffuser exit and inlet pressure , ρ is fluid density at the inlet and U_i is the mean velocity at diffuser inlet.

1.2.2 Ideal Pressure Recovery

Another parameter of interest is the ideal pressure recovery , C_{pi} ,which is the pressure recovery coefficient assuming an inviscid flow through diffuser ,which represent the maximum pressure recovery attainable by the given diffuser. When the definition of pressure recovery, the Bernoulli equation, and the conservation of mass and conservation of angular momentum principles are all employed, the following relationship is obtained for *Cpi* :

$$C_{pi} = 1 - \frac{1}{AR^2}$$

1.2.3 Diffuser Effectiveness η

A parameter used as a measure of diffuser performance is the diffuser effectiveness η

$$\eta = C_p / C_{pi}$$

1.2.4 Total Pressure Loss Coefficient :

the total pressure loss through the diffuser is generally cast in the form of a loss coefficient

$$K = \frac{\overline{p}_{01} - \overline{p}_{02}}{\frac{1}{2}\rho v^2_{av1}}$$

$$K = (\overline{u}_i^{\,2} - \overline{u}_e^{\,2})/U_i^{\,2} - C_p \qquad = (\alpha_i - \alpha_e / AR^2) - C_p$$

where p_{oi} is the total pressure in the core region at the exit, the over bar indicate the mass averaged quantity, and α_i and α_e are the kinetic energy parameters at the inlet and exit of the diffuser .

for the case where the velocity profile at the inlet of diffuser is flat with a thin wall boundary layer, $\alpha_i \approx 1$. However, due to the thickening of boundary layer through the

diffuser, α_e is generally greater than unity. Nonetheless, it is often assumed that kinetic energy coefficient are equal to unity, than

$$K = C_{pi} - C_p$$

1.2 Motivations:

The purpose of this study is to investigate the level of knowledge and in certain important areas the lack thereof, concerning the performance of annular diffusers. For decades investigators have conducted individual studies without a careful consideration of how all the studies may be interwoven. A pattern of consistent behavior among the database elements for annular diffusers is established in this investigation. However, it may be of even greater significance that the investigation reveals areas where critical design knowledge is missing. It will be observed that conducting individual investigations of annular diffuser performance has blinded most investigators from seeing the larger picture and the critical interactions between the different variables which have been discussed in the literature. This study begins by looking at historical data, then proceeds to investigate the parametric dependence, resulting in the development of a preliminary design set of equations and then finally by careful examination of further investigations which are needed before the annular diffuser design problem will be well understood.

Chapter 2

Literature Survey

Much of the extant data covering annular diffusers comes from the period from the 1950s through the 1980s. In this period of time, a considerable amount of research was done in the experimental laboratory to uncover some of the unusual performance characteristics of annular diffusers. By the late 1980s, however, the experimental research had reduced substantially due to a lack of government funding in a number of countries where the work had previously been extensive. It is, therefore, useful to review the data which has been made available and to look for patterns within this data. It is also necessary to determine how this data may best be used in future design studies and where it needs to be further improved. Much of the original data was taken in order to support studies of axial compressor discharge diffusion as flow leaves a compressor and enters a combustion chamber. Other work was done for exhaust diffusers of hydroelectric turbines, small gas turbines, and turbochargers. While these topics are still important today and there are important unresolved questions, the level of activity has reduced. Now important research topics must be carefully selected for the more limited studies possible in future years. Figure 1a shows a plot of many different annular diffuser data sets which cover a wide range of swirl angles, blockage, turbulence intensity, and geometric parameters. Figure 1b shows the classical diffuser performance map for an annular diffuser by Sovarn and Klomp (1967)[27]. This map was the first investigation to introduce the topic of aerodynamic blockage. The map actually is a generalized composite of many different investigations

. The Sovran and Klomp map actually has accuracies of roughly ±0.1 on *Cp* since the map itself is an aggregate of many different diffuser builds and does not correspond to one single or specific diffuser configuration. The difference in Figure 1a and Figure 1b is very important. Figure 1a is much less systematic than Figure 1b. Figure 1b is a systematic variation of certain geometric parameters, with many other parameters held constant. For example, Figure 1b corresponds to very low blockage (approximately

2%), low turbulence intensity, no swirl, and moderate variations of flow (wall) deflection angle. By contrast, Figure 1a has a wide variety of these parameters and forces the reviewer to think carefully about the role of these additional parameters. Ideally, one would like to see a very large collection of maps, such as in Figure 1b, to cover the list of variables just given, but these maps have never been prepared. To produce a map (such as Figure 1b) requires a large number of different geometries, a variety of inlet flow conditions and a large series of systematic tests. This has not been economically possible. Many dream of the day when this can be done by computational fluid dynamic methods (CFD), although this dream may still be quite remote. Consequently, it is important that we consider the variations in Figure 1a and attempt to determine how much of a systematic nature has been learned in the prior investigations.

In this early work of Hoadley and Hughes (1969)[11], an ideal pressure recovery contour is plotted parallel to the actual pressure recovery. This suggests that much of the effect of geometry and swirl can be taken care of in the ideal pressure recovery and that a sensible way of developing a correlation for static pressure recovery performance will be to use diffuser effectiveness which is $\eta = Cp / Cpi$ or in other words the ratio of the actual pressure recovery coefficient divided by the ideal pressure recovery coefficient. Figure 2 supports this basic notion and suggests that much of the swirl angle variation will be taken care of by this approach.. On the far right-hand side of the figure, the data trend is no longer exactly parallel to the ideal pressure recovery and tends to fall away more quickly. A variety of past experiences suggests that there is some development of progressive stalling occurring which will not be reflected in the ideal pressure recovery, but must be dealt with in the actual pressure recovery . Clearly, a first step is to concentrate on diffuser effectiveness and not upon *Cp*. We must therefore, establish a proper definition of ideal pressure recovery coefficient.

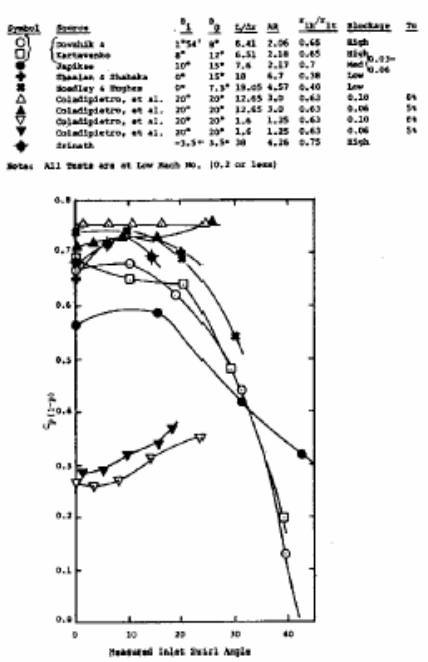

Figure 1a. Straight annular diffuser performance with swirl at various AR and blockage.

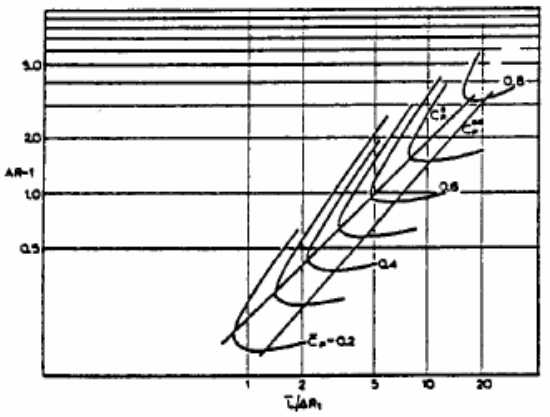

Figure 1b. Annular diffuser performance chart, B_1, ≃ .02 Sovran and Klomp (1967).

The ideal pressure recovery coefficient is derived directly from basic principles. It is the pressure recovery that would be achieved if the flow was strictly one dimensional, inviscid, filled the entire passage and, therefore, by implication, has no blockage, no boundary layer buildup, and no deviation of flow either entering or leaving.

Using this definition, we can now look at the entire data set. The first step is to partially remove the effect of geometry and swirl (as embodied in Figure 1) by using the definition of diffuser effectiveness, and then look for other dominate variables and trends. A variety of parameters was considered in looking at basic trends for η. Area ratio, $L/\Delta r$, $b2/b1$, $r1h/r1t$, $r2/r1$, and such parameters were initially considered in a general parameter sensitivity investigation. It was found that all the remaining geometric effects (those not handled in the *Cpi* relationship above) were best handled simply by diffuser area ratio. This first investigation was scoping in nature and pointed a direction in which to begin the modeling exercise.

Several annular diffuser studies have been published in which contoured walls were an essential part of the design problem. Thayer (1971)[30] reported that curved wall diffusers had pressure recovery as high as 0.61 to 0.65 for an area ratio of 2.15

Takehira et al (1977)[34] presented extensive data for a large set of both straight annular diffusers and curved wall diffusers, and determined that the use of strong curvature at the exit of diffuser was not debilitating but did produce a penalty compared to noncurved diffusers or diffusers with curvature at the inlet. Adkins et al (1983)[2] tested an annular diffuser of constant outer radius and a conical center body with cones of different angles. In general the pressure recovery increases with decreasing cone angle for various area ratios, but the 132º and sometimes the 45º cone angle produced lower pressure recoveries than an equivalent sudden expansion. This was attributed to a large and rapid separation at the base of the cone where the diffuser starts. Adding a radius to the base of the cone so that it smoothly blended into the upstream hub, was found to improve the performance. An extensive study of diffusers which, although annular, begin with a circular cross section was reported by Ishikawa and Nakamura (1989)[13]. The author found that the performance of the diffuser differed significantly depending on whether it is parallel or diverging for L/r_1 greater than about 2. When both types have the same non dimensional length and area ratio, the parallel diffuser has the higher C_P. The lines of optimum performance are also drawn. The line of C_P^* shows the best area ratio for a given non dimensional length, and the line of C_P^{**} shows the best non dimensional length for a given area ratio. In the case of the latter line, there is no difference between the parallel and diverging diffuser.

Ishikawa and Nakamura (1989)[13] also attempted to compare their results with those of Sovran and Klomp for a conventional annular diffuser for the same wall length and area ratio, their diffuser was superior, but since the inlet conditions were different in the two studies, this conclusion is only tentative.

Chapter 03

CFD Analysis in FLOTRAN

FLOTRAN is a finite element analysis program for solving fluid flow and conjugate heat transfer problems. The fluid flow problem is defined by the laws of conservation of mass, momentum, and energy. These laws are expressed in terms of partial differential equations which are discretized with a finite element based technique.
Assumptions about the fluid and the analysis are as follows:

1 There is only one phase.

2 The user must determine:

(a) If the problem is laminar (default) or turbulent

(b) If the incompressible (default) or the compressible algorithm must be invoked

The governing equations solved by FLOTRAN are the Navier-Stokes equations combined with the continuity equation, the thermal transport equation, and constitutive property relationships.

Navier-Stokes Equation $$U\frac{\partial U}{\partial x}+V\frac{\partial V}{\partial y}=-\frac{1}{\rho}\frac{\partial p}{\partial x}+\frac{1}{\rho}\frac{\partial \tau}{\partial y}$$

Continuity Equation $$\frac{\partial \rho}{\partial t}+\frac{\partial(\rho V_x)}{\partial x}+\frac{\partial(\rho V_y)}{\partial y}+\frac{\partial(\rho Vz)}{\partial z}=0$$

This equation represents a number of fluid flow equations:

Table 1 Basic Equations of fluid

ϕ	**Equation**	**D**	**S**
1	mass conserve.		0
u	x-momentum	μ	$-\frac{\partial P}{\partial x}+\rho g_x$
v	y-momentum	μ	$-\frac{\partial P}{\partial x}+\rho g_x$
w	z-momentum	μ	$-\frac{\partial P}{\partial x}+\rho g_x$
T	temp.(energy)	k	q
k	turb.k.e.	μ_t/σ_t	$\mu_t G-\rho\varepsilon$

ε	t. k.e. diss. rate	μ_t/σ_t	$C_1\mu_t\frac{\varepsilon}{k}G - C_2\rho\frac{\varepsilon^2}{k}$
			$G = \left(\frac{\partial u_i}{\partial x_j} + \frac{\partial u_j}{\partial x_i}\right)\frac{\partial u_i}{\partial x_j}$

3.2 FLOTRAN Features

- Steady-State or Transient Solution Algorithm
- Equal Order Approximation for Velocity and Pressure
    1. No staggered grids
    2. No mixed order interpolation
- Monotone Streamline Upwind Approximation for Advection Terms
    1. Increased accuracy over conventional upwind
    2. Stable at high Reynolds numbers
- Minimal Execution Time Requirements
    1. Segregated sequential solution
    2. Iterative solution methods
- Minimal Storage Requirements
    1. Bandwidth independent
    2. In-core solution method

3.2.1 FLOTRAN Capabilities

- 2-D or 3-D Geometries
- Ax symmetric Geometries
- Laminar or Turbulent Flow and/or Heat Transfer
- Forced, Free, or Mixed Convection
- Conduction
- Conjugate Heat Transfer
- Distributed Flow Resistances
- Porous Media
- Incompressible or Compressible Flow
- Steady State or Transient

- Total Energy Equation
- Global Convergence Status
- Boundary Conditions:
    1. Prescribed Nodal Values - Velocity, Pressure, Temperature, Turbulent Kinetic Energy, Turbulent Energy Dissipation.
    2. Prescribed Heat Flux
    3. Prescribed Heat Source
    4. Prescribed Film Coefficient
    5. Adiabatic
    6. Symmetry
    7. Periodic Boundaries

3.3 Getting Started Using FLOTRAN

FLOTRAN has been integrated with ANSYS. This integration allows users to build the finite element models using ANSYS PREP7 and to pass the model data to Flotran for the various analyses. Once the FLOTRAN analyses are done, the data can then be transferred to the ANSYS postprocessor, POST1.

IDEAS and PATRAN can also be used to pre- and post process finite element models for FLOTRAN analyses.

In this course, we will use only ANSYS for pre- and postprocesses.

3.3.1 FLOTRAN Processes

- Preprocessing (or model generation and B.C./I.C.) - ANSYS,
- Solution - FLOTRAN,
- Postprocessing (or results evaluation) - ANSYS.
-

3.3.1 FLOTRAN Modeling

Only two element types are valid for FLOTRAN analyses. FLOTRAN uses the MAT element attribute to distinguish fluid elements from solid elements. Fluid elements must have *MAT = 1*, and solid elements are identified by *MAT > 1*. The REAL ATTRIBUTE is to flag elements with distributed resistance.

3.3.1.1 Modeling Constraints

- Element Types
    1. Quad and triangles (2D) - PLANE55
    2. Hex and tet (3D) - SOLID70
- Element Material Number
    1. *MAT = 1* - Fluid Elements
    2. *MAT > 1* - Solid Elements
- Cartesian Coordinates
- Rotating Coordinates
- Cylindrical Coordinates

3.3.1.2 Modeling Guidelines

- Examine the solution domain for possible symmetries
- Sketch the geometry for planning the geometry model and the finite element model
- Anticipate the analysis requirements
    1. Regions of high gradients in the solution variables. These regions usually require finer meshes.
    2. Important Boundaries such as flow inlets, flow exits, heated areas, and constant temperature boundaries.
    3. Mesh size requirements to be considered with maximum limit of nodes and CPU and storage requirements.
- Sketch the proposed mesh
- Construct the geometry and elements with top-down or bottom-up technique

3.3.1.3Boundary Condition Types

- Symmetry boundaries
    - Geometry half symmetry or Mirror image
    - Align with a coordinate axis
    - Zero normal velocity on the boundaries
- Inflow boundaries - specify either inlet velocity or pressure
- Outflow boundaries - specify pressure only
- Wall boundaries - zero flow velocity on the wall

- Periodic Boundaries - corresponding boundaries with identical flows
- Thermal boundary conditions - do not affect flow boundary conditions
- Initial conditions - specified with separate boundary condition in each LOAD STEP(ANSYS)

3.3.1.4 Optimum Order for Setting Boundary conditions

- Symmetry boundaries
- Inflow boundaries
- Outflow boundaries
- Wall boundaries

When a boundary condition is repeatedly specified, the latter overwrite the former one. Unspecified flow boundaries are treated as natural boundary conditions where mass can enter or leave the boundaries.

3.3.2 FLOTRAN Solution

A complete pass through all the equations is called a global iteration consisting of

1. Approximate solution of each momentum equation in sequential fasion.
2. Solution of the pressure equation.
3. Calculation of velocities to conserve mass.
4. Solution of the energy equation.
5. Update of the laminar properties.
6. Solution of the turbulence equations.
7. Update of the turbulent properties.

The progress of the solution is monitored by observing the rate of change of the solution from one global iteration to the next. The analyst can restart the analysis until satisfied that the rate of change of the solution is small enough.

The approximate solution of the momentum equation is obtained through the use of a tri-diagonal matrix algorithm. The momentum equations are relaxed to provide a stable solution.

The pressure equation is solved with a pre-conditioned conjugate gradient routine. An incomplete Choleski decomposition provides the preconditioning. The approach is particularly well suited for practical applications because the solver requires very little

storage other than those associated with the non-zero matrix terms in the nonsymmetric momentum equation. The performance of the method is bandwidth independent and it is ideally suited towards use with irregular and unstructured finite element grids.

3.3.2.1 Results Evaluation

- Field Variable Information
    1. Velocity
    2. Pressure
    3. Temperature
    4. Total Temperature
    5. Turbulent Kinetic Energy
    6. Turbulent Dissipation Rate
    7. Density
    8. Molecular Viscosity
    9. Effective Viscosity
    10. Thermal Conductivity
- Calculated Field Quanities
    1. Stream Function (2D)
    2. Velocity Magnitude (3D)
    3. Wall Film Coefficients
    4. Wall Heat Fluxes
    5. Pressure Coefficient
    6. Mach Number
    7. Total Pressure
    8. Nodal Heat Fluxes
    9. Nodal Film Coefficients
- Solution Reliability Statistics
    1. Nodal Residuals
    2. Nodal Error Indicators
- Graphic Output:

1. All of the imaging capabilities (e.g., contour plots, vector plots, etc.) All FLOTRAN variables can be used for postprocessing.
2. Mass less Particle Tracking is available in the ANSYS and IDEAS programs.

3.3.3 FLOTRAN Postprocessing

The FLOTRAN results file, *<jobname&.res>* is a unformatted binary file that can be read by the FLREAD command in ANSYS postprocessing.

3.3.3.1 Read Results File:

FLREAD, jobname, ext

Where ext is the extension of FLOTRAN filename.

res Nodal results file for all degrees of freedom as well as properties

nqh Heat flux and filem coefficients

eid Error indicator file

*** Plot Results:**

PLNSOL, variable (Velocity, Temperature, Pressure, etc.)

*** Plot velocity vectors:**

PLVECT, V

*** Plot graphs along a line path:**

Define Path:

LPTATH,node1,node2,....node10

Define Name of Graph:

PDEF, User-define-name, Variable

Produce Graph:

PLPATH, User-define-name

*** Integrate Pressures:**

INTSRF, PRES

*** Particles Tracing:**

Define up to 50 points in problem domain

TRPOIN,x,y,z

TRPOIN,PICK

List existing points with TRPLIS

Delete points with TRPDEL

Execute particle tracing of any post processing variable

PLTRAC, FLUID, item, compon

*** 3D Contour Plots:**

/CTYPE,1

/EDGE,off

ASEL,S,EXT

NSLA,S,ALL,1

NSEL,INVE

PLNSOL,V,SUM

*** 3D Cross Section Contour Plots**

/TYPE,3,SECT

/FOCUS,3,RI,0,D4+RI

/VIEW,3,1,0,0

NSEL,s,loc,x,RI

ESLN,,0

PLNSOL,V,SUM

PLNSOL,PRESS

Transient results files use ANSYS POST26.

3.4 Error and Trouble Shooting

FLOTRAN error message indicates a fatal error. FLOTRAN performs a number of data checks to ensure that the problem posted is valid. There are, of course, many inputs that cannot be verified; users must verify them. Diverging solution, and unexpected results are often caused by invalid input.

3.4.1 Common Causes of Divergence

- Incorrect problem setup
    - Highly skewed or tapered finite elements
    - Missing or duplicate nodes
    - Incorrect or missing boundary conditions
    - Unreferenced nodes
    - Poorly defined problem domain

- Incorrect problem setup in FLOTRAN
    - Inconsistent property information
    - Invalid control parameters
- Tough fluids problem

3.4.2 Trouble Shooting Guide

- Users may check the boundary conditions by setting both Flow and Thermal in **Screen 1S** to F(false) and Iteration to 0. The FLOTRAN will generate a jobname.prt that tabulates the mass flows at all inlets and outlets. If unexpected inlets/outlets are listed, eliminate them.
- Make sure information on **Screen 2S** and **Screen 2P** are realistic and consistent.

  For example, a temperature data given in when it should be given in may give an unrealistic density and cause divergence.
- If the divergence occurs on the first few iterations, it is usually either a modeling error or an incorrect FLOTRAN data specification. If a FLOTRAN analysis runs for a short time (5-10 iterations) where it appears to converge and then diverges, it may be caused by improper run parameters. For example, a laminar flow analysis on a high Reynolds number situation may first converge then diverge.
- Reducing the relaxation parameters on Screen 4S may help the convergence. These parameters are set at 0.5 and may be reduced to 0.2-0.3 to better control the convergence. Another alternative is to lower the inertia number on Screen 4S.

If these methods still fail to converge, it may be possible to pre-condition the problem. This is done by raising the viscosity an appropriate order of magnitude to obtain a laminar solution and then introducing the turbulence.

3.5 FLOTRAN Applications

FLOTRAN has been applied to a variety of applications from a wide range of industries.

- AUTOMOTIVE
    1. Study of air flow over vehicles
    2. Passenger compartment flow
    3. Fluid flow, conjugate heat transfer analysis of engine exhaust manifolds and water jackets - Flow through radiator passages
    4. Flow analysis through various valve configurations

- AEROSPACE
    1. External flow over various wing configurations
    2. Internal flow analyses of nozzles and ducts
    3. Fluid flow, heat transfer analysis of aircraft passenger compartments
    4. Compressible flow analysis with shock/boundary layer interaction
    5. Thermal analyses
- ELECTRONICS
    1. Electronic cooling in a computer terminal
    2. Conjugate heat transfer analysis of IC package
    3. Heat transfer analysis of electronic fin array
    4. Heat transfer analysis of a simulated card cage
    5. Disk flow
- POWER
    1. Thermally stratified turbulent pipe flow
    2. Pressurized thermal shock
    3. Natural convection cooling
    4. Fluid bed reactor analysis
    5. Valve analysis
- HVAC
    1. Flow inside buildings
    2. Flow in ducts
    3. Flow in pipes
    4. Flow through coolant passages
    5. Heat exchanger analysis
- TURBO MACHINERY
    1. Torque converter flow analysis
    2. Flow through vaned and vane less diffusers
    3. Labyrinth seal flow
    4. Blade cooling analysis
    5. Flow in pump, compressor, turbine, impeller passages

Chapter 4

FLOTRAN Math Model

4.1 Fluid Flow Fundamentals

This chapter discusses the FLOTRAN solution method used with elements fluid141 and fluid142. These elements are used for the calculation of 2-D and 3-D velocity and pressure distributions in a single phase, Newtonian fluid. Thermal effects, if present, can be modeled as well.

The fluid flow problem is defined by the laws of conservation of mass, momentum, and energy. These laws are expressed in terms of partial differential equations which are discretized with a finite element based technique.

Assumptions about the fluid and the analysis are as follows:

1. There is only one phase.
2. The user must determine: (a) if the problem is laminar or turbulent; (b) if the incompressible (default) or the compressible algorithm must be invoked.

4.1.1. Continuity Equation

From the law of conservation of mass law comes the continuity equation:

$$U\frac{\partial U}{\partial x}+V\frac{\partial V}{\partial y}=-\frac{1}{\rho}\frac{\partial p}{\partial x}+\frac{1}{\rho}\frac{\partial \tau}{\partial y}$$
$$\frac{\partial \rho}{\partial t}+\frac{\partial(\rho V_x)}{\partial x}+\frac{\partial(\rho V_y)}{\partial y}+\frac{\partial(\rho Vz)}{\partial z}=0 \qquad (4\text{–}1)$$

where:

V_x, V_y and V_z = components of the velocity vector in the x, y and z directions, respectively

ρ = density

x, y, z = global Cartesian coordinates

t = time

The rate of change of density can be replaced by the rate of change of pressure and the rate at which density changes with pressure:

$$\frac{\partial \rho}{\partial t} = \frac{\partial \rho}{\partial P}\frac{\partial P}{\partial t} \tag{4–2}$$

where:

P = pressure

The evaluation of the derivative of the density with respect to pressure comes from the equation of state. If the compressible algorithm is used, an ideal gas is assumed:

$$\rho = \frac{P}{RT} \Rightarrow \frac{\partial \rho}{\partial t} = \frac{1}{RT} \tag{4–3}$$

where:

R = gas constant

T = temperature

If the incompressible solution algorithm is used (the default), the user can control the specification of the value with:

$$\frac{\partial \rho}{\partial P} = \frac{1}{\beta} \tag{4–4}$$

where:

β = bulk modulus

The default value of 10^{15} for β implies that for a perfectly incompressible fluid, pressure waves will travel infinitely fast throughout the entire problem domain, e.g. a change in mass flow will be seen downstream immediately.

4.1.2. Momentum Equation

In a Newtonian fluid, the relationship between the stress and rate of deformation of the fluid is:

$$\tau_{ij} = -P\delta_{IJ} + \mu\left(\frac{\partial u_i}{\partial x_j} + \frac{\partial u_j}{\partial x_i}\right) + \delta_{ij}\lambda\frac{\partial u_i}{\partial x_i} \tag{4–5}$$

where:

τ_{ij} = stress tensor

u_i = orthogonal velocities ($u_1 = v_x$, $u_2 = v_y$, $u_3 = v_z$)

μ = dynamic viscosity

λ = second coefficient of viscosity

The final term, the product of the second coefficient of viscosity and the divergence of the velocity, is zero for a constant density fluid and is considered small enough to neglect in a compressible fluid. Equation 4.5 transforms the momentum equations to the Navier-Stokes equations; however, these will still be referred to as the momentum equations elsewhere in this chapter. The momentum equations, without further assumptions regarding the properties, are as follows:

$$\frac{\partial(\rho V_x)}{\partial t}+\frac{\partial(\rho V_x V_x)}{\partial x}+\frac{\partial(\rho V_y V_x)}{\partial y}+\frac{\partial(\rho V_z V_x)}{\partial z}=\rho g_x-\frac{\partial P}{\partial x}+R_x+\frac{\partial}{\partial x}\left(\mu_e\frac{\partial V_x}{\partial x}\right)+\frac{\partial}{\partial y}\left(\mu_e\frac{\partial V_x}{\partial y}\right)+\frac{\partial}{\partial z}\left(\mu_e\frac{\partial V_x}{\partial z}\right)+T_x \quad (4\text{–}6)$$

$$\frac{\partial(\rho V_y)}{\partial t}+\frac{\partial(\rho V_x V_y)}{\partial x}+\frac{\partial(\rho V_y V_y)}{\partial y}+\frac{\partial(\rho V_z V_y)}{\partial z}=\rho g_y-\frac{\partial P}{\partial y}+R_y+\frac{\partial}{\partial x}\left(\mu_e\frac{\partial V_y}{\partial x}\right)+\frac{\partial}{\partial y}\left(\mu_e\frac{\partial V_y}{\partial y}\right)+\frac{\partial}{\partial z}\left(\mu_e\frac{\partial V_y}{\partial z}\right)+T_y \quad (4\text{–}7)$$

$$\frac{\partial(\rho V_z)}{\partial t}+\frac{\partial(\rho V_x V_z)}{\partial x}+\frac{\partial(\rho V_y V_z)}{\partial y}+\frac{\partial(\rho V_z V_z)}{\partial z}=\rho g_z-\frac{\partial P}{\partial z}+R_z+\frac{\partial}{\partial x}\left(\mu_e\frac{\partial V_z}{\partial x}\right)+\frac{\partial}{\partial y}\left(\mu_e\frac{\partial V_z}{\partial y}\right)+\frac{\partial}{\partial z}\left(\mu_e\frac{\partial V_z}{\partial z}\right)+T_z \quad (4\text{–}8)$$

where:

g_x, g_y, g_z = components of acceleration due to gravity

ρ = density

μ_e = effective viscosity

R_x, R_y, R_z = distributed resistances

T_x, T_y, T_z = viscous loss terms

For a laminar case, the effective viscosity is merely the dynamic viscosity, a fluid property. The effective viscosity for the turbulence model is described later in this section. The terms R_x, R_y R_z represent any source terms the user may wish to add. An example is distributed resistance, used to model the effect of some geometric feature without modeling its geometry. Examples of this include flow through screens and porous media.

The terms T_x, T_y T_z are viscous loss terms which are eliminated in the incompressible, constant property case. The order of the differentiation is reversed in each term, reducing the term to a derivative of the continuity equation, which is zero.

$$\frac{\partial}{\partial x}\left(\mu\frac{\partial V_x}{\partial x}\right)+\frac{\partial}{\partial y}\left(\mu\frac{\partial V_y}{\partial x}\right)+\frac{\partial}{\partial z}\left(\mu\frac{\partial V_z}{\partial x}\right)=T_x \qquad (4–9)$$

$$\frac{\partial}{\partial x}\left(\mu\frac{\partial V_x}{\partial y}\right)+\frac{\partial}{\partial y}\left(\mu\frac{\partial V_y}{\partial y}\right)+\frac{\partial}{\partial z}\left(\mu\frac{\partial V_z}{\partial y}\right)=T_y \qquad (4–10)$$

$$\frac{\partial}{\partial x}\left(\mu\frac{\partial V_x}{\partial z}\right)+\frac{\partial}{\partial y}\left(\mu\frac{\partial V_y}{\partial z}\right)+\frac{\partial}{\partial z}\left(\mu\frac{\partial V_z}{\partial z}\right)=T_z \qquad (4–11)$$

The conservation of energy can be expressed in terms of the stagnation (total) temperature, often useful in highly compressible flows, or the static temperature, appropriate for low speed incompressible analyses.

4.1.3. Compressible Energy Equation

The complete energy equation is solved in the compressible case with heat transfer In terms of the total (or stagnation) temperature, the energy equation is:

$$\frac{\partial}{\partial t}\left(\rho C_P T_o\right)+\frac{\partial}{\partial x}\left(\rho V_x C_p T_o\right)+\frac{\partial}{\partial y}\left(\rho V_y C_p T_o\right)+\frac{\partial}{\partial z}\left(\rho V_z C_p T_o\right)= \frac{\partial}{\partial x}\left(K\frac{\partial T_o}{\partial x}\right)+\frac{\partial}{\partial y}\left(K\frac{\partial T_o}{\partial y}\right)+\frac{\partial}{\partial z}\left(K\frac{\partial T_o}{\partial z}\right)+W^V+E^K+Q_V+\Phi+\frac{\partial P}{\partial t} \qquad (4–12)$$

where:

C_p = specific heat

T_o = total (or stagnation) temperature

K = thermal conductivity

W^v = viscous work term

Q_v = volumetric heat source

Φ = viscous heat generation term

E^k = kinetic energy

The static temperature is calculated from the total temperature from the kinetic energy:

$$T = T_o - \frac{v^2}{2c_p} \tag{4–13}$$

where:

T = static temperature

v = magnitude of the fluid velocity vector

The static and total temperatures for the non-fluid nodes will be the same.

The W^v, E^k and Φ terms are described next.

The viscous work term using tensor notation is:

$$W^V = u_i \mu \left(\frac{\partial}{\partial x} \right) \tag{4–14}$$

where the repetition of a subscript implies a summation over the three orthogonal directions.

The kinetic energy term is

$$W^V = u_i \mu \left(\frac{\partial}{\partial x_i} \frac{\partial u_j}{\partial x_i} + \frac{\partial}{\partial x_k} \frac{\partial u_k}{\partial x_j} \right) \tag{4–15}$$

Finally, the viscous dissipation term in tensor notation is

$$\phi = \mu \left(\frac{\partial u_i}{\partial x_k} + \frac{\partial u_k}{\partial x_i} \right) \frac{\partial u_i}{\partial x_k} \tag{4–16}$$

In the absence of heat transfer (i.e., the adiabatic compressible case), equation 4–13 is used to calculate the static temperature from the total temperature specified.

4.1.4. Incompressible Energy Equation

The energy equation for the incompressible case may be derived from the one for the compressible case by neglecting the viscous work (W^v), the pressure work, viscous dissipation (f), and the kinetic energy (E^k). As the kinetic energy is neglected, the static temperature (T) and the total temperature (T_o) are the same. The energy equation now takes the form of a thermal transport equation for the static temperature:

$$\frac{\partial}{\partial t}\left(\rho C_p T\right)+\frac{\partial}{\partial x}\left(\rho V_x C_p T\right)+\frac{\partial}{\partial y}\left(\rho V_y C_p T\right)+\frac{\partial}{\partial z}\left(\rho V_z C_p T\right)= \frac{\partial}{\partial x}\left(K\frac{\partial T}{\partial x}\right)+\frac{\partial}{\partial y}\left(K\frac{\partial T}{\partial y}\right)+\frac{\partial}{\partial z}\left(K\frac{\partial T}{\partial z}\right)+Q_V \quad (4–17)$$

4.1.5. Turbulence

If inertial effects are great enough with respect to viscous effects, the flow may be turbulent. The user is responsible for deciding whether or not the flow is turbulent . Turbulence means that the instantaneous velocity is fluctuating at every point in the flow field. The velocity is thus expressed in terms of a mean value and a fluctuating component:

$$V_x = \bar{V}_x + V_x^{\,r} \quad (4–18)$$

where:

$\overline{V_x}$ = mean component of velocity in x-direction

$V_x^{\,r}$ = fluctuating component of velocity in x-direction

If an expression such as this is used for the instantaneous velocity in the Navier-Stokes equations, the equations may then be time averaged, noting that the time average of the fluctuating component is zero, and the time average of the instantaneous value is the average value. The time interval for the integration is arbitrarily chosen as long enough for this to be true and short enough so that “real time” transient effects do not affect this integration.

$$\frac{1}{\delta t}\int_0^{\delta_t} V_x^{\,r}\,dt = 0;\ \frac{1}{\delta t}\int_0^{\delta_t} V_x\,dt = \bar{V}_x \quad (4–19)$$

After the substitution of Equation 4–18 into the momentum equations, the time averaging leads to additional terms. The velocities in the momentum equations are the averaged ones, and we drop the bar in the subsequent expression of the momentum equations, so that the absence of a bar now means the mean value. The extra terms are:

$$\sigma_x^{\,R} = -\frac{\partial}{\partial x}\left(\overline{\rho V_x^{\,r} V_x^{\,r}}\right)-\frac{\partial}{\partial y}\left(\overline{\rho V_x^{\,r} V_y^{\,r}}\right)-\frac{\partial}{\partial z}\left(\overline{\rho V_x^{\,r} V_z^{\,r}}\right) \quad (4–20)$$

$$\sigma_y{}^R = -\frac{\partial}{\partial x}\left(\overline{\rho V_y{}^r V_x{}^r}\right) - \frac{\partial}{\partial y}\left(\overline{\rho V_y{}^r V_y{}^r}\right) - \frac{\partial}{\partial z}\left(\overline{\rho V_y{}^r V_z{}^r}\right) \tag{4–21}$$

$$\sigma_z{}^R = -\frac{\partial}{\partial x}\left(\overline{\rho V_z{}^r V_x{}^r}\right) - \frac{\partial}{\partial y}\left(\overline{\rho V_z{}^r V_y{}^r}\right) - \frac{\partial}{\partial z}\left(\overline{\rho V_z{}^r V_z{}^r}\right) \tag{4–22}$$

where:

σ^R = Reynolds stress terms

In the eddy viscosity approach to turbulence modeling one puts these terms into the form of a viscous stress term with an unknown coefficient, the turbulent viscosity. For example:

$$-\overline{\rho V_x V_y} = \mu_t \frac{\partial V_x}{\partial y} \tag{4–23}$$

The main advantage of this strategy comes from the observation that the representation of σ^R is of exactly the same form as that of the diffusion terms in the original equations. The two terms can be combined if an effective viscosity is defined as the sum of the laminar viscosity and the turbulent viscosity:

$$\mu_e = \mu + \mu_t \tag{4–24}$$

The solution to the turbulence problem then revolves around the solution of the turbulent viscosity.

Note that neither the Reynolds stress nor turbulent heat flux terms contain a fluctuating density because of the application of Favre averaging to equation 4–20 to equation 4–22. Bilger(187) gives an excellent description of Favre averaging. Basically this technique weights each term by the mean density to create a Favre averaged value for variable φ which does not contain a fluctuating density:

$$\tilde{\phi} = \frac{\overline{\rho\phi}}{\overline{\rho}} \tag{4–25}$$

The tilde indicates the Favre averaged variable. For brevity, reference is made to Bilger [37]for further details.

There are eight turbulence models available in FLOTRAN . The model acronyms and names are as follows:

- Standard k-ε Model
- Zero Equation Model
- RNG - (Re-normalized Group Model)
- NKE - (New k-ε Model due to Shih)
- GIR - (Model due to Girimaji)
- SZL - (Shi, Zhu, Lumley Model)
- Standard k-ω Model
- SST - (Shear Stress Transport Model)

The simplest model is the Zero Equation Model, and the other five models are the two equation standard k-ε model and four extensions of it. The final two models are the Standard k-ω Model and SST model. In the Zero Equation Model, the turbulent viscosity is calculated as:

$$c = \rho L_s^{\,2} \sqrt{\Phi} \tag{4–26}$$

where:

μ_t = turbulent viscosity

Φ = viscous dissipation (Equation 4–16)

$$L_s = \begin{cases} L_x & if \;\; L_x > 0.0 \\ \min\begin{Bmatrix} 0.4L_n \\ 0.09L_c \end{Bmatrix} & if \;\; L_x \le 0.0 \end{cases}$$

L_x = length scale

L_n = shortest distance from the node to the closest wall

L_c = characteristic length scale

In the k-ε model and its extensions, the turbulent viscosity is calculated as a function of the turbulence parameters kinetic energy k and its dissipation rate ε using Equation 4–27. In the RNG and standard models, C_μ is constant, while it varies in the other models.

$$\mu_t = C_\mu \rho \frac{k^2}{\varepsilon} \tag{4–27}$$

where:

C_μ = turbulence constant

k = turbulent kinetic energy (input/output as ENKE)

ε = turbulent kinetic energy dissipation rate (input/output as ENDS)

In the k-ω model and SST model, the turbulent viscosity is calculated as:

$$\mu_t = \rho \frac{k}{\omega} \tag{4.28}$$

Here ω is defined as:

$$\omega = \frac{\varepsilon}{C_\mu k} \tag{4.29}$$

where:

ω = specific dissipation rate

The k-ε model and its extensions entail solving partial differential equations for turbulent kinetic energy and its dissipation rate whereas the k-ω and SST models entail solving partial differential equations for the turbulent kinetic energy and the specific dissipation rate. The equations below are for the standard k-ε model. The different calculations for the other k-ε models will be discussed in turn. The basic equations are as follows:

4.1.5.1. Standard k-ε Model

The reader is referred to Spalding and Launder (37) for details.

The Turbulent Kinetic Energy equation is:

$$\begin{aligned}\frac{\partial pk}{\partial t} + \frac{\partial (pV_x k)}{\partial x} + \frac{\partial (pV_y k)}{\partial y} + \frac{\partial (pV_z k)}{\partial z} = \frac{\partial}{\partial x}\left(\frac{\mu_t}{\sigma_k}\frac{\partial k}{\partial x}\right) + \frac{\partial}{\partial y}\left(\frac{\mu_t}{\sigma_k}\frac{\partial k}{\partial y}\right) + \frac{\partial}{\partial z}\left(\frac{\mu_t}{\sigma_k}\frac{\partial k}{\partial z}\right) \\ + \mu_t \Phi - \rho\varepsilon + \frac{C_4 \beta \mu_t}{\sigma_t}\left(g_x \frac{\partial T}{\partial x} + g_y \frac{\partial T}{\partial y} + g_z \frac{\partial T}{\partial z}\right)\end{aligned} \tag{4.30}$$

The Dissipation Rate equation is:

$$\frac{\partial p\varepsilon}{\partial t}+\frac{\partial\left(pV_x\varepsilon\right)}{\partial x}+\frac{\partial\left(pV_y\varepsilon\right)}{\partial y}+\frac{\partial\left(pV_z\varepsilon\right)}{\partial z}=\frac{\partial}{\partial x}\left(\frac{\mu_t}{\sigma_k}\frac{\partial\varepsilon}{\partial x}\right)+\frac{\partial}{\partial y}\left(\frac{\mu_t}{\sigma_k}\frac{\partial\varepsilon}{\partial y}\right)+\frac{\partial}{\partial z}\left(\frac{\mu_t}{\sigma_k}\frac{\partial\varepsilon}{\partial z}\right) \qquad (4.31)$$
$$+C_1\varepsilon\mu_t\frac{\varepsilon}{k}\Phi-C_2\rho\frac{\varepsilon^2}{k}+\frac{C_\mu\left(1-C_3\right)\beta\rho k}{\sigma_t}\left(g_x\frac{\partial T}{\partial x}+g_y\frac{\partial T}{\partial y}+g_z\frac{\partial T}{\partial z}\right)$$

The final term in each equation are terms used to model the effect of buoyancy and are described by Viollet(37). Default values for the various constants in the standard model are provided by Lauder and Spalding(37) and are given in

The solution to the turbulence equations is used to calculate the effective viscosity and the effective thermal conductivity:

$$\mu_e=\mu+C_\alpha\rho\frac{k^2}{\varepsilon} \qquad (4–32)$$

$$k_e=k+\frac{\mu_t C_p}{\sigma_t} \qquad (4–33)$$

where:

μ_e = effective viscosity

K_e = effective conductivity

σ_t = Turbulent Prandtl (Schmidt) Number

The four extensions to the standard k-ε model have changes in either the C_μ term or in the source term of the dissipation equation. The new functions utilize two invariants constructed from the symmetric deformation tensor S_{ij}, and the antisymmetric rotation tensor W_{ij}. These are based on the velocity components v_k in the flow field.

$$S_{ij}=\frac{1}{2}\left(V_{i,j}+V_{j,i}\right) \qquad (4–34)$$

$$W_{ij}=\frac{1}{2}\left(V_{i,j}-V_{j,i}\right)+C_r\Omega_m\varepsilon_{mij} \qquad (4–35)$$

where:

C_r = constant depending on turbulence model used

Ω_m = angular velocity of the coordinate system

ε_{mij} = alternating tensor operator

The invariants are:

$$\eta = \frac{k}{\varepsilon}\sqrt{2S_{ij}S_{ij}} \tag{4–36}$$

and

$$\xi = \frac{k}{\varepsilon}\sqrt{2\,W_{ij}W_{ij}} \tag{4–37}$$

4.1.5.2. RNG Turbulence Model

In the RNG model, the constant $C_{1\varepsilon}$ in the dissipation Equation 4–31, is replaced by a function of one of the invariants.

$$C_{1\varepsilon} = 1.42 - \frac{\eta\left(1-\frac{\eta}{\eta_\alpha}\right)}{1+\beta\eta^3} \tag{4–38}$$

In the RNG model a constant C_μ is used. The value is specified with a separate command than the one used to specify the C_μ in the standard model. The same is true of the constant C_2. As shown in the above table, the diffusion multipliers have different values than the default model, and these parameters also have their own commands for the RNG model. The value of the rotational constant C_r in the RNG model is 0.0. Quantities in Equation 4–31 not specified .

4.1.5.3. NKE Turbulence Model

The NKE Turbulence model uses both a variable C_μ term and a new dissipation source term. The C_μ function used by the NKE model is a function of the invariants.

(4–39)

The production term for dissipation takes on a different form. From equation 4.31, the production term for the standard model is:

$$C_{1\varepsilon}\mu_t \frac{\varepsilon}{k}\Phi \tag{4–40}$$

The NKE model replaces this with:

$$\rho\, C_{1\varepsilon}\sqrt{2\, S_{ij}S_{ij}}\varepsilon \tag{4–41}$$

The constant in the dissipation rate Equation 4–31 is modified in the NKE model to be:

$$C_{1\varepsilon} = \max\left(C_{1M}\frac{\eta}{\eta+5}\right) \tag{4–42}$$

The constant C_2 in the dissipation Equation 4–31 of the NKE model has a different value than that for the corresponding term in the standard model. Also, the values for the diffusion multipliers are different. Commands are provided for these variables to distinguish them from the standard model parameters. So for the NKE model, the input parameters are as follows:

The value of the rotational constant C_r in the NKE model is 3.0. All parameters in Equation 4–30 and Equation4–31 not covered by this table are covered in Table 4.1: "Standard Model Coefficients"

4.1.5.4. GIR Turbulence Model

The Girimaji model relies on a complex function for the calculation of the C_μ coefficient. The coefficients in Table 4.4: "GIR Turbulence Model Coefficients" are used.

These input values are used in a series of calculations as follows First of all, the coefficients L_1^0 to L_4 have to be determined from the input coefficients. Note, these coefficients are also needed for the coefficients of the nonlinear terms of this model, which will be discussed later.

$$\begin{aligned} L_1^0 &= \frac{C_1^0}{2} - 1 \quad : L_1^1 = C_1^1 + 1 \qquad ; L_2 = \frac{C_2}{2} - \frac{2}{3} \\ L_3 &= \frac{C_3}{2} - 1 \quad ; L_4 = \frac{C_4}{2} - 1 \end{aligned} \tag{4–43}$$

Secondly, the following coefficients have to be calculated:

$$
\begin{aligned}
p &= \frac{-2L_1^0}{\frac{1}{2}\eta^2 L_1^1} \qquad ;r = \frac{L_1^0 L_2}{\left(\frac{1}{2}\eta^2 L_1^1\right)^2} \\
\Theta &= arc\cos\frac{-b/2}{\sqrt{-a^3/27}} \\
q &= \frac{1}{\left(\frac{1}{2}\eta^2 L_1^1\right)^2}\left[\left(L_1^0\right)^2 + \frac{1}{2}\eta^2 L_1^1 L_2 - \frac{1}{3}\eta^2\left(L_3\right)^2 + \zeta^2\left(L_4\right)^2\right] \\
C_1 &= q - \frac{p^2}{3} \quad ;b = \frac{1}{27}\left(2p^3 - 9pq + 27r\right) \quad ;D = \frac{b^2}{4} + \frac{a^3}{27}
\end{aligned}
\tag{4–44}
$$

With these coefficients we can now determine the coefficient C_μ from the following set of equations:

$$
C_\mu = \begin{cases}
L_1^0 L_2 \Big/ \left[\left(L_1^0\right)^2 - -\frac{1}{3}\eta^2\left(L_3\right)^2 + \zeta^2\left(L_4\right)^2\right] & if\ L_1^1 = 0\ \ or\ \eta = 0 \\
-\frac{p}{3} + \left(-\frac{b}{2} + \sqrt{D}\right)^{1/3} + \left(-\frac{b}{2} + \sqrt{D}\right)^{1/3} & if\ D > 0 \\
-\frac{p}{3} + 2\sqrt{\frac{-a}{3}}\cos\left(\frac{\theta}{3}\right) & if\ D < 0, b < 0 \\
-\frac{p}{3} + 2\sqrt{\frac{-a}{3}}\cos\left(\frac{\theta}{3} + \frac{2}{3}\pi\right) & if\ D < 0, b < 0
\end{cases}
\tag{4–45}
$$

and for the GIR model, the rotational term constant C_r is

$$
C_r = \frac{C_4 - 4}{C_4 - 2} \tag{4–46}
$$

4.1.5.5. SZL Turbulence Model

The Shi-Zhu-Lemley turbulence model uses a simple expression for the C_μ coefficient and uses the standard dissipation source terms. The user controls three constants in the calculation of the coefficients:

$$
C_\mu = \frac{A_{s1}}{A_{s2} + \eta + A_{s3}\zeta} \tag{4–47}
$$

The constants and their defaults are as follows:

The value of the rotational constant C_r for the SZL model is 4.0.

4.1.5.6. Standard k-ω Model

The k-ω model solves for the turbulent kinetic energy k and the specific dissipation rate ω (Wilcox(37). As in the k-ε based turbulence models, the quantity k represents the exact kinetic energy of turbulence. The other quantity ω represents the ratio of the turbulent dissipation rate ε to the turbulent kinetic energy k, i.e., is the rate of dissipation of turbulence per unit energy..

The turbulent kinetic energy equation is:

$$\frac{\partial pk}{\partial t}+\frac{\partial (pV_x k)}{\partial x}+\frac{\partial (pV_y k)}{\partial y}+\frac{\partial (pV_z k)}{\partial z}=\frac{\partial}{\partial x}\left[\left(\mu+\frac{\mu_t}{\sigma_k}\right)\frac{\partial k}{\partial x}\right]+\frac{\partial}{\partial y}\left[\left(\mu+\frac{\mu_t}{\sigma_k}\right)\frac{\partial k}{\partial y}\right]+\frac{\partial}{\partial z}\left[\left(\mu+\frac{\mu_t}{\sigma_k}\right)\frac{\partial k}{\partial z}\right] + \mu_t\Phi - C_\mu \rho k\omega^2 + \frac{C_4\beta\mu_t}{\sigma_k}\left(g_x\frac{\partial T}{\partial x}+g_y\frac{\partial T}{\partial y}+g_z\frac{\partial T}{\partial z}\right) \quad (4\text{–}48)$$

The specific dissipation rate equation is:

$$\frac{\partial p\omega}{\partial t}+\frac{\partial V_x\omega}{\partial x}+\frac{\partial V_y\omega}{\partial y}+\frac{\partial V_z\omega}{\partial z}=\frac{\partial}{\partial x}\left[\left(\mu+\frac{\mu_t}{\sigma_\omega}\right)\frac{\partial \omega}{\partial x}\right]+\frac{\partial}{\partial y}\left[\left(\mu+\frac{\mu_t}{\sigma_\omega}\right)\frac{\partial \omega}{\partial y}\right]+\frac{\partial}{\partial z}\left[\left(\mu+\frac{\mu_t}{\sigma_\omega}\right)\frac{\partial \omega}{\partial z}\right] + \gamma\rho\Phi - \beta'\rho\omega^2 + \frac{(1-C_3)\beta\rho}{\sigma_t}\left(g_x\frac{\partial T}{\partial x}+g_y\frac{\partial T}{\partial y}+g_z\frac{\partial T}{\partial z}\right) \quad (4\text{–}49)$$

The final term in Equation 4–48 and Equation 4–49 is derived from the standard k-ε model to model the effect of buoyancy. Default values for the model constants in the k-ω model are provided by Wilcox(349). Some values are the same with the standard k-ε model and are thus given in Table 4.1: "Standard Model Coefficients", whereas the other values are given in Table 46: "The k-ω Model Coefficients".

The k-ω model has the advantage near the walls to predict the turbulence length scale accurately in the presence of adverse pressure gradient, but it suffers from strong sensitivity to the free-stream turbulence levels. Its deficiency away from the walls can be overcome by switching to the k-ε model away from the walls with the use of the SST model.

4.1.5.7. SST Turbulence Model

The SST turbulence model combines advantages of both the standard k-ε model and the k-ω model. As compared to the turbulence equations in the k-ω model, the SST model first modifies the turbulence production term in the turbulent kinetic energy equation. From Equation 4.48, the production term from the k-ω model is:

$$P_t = \mu_t \Phi \tag{4–50}$$

The SST model replaces it with:

$$P_t = \min\left(\mu_t \Phi \, , C_{lmt} \varepsilon\right) \tag{4–51}$$

By default, the limiting value of C_{lmt} is set to 10^{15}, so Equation 4–51 is essentially the same with Equation 4–50. However, Equation 4–51 allows the SST model to eliminate the excessive build-up of turbulence in stagnation regions for some flow problems with the use of a moderate value of C_{lmt}. Further, the SST model adds a new dissipation source term in the specific dissipation rate equation:

$$\frac{(1-F_1)2\rho\sigma_{\omega 2}}{\omega}\left[\frac{\partial k}{\partial x}\frac{\partial \omega}{\partial x}+\frac{\partial k}{\partial y}\frac{\partial \omega}{\partial y}+\frac{\partial k}{\partial z}\frac{\partial \omega}{\partial z}\right] \tag{4–52}$$

Here, F_1 is a blending function that is one near the wall surface and zero far away from the wall. The expression of the bending function F_1 is given by Menter(350), and with the help of F_1, the SST model automatically switches to the k-ω model in the near region and the k-ε model away from the walls. The model coefficients are all calculated as functions of F_1:

$$\varphi = F_1\varphi_1 + (1-F_1)\varphi_2 \tag{7–53}$$

Here, φ stands for the model coefficient (σ_k, σ_ω, β', γ) of the SST model, and φ_1 and φ_2 stand for the model coefficient of the k-ω model and the k-ε model respectively. Default values for the various constants in the SST model are provided by Menter(350), and are given in Table 4.7: "The SST Model Coefficients".

4.1.5.8. Near-Wall Treatment

All of the above turbulence models except the Zero Equation Model use the near-wall treatment discussed here. The near-wall treatment for the k-ω model and SST model are

slightly different from the following discussions. Refer to Wilcox (349) and Menter (350) for differences for those two models.

The k-ε models are not valid immediately adjacent to the walls. A wall turbulence model is used for the wall elements. Given the current value of the velocity parallel to the wall at a certain distance from the wall, an approximate iterative solution is obtained for the wall shear stress. The equation is known as the "Log-Law of the Wall" and is discussed in White (37) and Launder and Spalding(37).

$$\frac{V_{\tan}}{\sqrt{\frac{\tau}{\rho}}} = \frac{1}{\kappa}\left(\ln\frac{E\delta}{\nu}\sqrt{\frac{\tau}{\rho}}\right) \tag{4–54}$$

where:

$v_{\tan}$ = velocity parallel to the wall

τ = shear stress

ν = kinematic viscosity (m/r)

κ = slope parameter of law of the wall

E = law of the wall constant

δ = distance from the wall

The default values of κ and E are 0.4 and 9.0 respectively, the latter corresponding to a smooth wall condition.From the shear stress comes the calculation of a viscosity:

$$\mu_{\varpi} = \delta\frac{\tau}{V_{\tan}} \tag{4–55}$$

The wall element viscosity value is the larger of the laminar viscosity and that calculated from Equation 4–55.

Near wall values of the turbulent kinetic energy are obtained from the k-ε model. The near wall value of the dissipation rate is dominated by the length scale and is given by Equation 4–56.

$$\varepsilon_{nW} = \frac{C_{\mu}^{(0.75)} k_{nW}^{(1.5)}}{\kappa \delta} \tag{4–56}$$

where:

ε_{nw} = near wall dissipation rate

k_{nw} = near wall kinetic energy

The user may elect to use an alternative wall formulation (accessed with the FLDATA24,TURB,WALL,EQLB command) directly based on the equality of turbulence production and dissipation. This condition leads to the following expression for the wall parameter y+

$$y^{+} = \frac{C_{\mu}^{1/4} \rho \kappa_{nW}^{1/2} \delta}{\mu} \tag{4–57}$$

The wall element effective viscosity and thermal conductivity are then based directly on the value of y+. The laminar sublayer extends to y_t^+ (input on the FLDATA24,TURB,TRAN command) with the default being 11.5.

For y+ < y_t^+

$$\begin{aligned} \mu_{eff} &= \mu \\ k_{eff} &= k \end{aligned} \tag{4–58}$$

For y+ ≥ y_t^+ :

$$\mu_{eff} = \frac{\mu y^{+}}{\frac{1}{\kappa} \ln\left(E y^{+}\right)} \tag{4–59}$$

$$k_{eff} = \frac{C_p}{\sigma_t} \frac{\mu y^{+}}{\left(\frac{1}{\kappa} \ln E y^{+} + P_{fn}\right)} \tag{4–60}$$

where:

n = natural logarithm

$$P_{fn} = \frac{(\pi/4)}{\sin(\pi/4)}\left(\frac{A}{\kappa}\right)^{1/2}\left(\frac{\mathrm{Pr}}{\sigma_t}-1\right)/\left(\frac{\mathrm{Pr}}{\sigma_t}\right)^{1/4}$$

Pr = Prandtl number

Although the wall treatment should not affect the laminar solution, the shear stress calculation is part of the wall algorithm. Thus, shear stresses from the equilibrium model will differ slightly from those obtained from the default treatment, as described in Equation 4–54 thru equation 4.56.

4.1.6. Pressure

For numerical accuracy reasons, the algorithm solves for a relative pressure rather than an absolute pressure. Considering the possibility that the equations are solved in a rotating coordinate system, the defining expression for the relative pressure is:

$$P_{abs} = P_{ref} + P_{rel} - \rho_0\{g\}\cdot\{r\} + \frac{1}{2}\rho_0(\{\omega\}\times\{\omega\}\times\{r\})\cdot\{r\} \qquad (4\text{–}61)$$

where:

ρ_o = reference density (calculated from the equation of state defined by the property type using the nominal temperature

P_{ref} = reference pressure

$\{g\}$ = acceleration vector due to gravity

P_{abs} = absolute pressure

P_{rel} = relative pressure

$\{r\}$ = position vector of the fluid particle with respect to the rotating coordinate system

$\{\omega\}$ = constant angular velocity vector of the coordinate system

Combining the momentum equations (equation 4.6 through equation 4.8) into vector form and again considering a rotating coordinate system, the result is:

$$\rho\frac{D\{V\}}{Dt} + 2\rho\{\omega\}\times\{V\} + \rho\{\omega\}\times\{\omega\}\times\{r\} = \rho\{g\} - \nabla P_{abs} + \mu\nabla^2\{V\} \qquad (4\text{–}62)$$

where:

$\{V\}$ = vector velocity in the rotating coordinate system

μ = fluid viscosity (assumed constant for simplicity)

ρ = fluid density

In the absence of rotation, $\{V\}$ is simply the velocity vector in the global coordinate system. The negative of the gradient of the absolute pressure is:

$$-\nabla P_{abs} = -\nabla P_{rel} - \rho_0 \{g\} \cdot \{r\} + \rho_0 \{\omega\} \times \{\omega\} \times \{r\} \quad (4\text{–}63)$$

Inserting this expression into the vector form of the momentum equation puts it in terms of the relative pressure and the density differences.

$$\rho \frac{D\{V\}}{Dt} + 2\rho\{\omega\} \times \{V\} + (\rho - \rho_0)\{\omega\} \times \{\omega\} \times \{r\} = (\rho - \rho_0)\{g\} - \nabla P_{rel} + \mu \nabla^2 \{V\} \quad (4\text{–}64)$$

This form has the desirable feature (from a numerical precision standpoint) of expressing the forcing function due to gravity and the centrifugal acceleration in terms of density differences. For convenience, the relative pressure output is that measured in the stationary global coordinate system. That is, the rotational terms are subtracted from the pressure calculated by the algorithm. Conversely, the total pressure is output in terms of the rotating coordinate system frame. This is done for the convenience of those working in turbomachinery applications.

Chapter 5

Results and Discussion

Investigation of parallel hub annular diffuser has been carried out with help of FLOTRAN of ANSYS 9.0, a CFD tool with varying area ratio and divergence angle. Analysis gives the effect of area ratio and divergence angle on pressure recovery coefficient, boundary layer effect, reverse flow in diverging part of diffuser and static pressure on hub and casing wall.

5.1 Inlet Flow Conditions

Inlet flow conditions are necessary factor for obtaining the performance of a diffuser. In addition to the importance of the boundary layer at inlet as an influence on the subsequent diffusion process, the pressure measurement obtained at this station are used in the determination of the overall diffuser performance coefficient. The boundary layer ,similar to fully developed pipe flow , filled the entire annulus, and the use of flow controls had no effect on the velocity profile had no effect on the inlet conditions for the range tested. For axial flow the velocity profile are nearly symmetrical about the annulus center line.

5.2 Velocity Distribution

Figures from .2 to 17shows the velocity and pressure distribution along the annular diffuser length. Figure no 12 shows the various type of velocity vector presentation of air flow for AR = 5 and divergence angle 20deg, similar vector diagram for other are plotted.

We can observe from graphs the reverse flow occurs at exit near the casing wall, he turbulence and reverse flow area increases with increasing divergence angle. We can observe from these graphs at inlet the velocity distribution is symmetrical and flow is stick with annular hub and casing wall

For the lower divergence angle as divergence increases the separation length at casing increases it tend to approach to inlet, as it progress in the diverging part near casing wall

of diffuser shown in figures by blue colour, it is more prone to separation and this is the part where reverse flow occurs ,this can be noticed in vector diagrams of velocity.

In figure 12 we observed that maximum velocity is higher than inlet velocity in diffusers some part, because due to increased boundary layer effect at exit and reverse flow a wedge section created between hub and casing where the air flows with higher velocity than inlet this condition is not present for lower divergence angles. This phenomenon is similar for other diffuser configurations and this limits the diffuser length.

Velocity in x direction is higher near the hub wall than the casing wall and boundary layer effects is less. Velocity at outlet of diffuser is more unstable at higher divergence angles and short length. For higher divergence angle (more than 10deg.) don't give good pressure recovery without controlling the fluid flow. For short and higher divergence angle annular diffuser the outlet flow should be stable by any means to get the pressure recovery.

In longer diffusers or low area ratio flow remains stable through the diffuser.

5.3 Static Pressure

Static pressure near hub wall is lower than the casing wall. At the hub the velocity is higher than casing that is one of the reasons to this phenomenon. Reverse flow near casing wall cause the whirling flow and eddies generation that reduce the increases the static pressure. Various graphs of static pressure is plotted from figure 2 to17 and 18 to 72 for different area ratio and divergence angle.

For the lower Reynolds number the lower static pressure is higher than for higher Reynolds numbers. Pressure at tip at inlet is low as flow precede it changes sharply than hub wall pressure. At low Mach number the difference between hub and tip wall pressure is low as Reynolds number increases the difference increase due to increase of irreversibility's at tip wall. In color map of pressure attached in appendix we see the pressure increase is smooth for long diffusers and it becomes more unstable and varying as the diffuser length decreases. From the static pressure charts from fig no .18 to 72 observed that changes in pressure at entrance section is more sharply than the rear diffusion section of diffuser. Static pressure is not changes in annular height for long and

low divergence angle diffusers ,bur for short diffusers it changes with annular height at inlet of diffusers.

5.4 Static Pressure Recovery Coefficient

Pressure recovery graphs are plotted (figure no. 18 to 72) with the non dimension length (X/L) for various annular diffusers geometries. It is observed that the pressure recovery coefficient is not vary significantly with velocity the range for tested. As the velocity at inlet increases the pressure recovery coefficient suppose to increase but it does not change significantly due to increase in the irreversibility's, namely reverse flow ,back flow at exit near casing wall ,whirl, in diffusion section. From the pressure recovery charts it observed that the shape of the pressure recovery charts are similar to the pressure charts at hub and tip. Pressure recovery chart characteristics are similar to the pressure charts. Pressure recovery coefficient is high for long and stable flow in diffusers

For higher recovery it is necessary to stabilize the flow in diffusion section , without stabilizing the flow FLOTRAN does not give the authentic results.

5.5 Mach number

Analysis carried out for low subsonic range, the effect of Mach number is negligible for this range on pressure recovery coefficient and pressure recovery. Present analysis mach number vary from 0.14 to 0.46, for same area ratio there is no significant changes with varying Mach number. All these shown in figure attached in appendix. Mach number charts are plotted (fig. 73 to 75) these show the different mach numbers for different combination of angle and area ratio. From figures we can see that as Mach number increases it boundary layer at tip wall thicken and a steeper graph obtained. Boundary layer near the hub wall is thinner than tip wall Mach number increase sharply near hub wall then decrease drastically towards the tip wall.

At higher angles FLOTRAN does not give the results for low dense meshing and we can not get solution until flow would not stabilize at exit and inlet. So to get solution flow at exit must stabilize by putting some controlling method like flow development length at exit.

Chapter 6

Conclusion and Future Scope

Analysis presented here have the conclusion are

1. Flow remains stable in entry of annular diffuser but later it separates after divergence angle 5 deg and more. As divergence angle increases the turbulence at exit of diffuser increase at vary high rate.
2. Flow should be fully develop and stable for good pressure recovery so if flow is not stable use the flow stabilizing means to stable it.
3. Pressure recovery coefficient increase with the diffuser length and for lower diverging angles and lower area ratio it is low as compared to lower diverging angle and higher area ratio.
4. Static pressure at casing wall is higher than hub wall; boundary layer effect is more significant at casing wall and increases with increase in divergence. As the outer area increases the kinetic energy dissipation increase and tend to unstable the flow at outlet. Turbulence increases with the decrease of effective length of diffuser and this is deciding the diffuser minimum length for the required pressure recovery.
5. For the get good results with FLOTRAN user must know the flow conditions and regime. User must know the behavior of flow an according to that needs to define the appropriate coefficients and iteration to solve the problem. The regions of high irreversibility's needs fine mesh for good results.
6. At the low range of Mach number (up to the 0.6)does not affect the pressure recovery.

6.1 Future Scope

The search for consistent behavioral patterns has revealed weaknesses both in the data and in the opportunity to conduct meaningful additional investigations. For the first approximation, geometry has been reasonably modeled with the *Cpi* and the η(*AR)* relationships. However, it is almost certain that additional tests with further geometric variations (and for annular diffusers a very wide range of geometric combinations is possible) would afford more precise correlations. Nonetheless, this is not a major area needing further investigation. The dual trend characteristics for both the swirl angle dependence and the inlet aerodynamic blockage dependence point to a clear need for further investigation. Systematic tests are needed with a variety of diffusers to determine which parameters control the development with stall within the annular diffuser

The development of stall would depend not only on geometric variables, but on a variety of different inlet profile parameters. Inlet velocity profiles constitute the area of greatest need for further investigation

Most of these problems can be resolved by using computational fluid dynamics (CFD). CFD can certainly be used today to conduct 'what if' studies of different possible inlet profile parameters and different geometric variations. It should not, however, be considered a definitive tool at the present time

Several fundamental problems keep CFD from being used as the definitive tool; these include serious problems in the basic turbulence model plus problems in discretization, artificial viscosity or damping, and effective grid generation.

REFERENCES

1. Ackert ,J. 1967. Aspect Of Internal Flow. Fluid Mechanics Of Internal Flow ,Ed. Sovaran G., Elsvier Amsterdum,pp1.
2. Adkins R.C ,Jacobsen OH , Chevealier P 1983 A Premilary Study of Annular Diffuser With Constant Diameter Outer Wall. ASME paper no. 83-GT-218
3. Adkins R.C.,1983. A simple Method For Design Optimum Annular Diffusers. ASME Paper No. 83-GT-42.
4. Awai T., Nakagawa T., Sakai T,1986. Study of Axially Curved Mixed Flow Vane less Diffuser .Bull JSME 29, 1759-1764.
5. Cockrell, D.J., Markland, E., 1963 .A Review of Incompressible Diffuser Flow. Aircraft Engg. Volume 35 , pp 286.
6. Coladipietro, R., Schneider, J.M., Sridhar, K.1974. “Effects of Inlet Flow Conditions on the Performance of Equiangular Annular Diffusers,” Trans. CSME 3 (2): pp. 75-82.
7. Dovzhik, S.A., Kartavenko, V.M.,1975. “Measurement of the Effect of Flow Swirl on the Efficiency of Annular Ducts and exhaust Nozzles of Axial Turbomachines,” Fluid Mechanics/Soviet Research 4(4): 156-172.
8. Goebel, J. H., Japikse, D., “The Performance of an Annular Diffuser Subject to Various Inlet Blockage and Rotor Discharge Effects,” Consortium Final Report, Creare TN-325, March 1981.
9. Hesterman R, Kim S ,Ban Khalid A, Wittigs 1995. Flow Field And Performances Characteristics Of Combustor Diffusers: A Basic Study. Trans. ASME Journal Engineering for Gaas Turbine and Power 117: pp 686-694.
10. Hoadley D,1970. Three Dimensional Turbulent Boundary Layers in an Annular Diffuser. PhD Thesis University of Canbrige.
11. Hoadley, D., Hughes, D.W.,1969. “Swirling Flow in an Annular Diffuser,” University of Cambridge, Department of Engineering, Report CUED/A-Turbo/TR5.

12. Howard, J. H. G., Thorton –Trump A. B., Henseler H. J. 1967" Performance And Flow Regime For Annular Diffusers".ASME paper no . 67-WA/FE-21.
13. Ishkawa K,Nakamura I 1989"An Experimental Study on The Performance of Mixed Flow Type Conical Wall Annular Diffuser " ASME FED-69.
14. Japikse, D., 1986. "A New Diffuser Mapping Technique – Studies in Component Performance: Part 1," ASME Paper No. 84-GT-237, Amsterdam, June 1984; also, Journal of Fluids Engineering, Vol. 108, No. 2. pp. 148-156.
15. Japikse, D., and Pampreen, R., "Annular Diffuser Performance for an Automotive Gas Turbine," ASME Publication 78-GT-147. 1978.
16. Japikse, D.,1980. "The Influence of Inlet Turbulence on Diffuser Performance," Concepts ETI, Inc., Design Data Sheet No. 1, .
17. Japikse, D.,2000. "Performance of Annular Diffusers Subject to Inlet Flow Field Variations and Exit Distortion," presented at the ISROMAC conference in Honolulu, Hawaii, March 26-30,.
18. Johanston I.H.,1959. Effect Of Inlet Conditions On The Flow In Annular Diffusers. National Gas Turbine Establishment Memo No.167,Cp No.178
19. Jonston J P 1959 "Summary of Results of Test on Short Conical Diffuser With Flow Control Inserts: as of June 1,1959.Ingersoll – Rand TN no 71.
20. Juhasz,A.J. 1974. Performance Of An Asymmetric Annular Diffuser With Non Diverging Inner Wall Using Sution .NASA TN -7575.
21. kamonicek V, Hibs M,1974.Results Of Experimental And Theoretical Investigation Of Annular Diffuser. CSIRO,Division of Mechanical Engg.
22. Klein, A., 1995. Characteristics of Combustor Diffusers. Prog .Aerospace Sci. 31: 171-271
23. Moller E.S,1965. Radial Diffuser Using Incompressible Flow Between Disks. ASME paper no. 65-FE-12.
24. Moller E.S.,1965.Radial Flow Without Swirl Between Parallel Disks Havimg Both Supersonic And Subsonic Resions .ASME paper no. 65-FE-11.
25. Shaalan, M.R.A., Shabaka, I.M.M.,1975. "An Experimental Investigation of the Swirling Flow Performance of an Annular Diffuser at Low Speed," ASME Paper No. 75-WA/FE-17.

26. Sharan V K, 1972.Diffuser Performance Co-Relations. JASI, Volume 24,pp415.
27. Sovran, G., Klomp, E.D.,1967. “Experimentally Determined Optimum Geometries for Rectilinear Diffusers with Rectangular, Conical or Annular Cross-Section,” Fluid Dynamics of Internal Flow, Elsevier Publishing Company.
28. Srinath T 1968 “ An Investigation of The Effects of Swirl on The Flow Regimes and Performance of Annular Diffuser With Equal Inner and Outer Cone Angles .” M.A. Science Thesis , University of Waterloo Canada
29. Stafford ,W . Willber, Jams T. Higginbothom, 1955. Investigation of Two Short Annular Diffuser Configurations Utilizing Suction and Injection as Means of Boundary Layer Control. NACA RM L54K18.
30. Stafford W.Willbur, James T.H.1957. Investigation Of Short Annular Diffuser Configuration Utilizing Suction As A Means Of Boundary Layer Control. NACA TN-3996
31. Stevan S. J., Williams G.J., 1980. The Influence of Inlet Conditions on The Performance of Annular Diffuser . Trans. ASME Journal Fluids Engg. 102,357-363.
32. Steven S.J.,Williams G.J.,1969. Performance Of Annular Diffusers. Gas Turbine Collaboration Committee Report No. 299.
33. Stevens S.J., Fry P.,1973 . Measurements of The Boundary Layer Growth in Annular Diffusers . Journal Aircraft Feb., pp 73-89.
34. Takehira, A., et al.,”An Experimental Study of the Annular Diffusers in Axial-Flow Compressors and Turbines,” Japan Society of Mechanical Engineers, Paper No.39, 1977.
35. Thayer E B 1971”Evaluationof Curved Wall Annular Diffuser “ ASME paper no .71-WA/FE-35
36. Wood, C .C., Henary, J.R., 1958. Effects of Shock Boundary Layer Interaction on The Long and Short Subsonic Annular Diffuser .NACA RM L58A31.
37. ANSYS 9.0 FLOTRAN user guide.

Table 2 Geometric Parameters For Tested Annular Diffuser

AR	D_o	L_5	L_{10}	L_{15}	L_{20}	L_{25}
2	**198**	**277**	**137**	**90**	**63**	**26**
3	**240**	**498**	**247**	**163**	**120**	**80**
4	**270**	**690**	**342**	**225**	**165**	**129**
5	**300**	**857**	**425**	**280**	**206**	**161**
6	**326**	**1011**	**502**	**330**	**243**	**190**

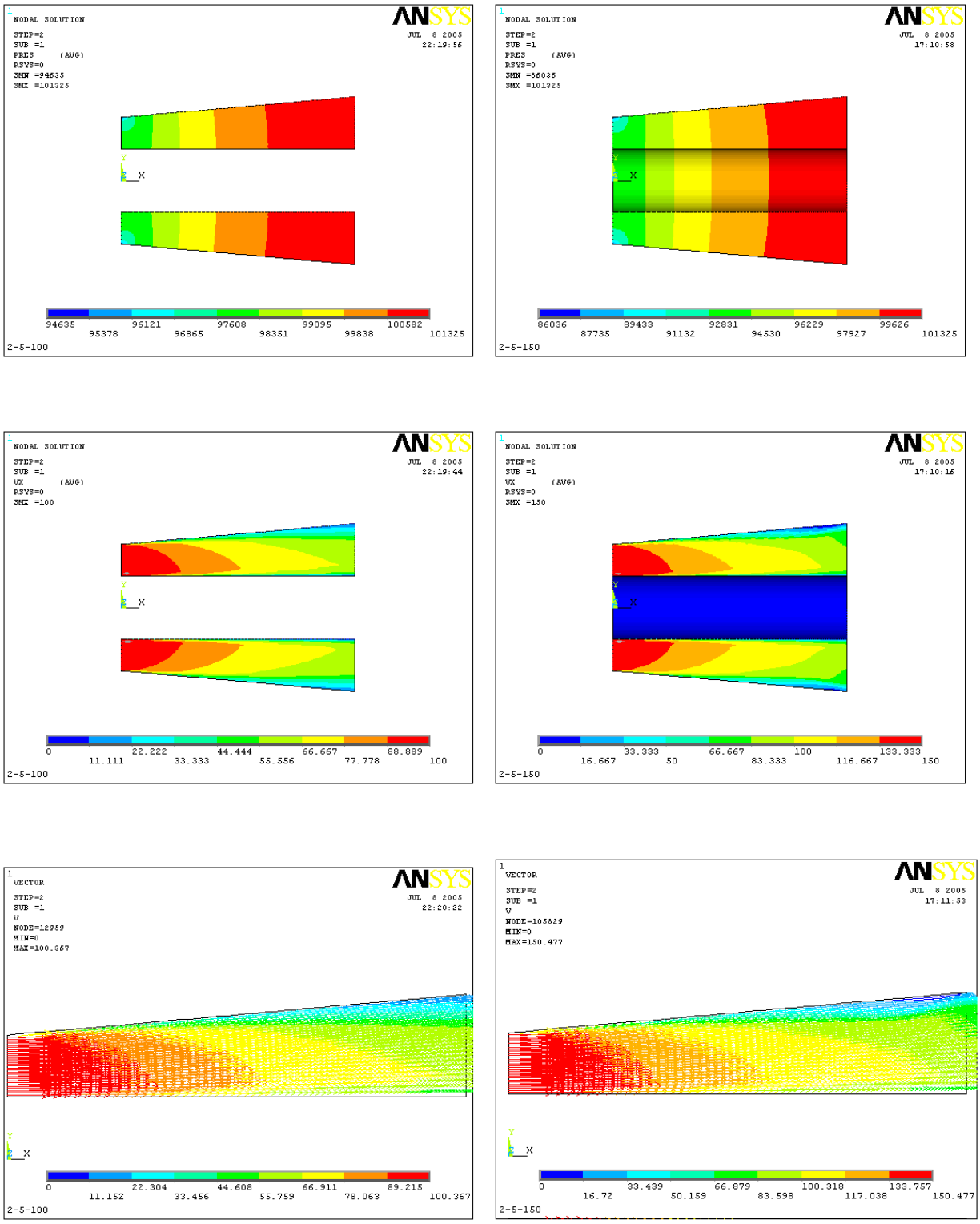

Fig 2 Diffuser AR = 2; α = 5 deg.; Re= 5.15×10^5 -7.7×10^5

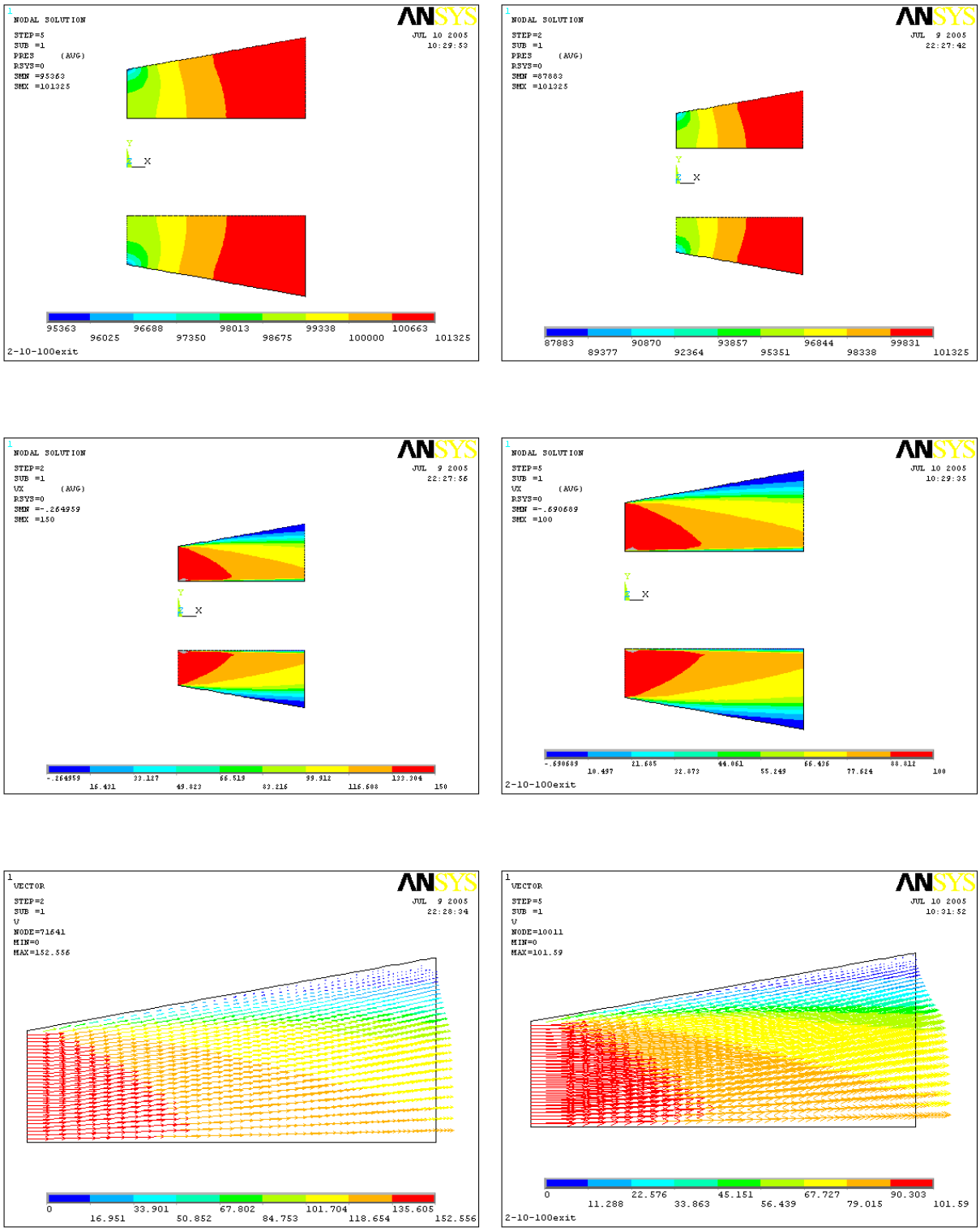

Fig 3 Diffuser AR = 2; α = 10 deg.; Re= 5.15×10^5 -7.7×10^5

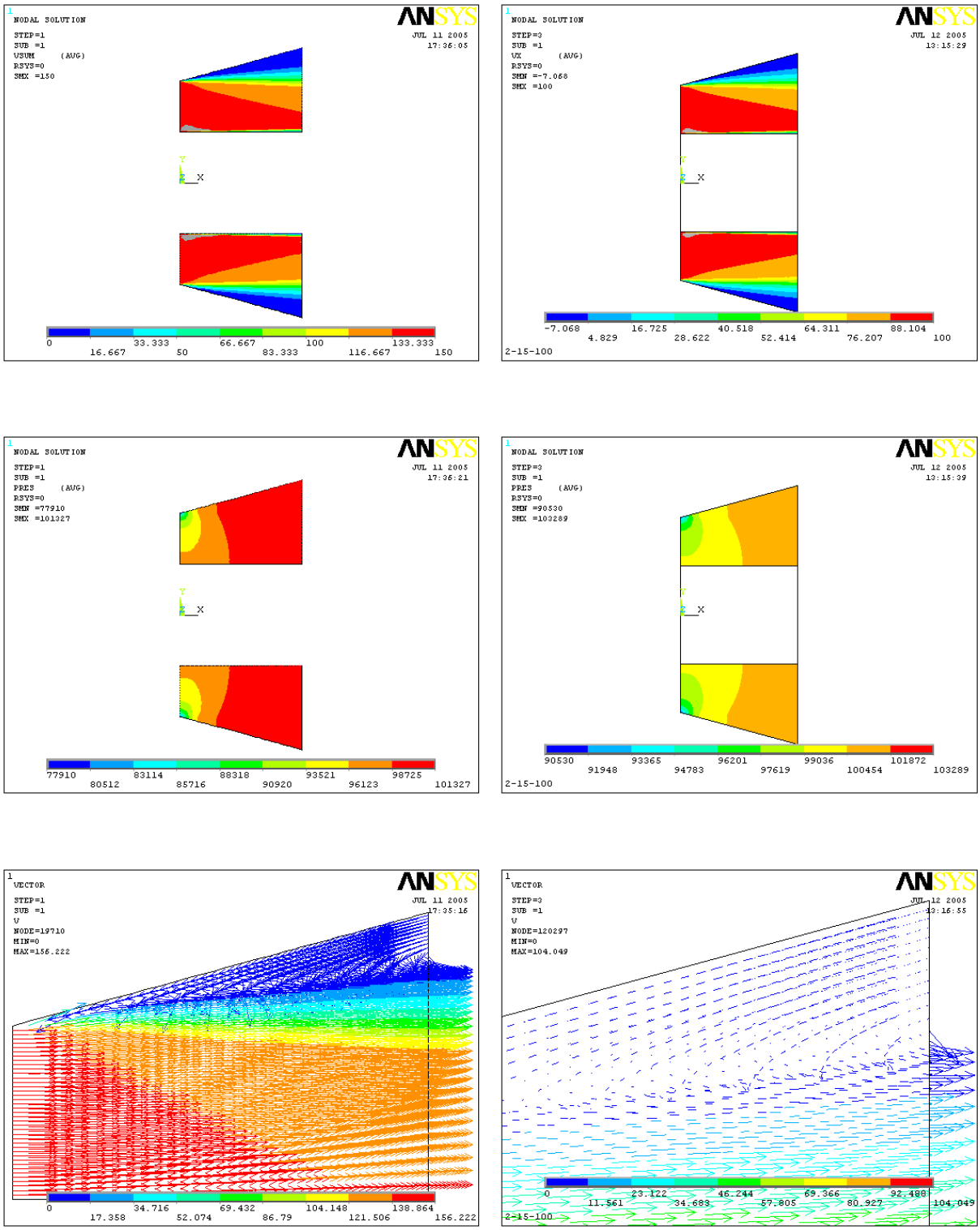

Fig 4 Diffuser AR = 2; α = 15 deg.; Re= 5.15×10^5 -7.7×10^5

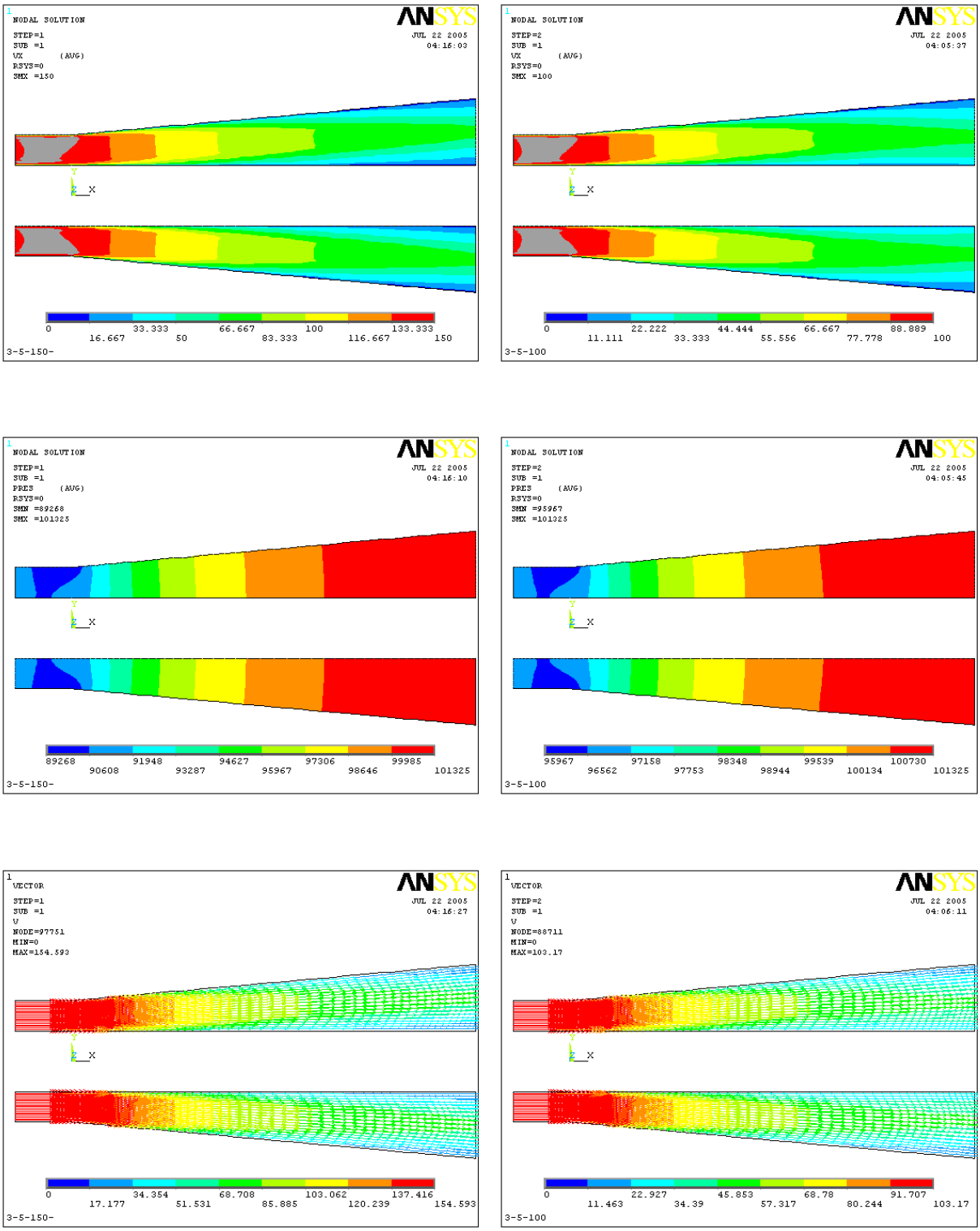

Fig 5 Diffuser AR = 3; α = 5 deg.; Re= 5.15×10^5 -7.7×10^5

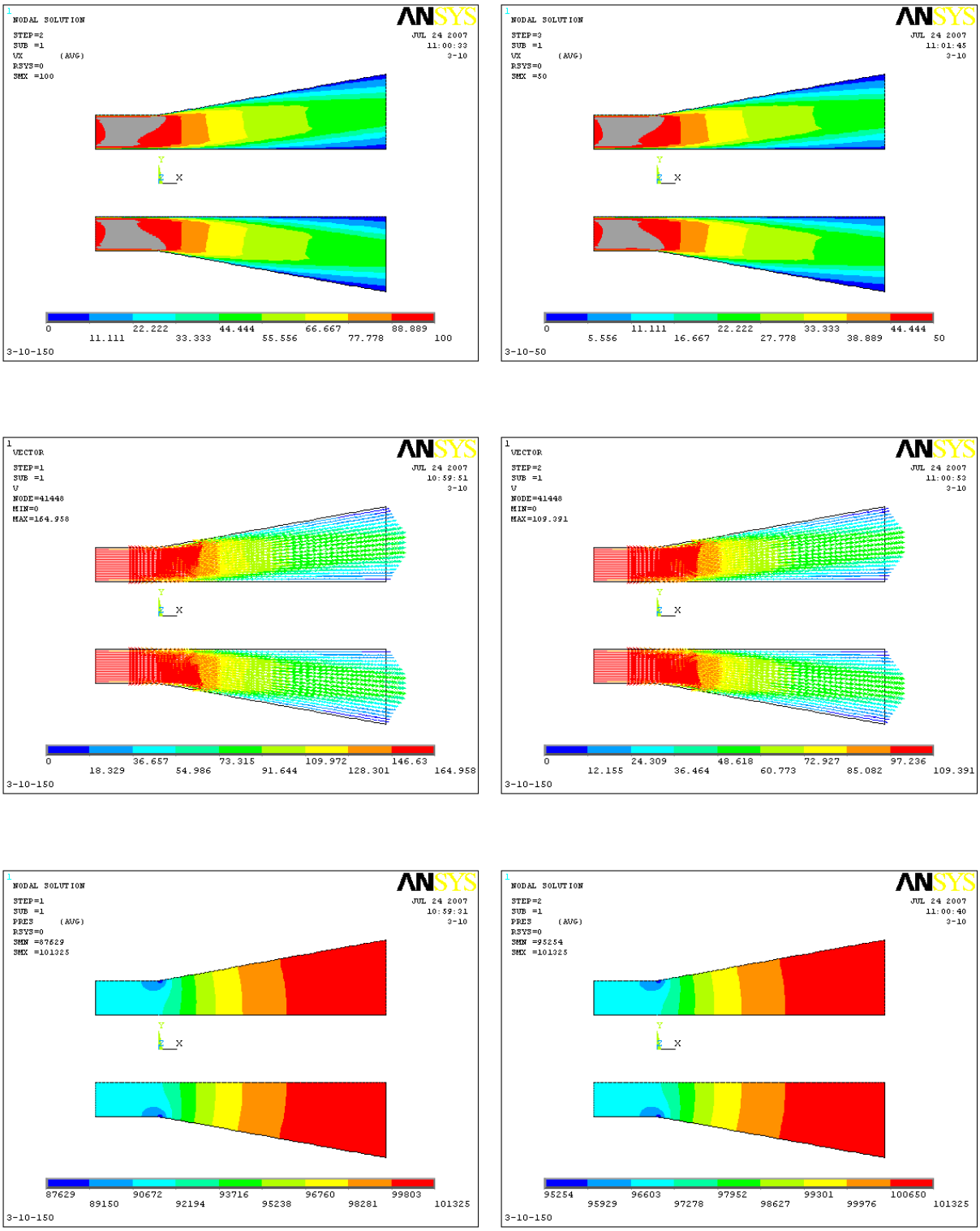

Fig 6 Diffuser AR = 3; α = 10 deg.; Re= 5.15×10^5 -7.7×10^5

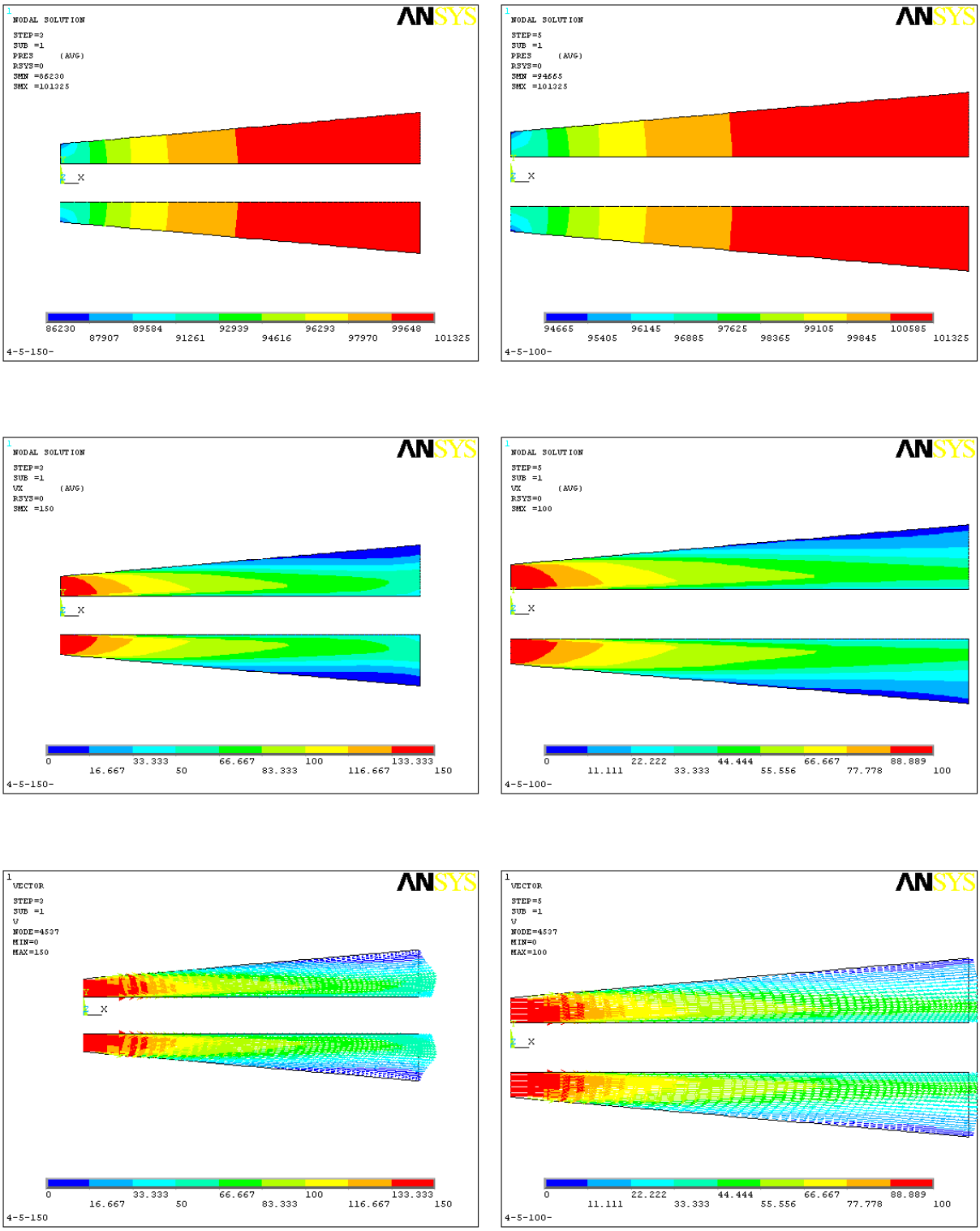

Fig 7 Diffuser AR = 4; α = 5 deg.; Re= 5.15×10^5 -7.7×10^5

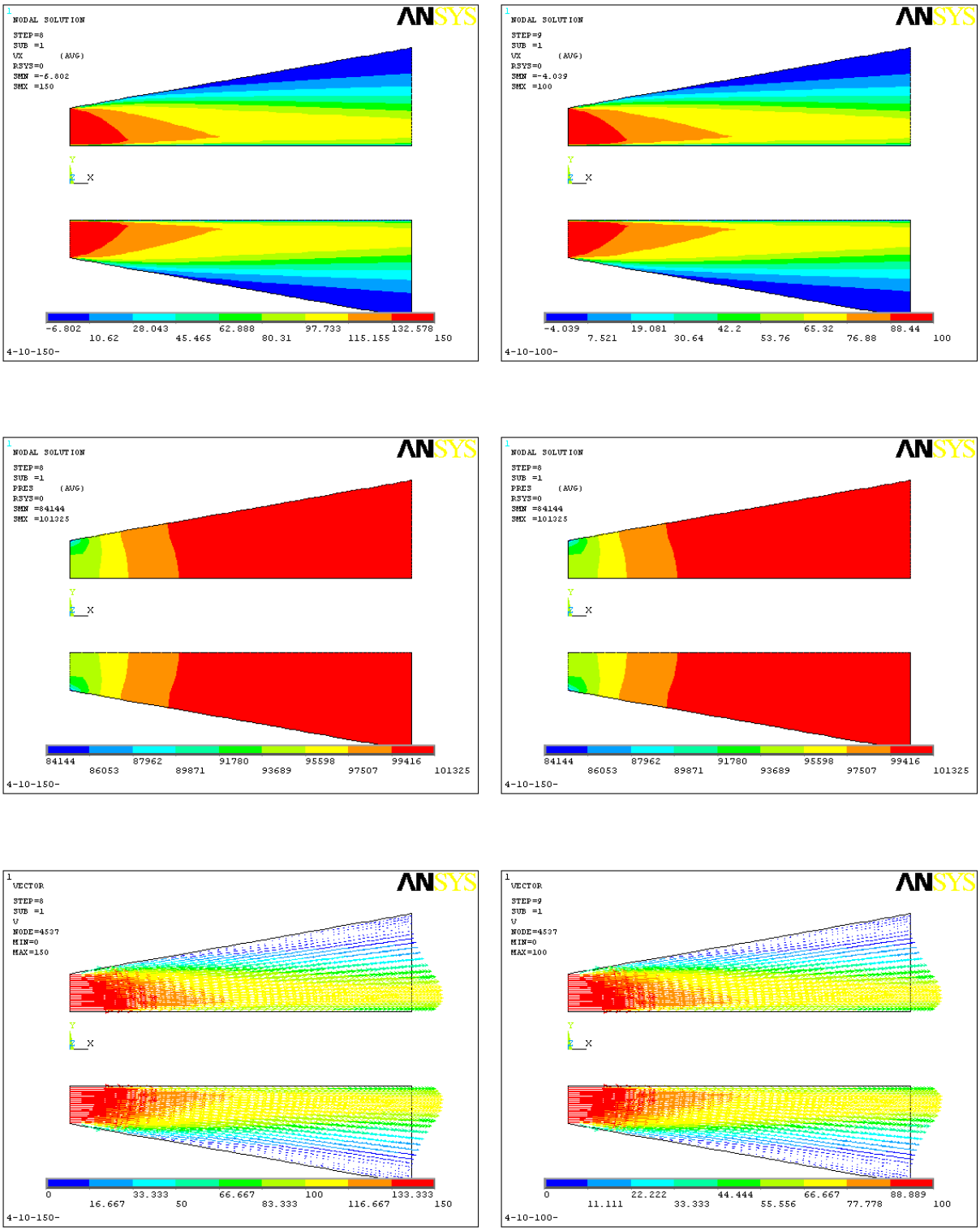

Fig 8 Diffuser AR = 4; α = 10 deg.; Re= 5.15×10^5 -7.7×10^5

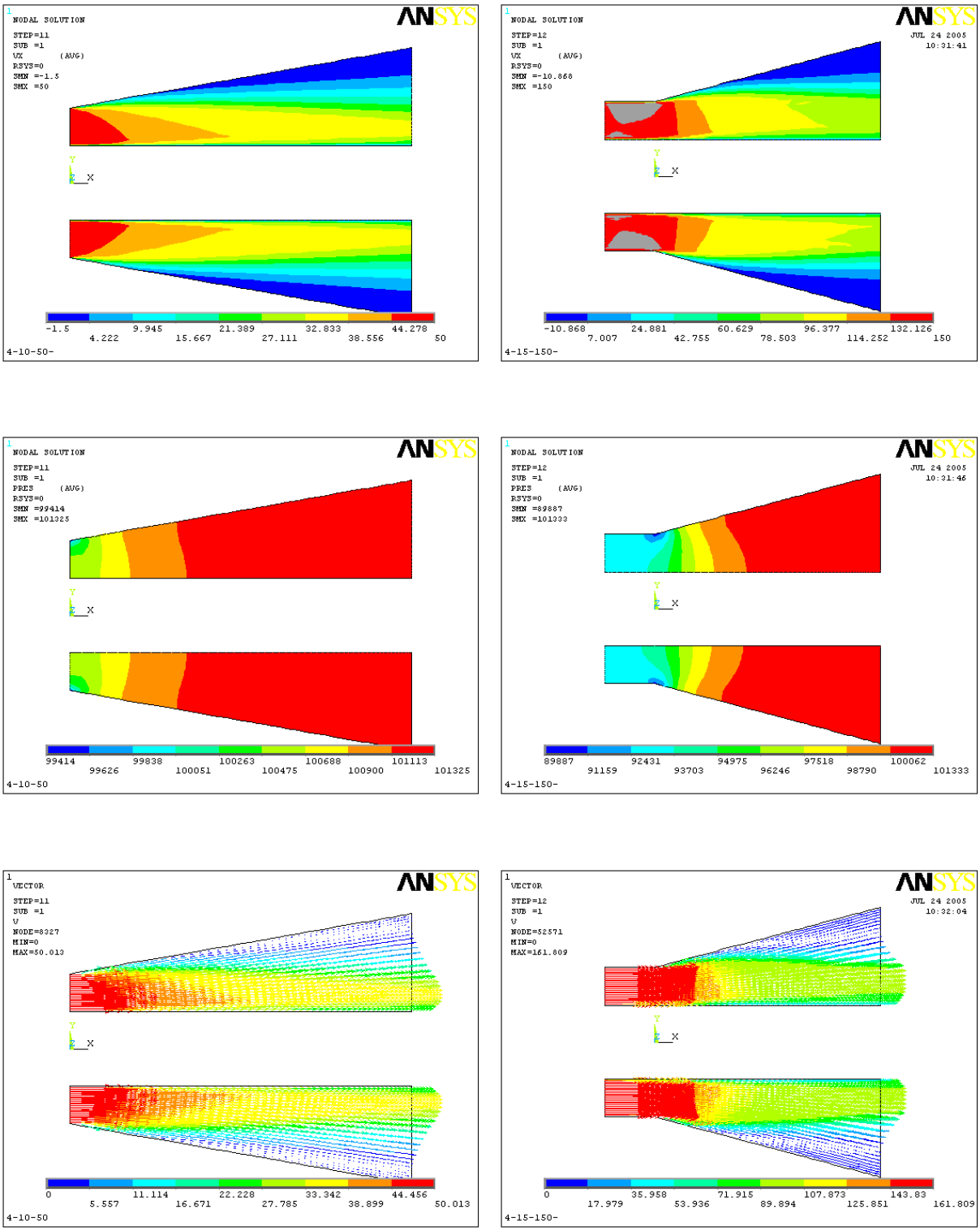

Fig 9 Diffuser AR = 4; α = 10 deg; α =15 deg; Re= 2.5×10^5

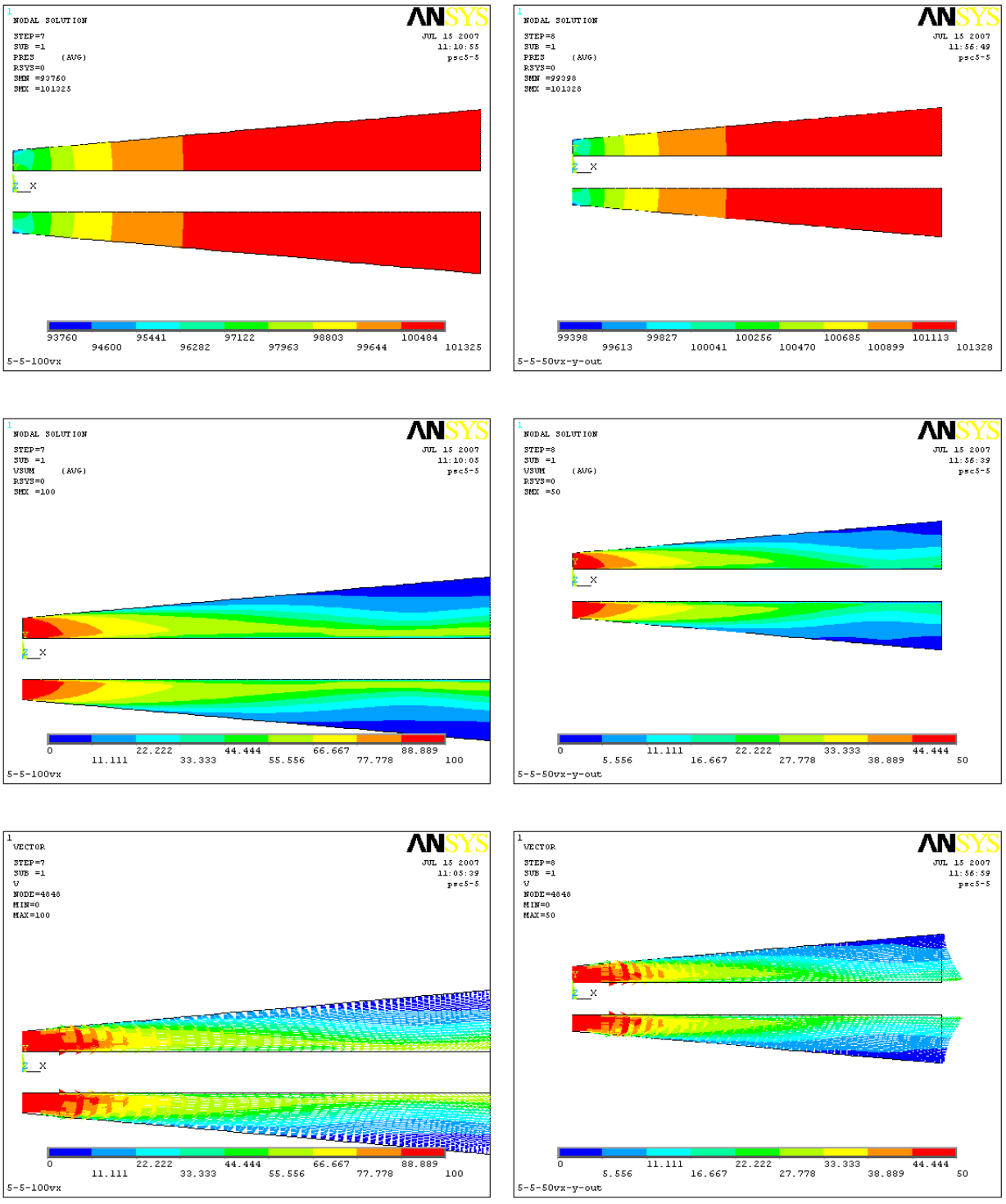

Fig 10 Diffuser AR = 5; α = 5 deg.; Re= 5.15×10^5 ; Re=7.7×10^5

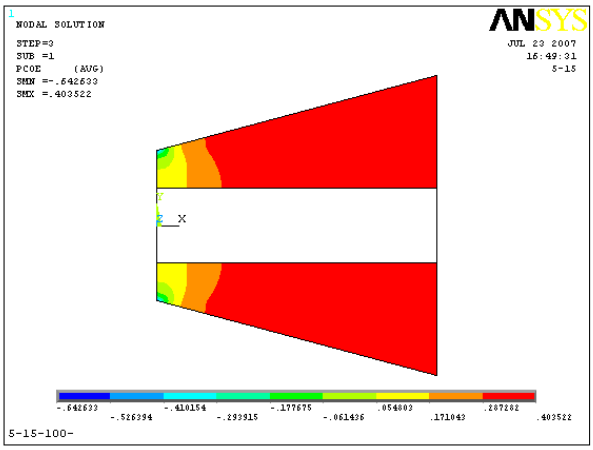

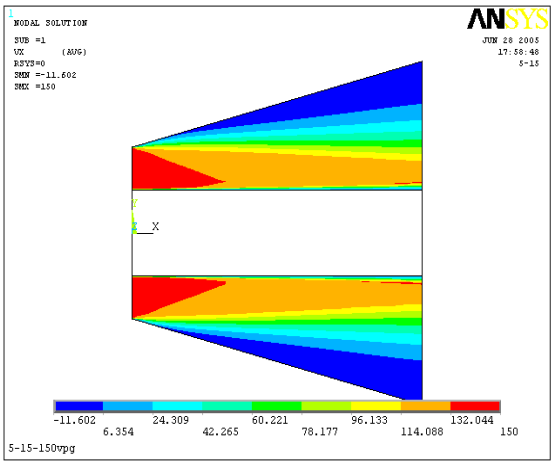

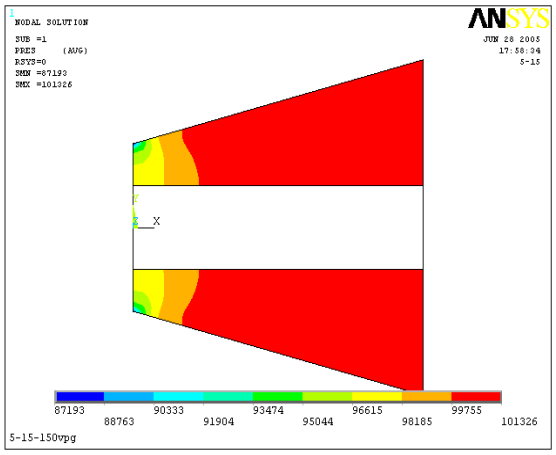

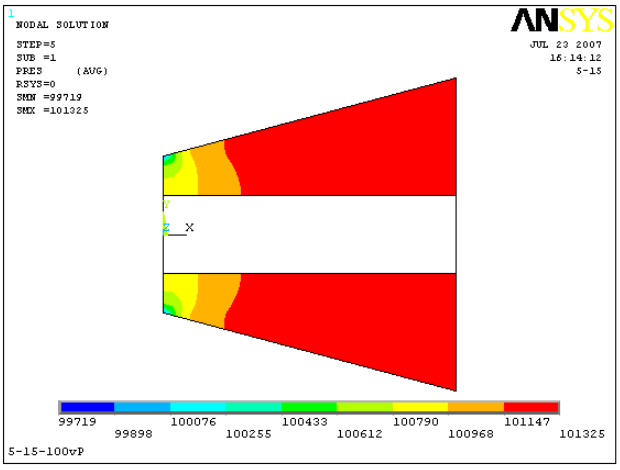

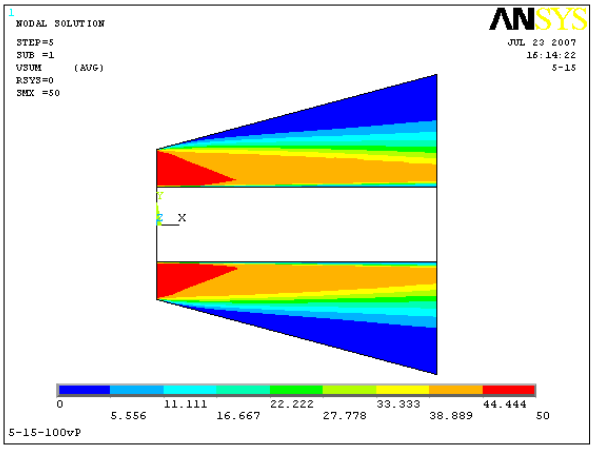

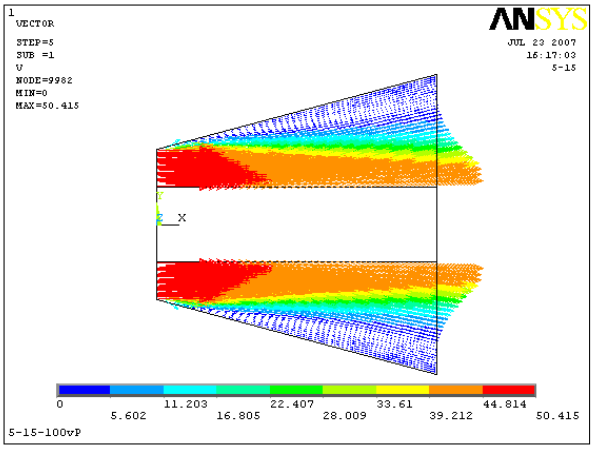

Fig 11 Diffuser AR = 5; α = 15 deg.; Re= 5.15×10^5 -7.7×10^5

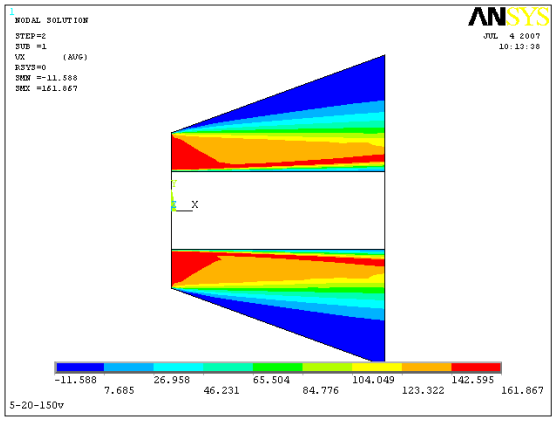

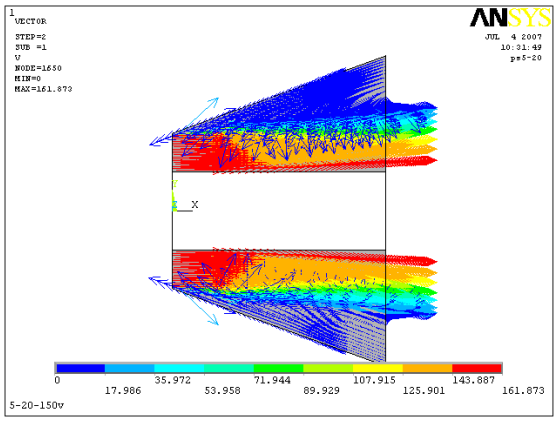

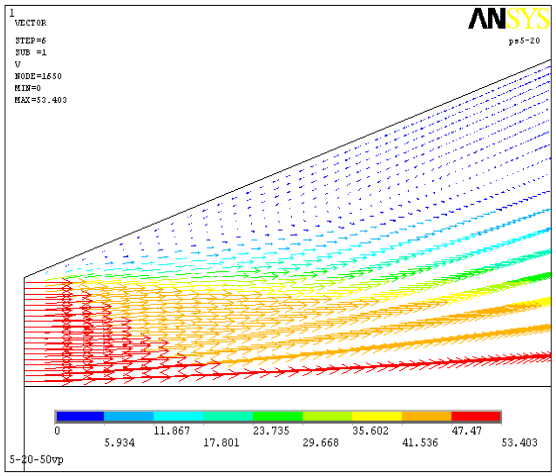

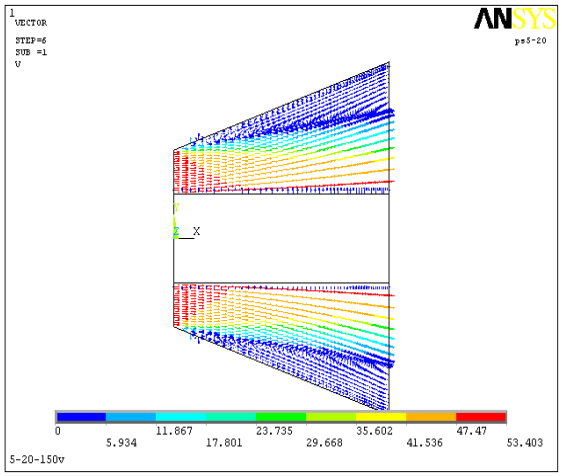

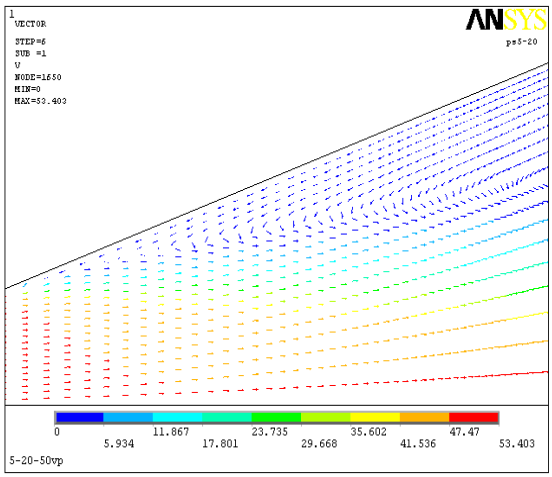

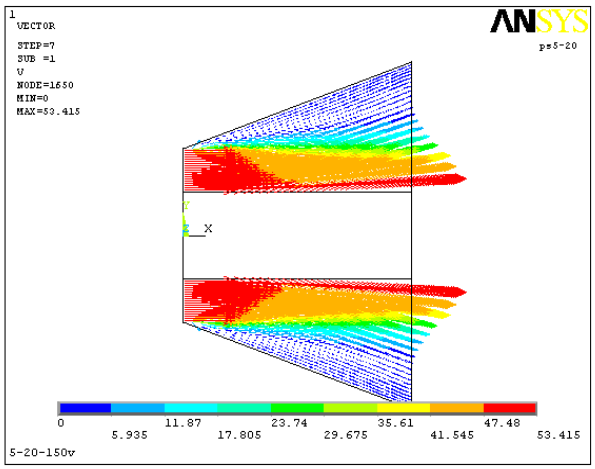

Fig 12 Diffuser AR = 5; α = 20deg; Re= 5.15×10^5 -7.7×10^5

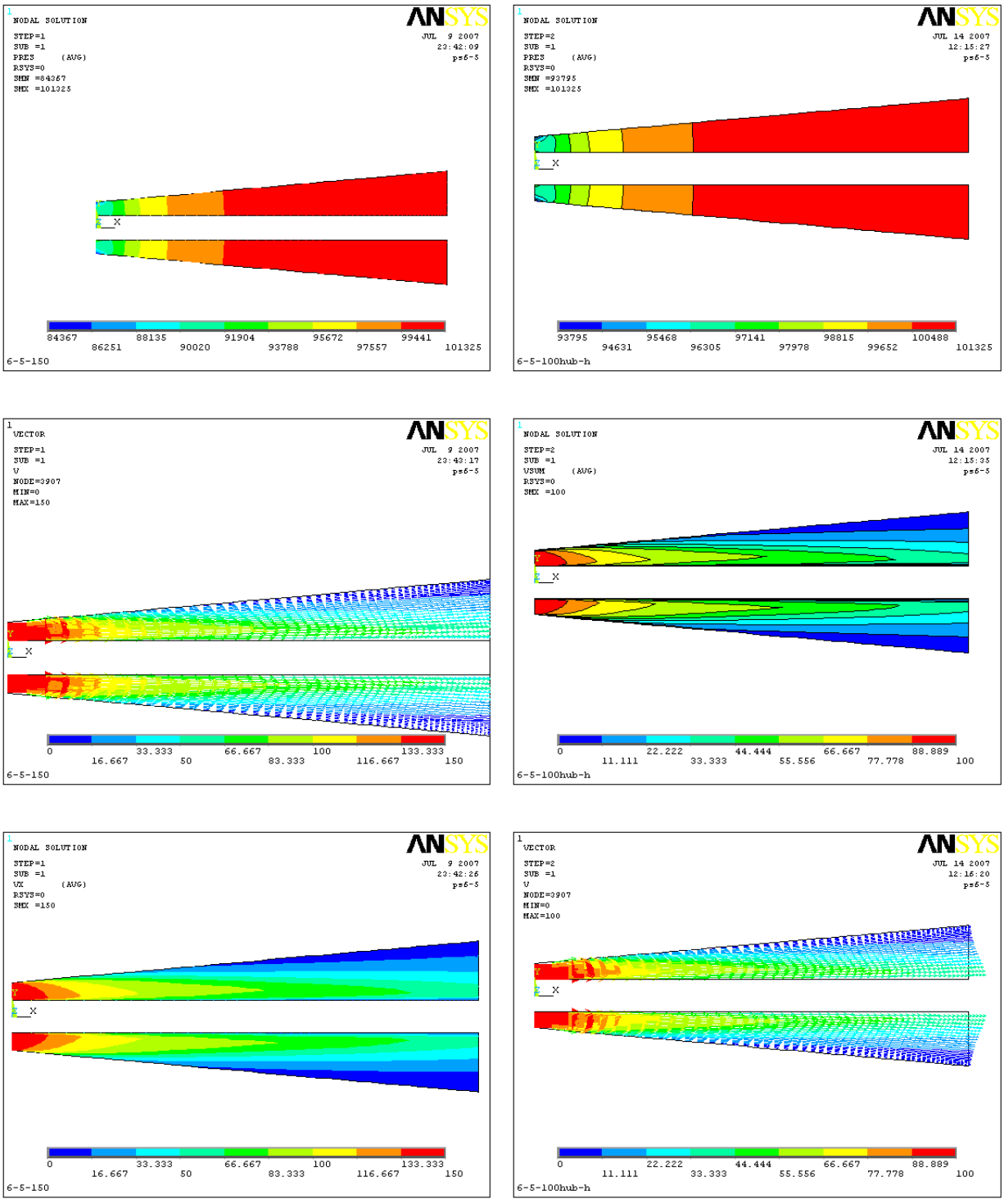

Fig 13 Diffuser AR = 6; α = 5 deg.; Re= 5.15×10^5 ; Re=7.7×10^5

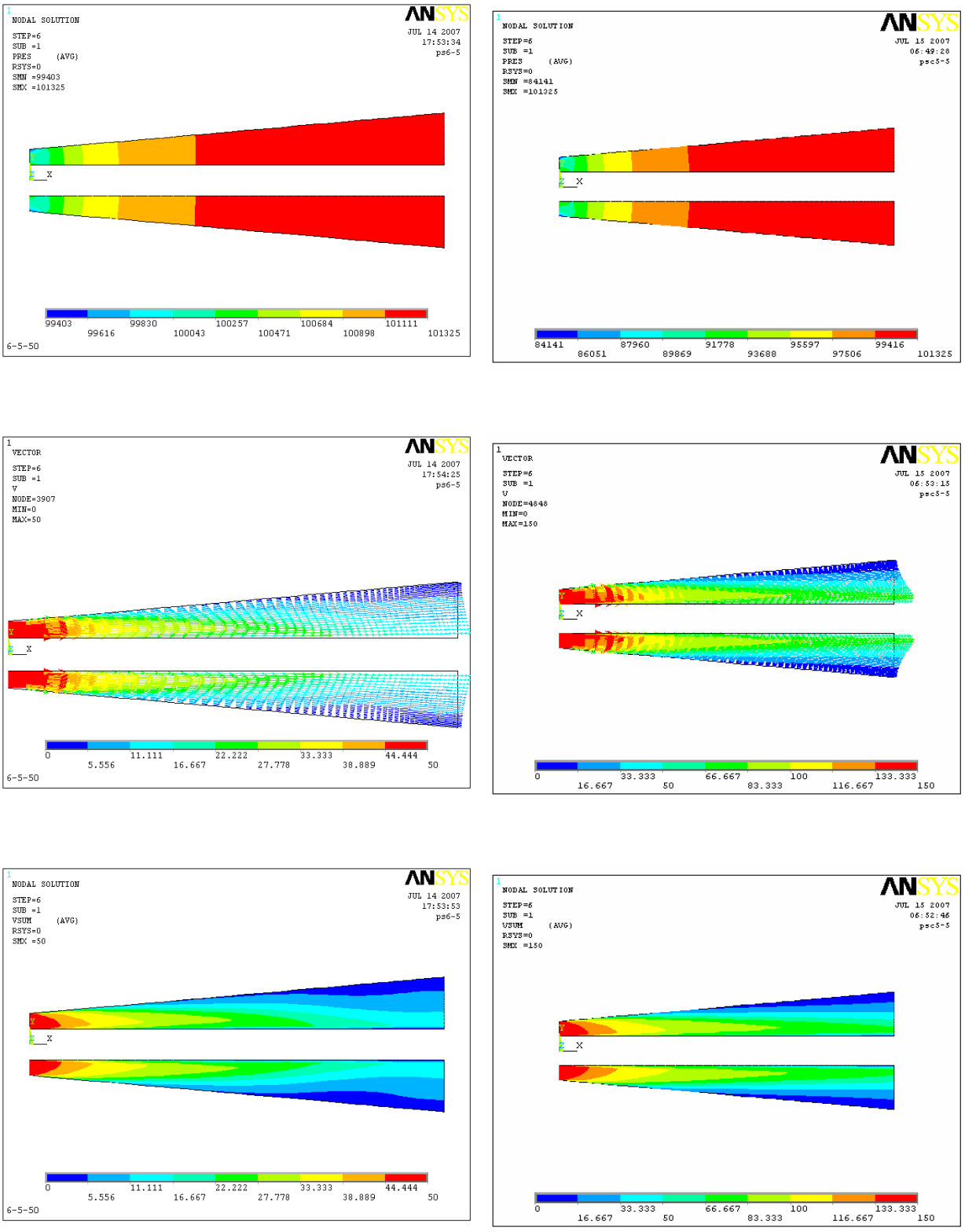

Fig 14 Diffuser AR = 5; AR = 6 α = 5 deg.; Re= 2.5×10^5

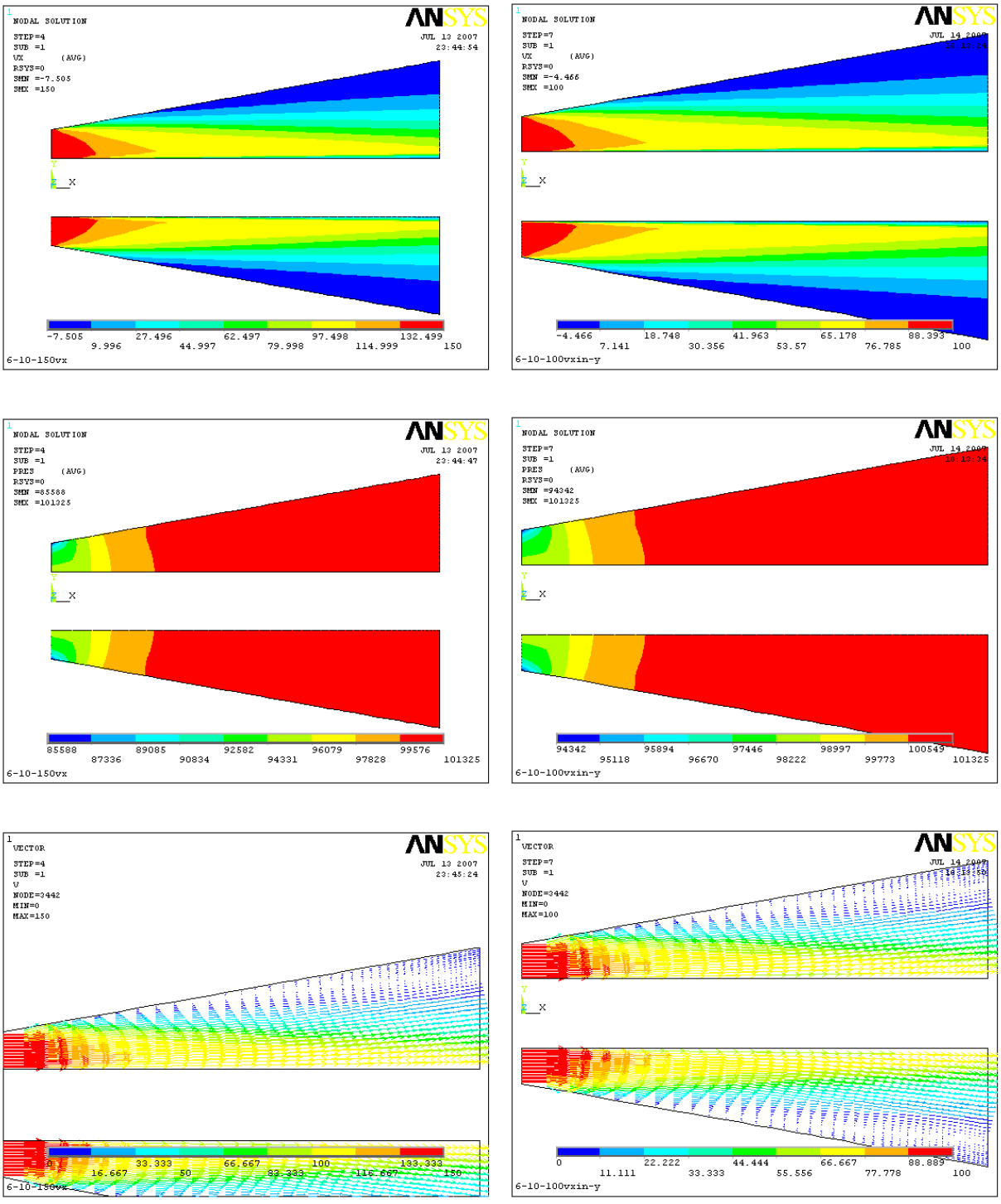

Fig 15 Diffuser AR = 6; α = 10 deg.; Re= 5.15×10^5 ; Re= 7.7×10^5

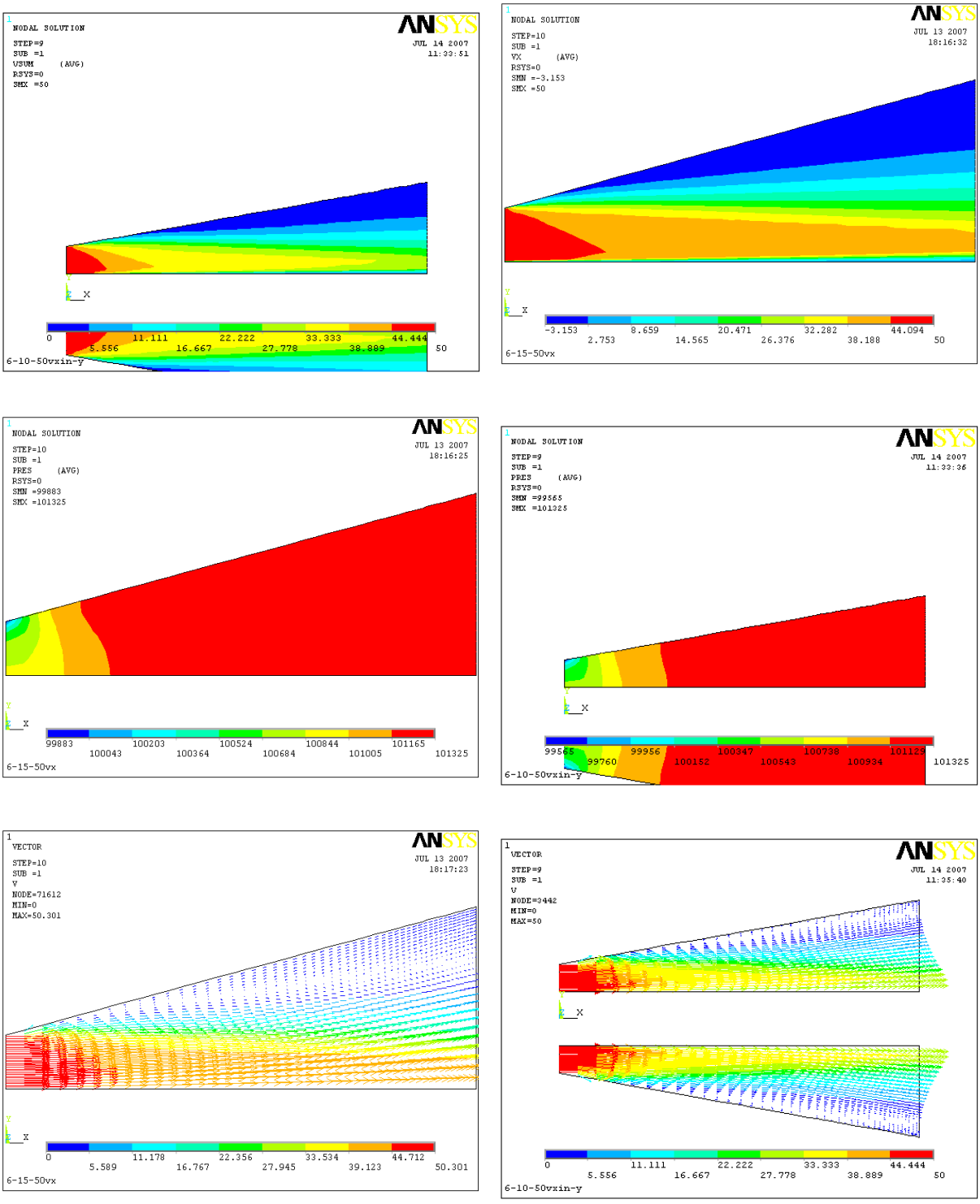

Fig 16Diffuser AR = 6; α = 15 deg.; α = 10deg; Re= 2.5×10^5

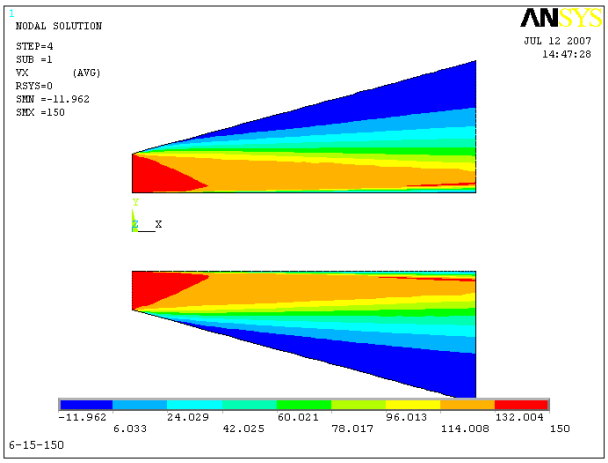

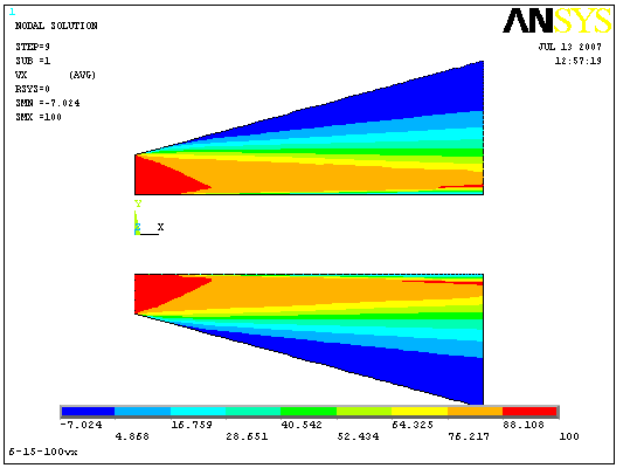

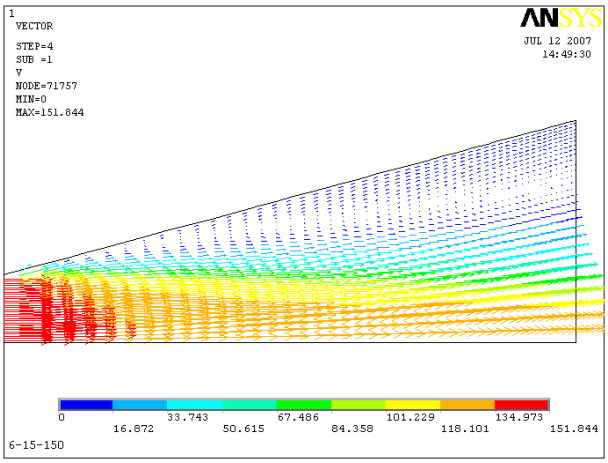

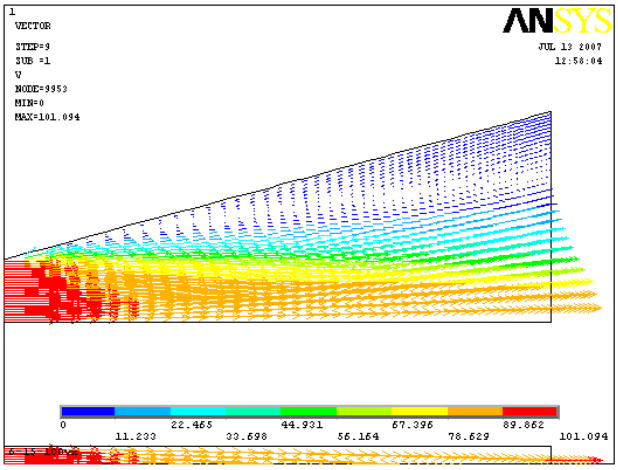

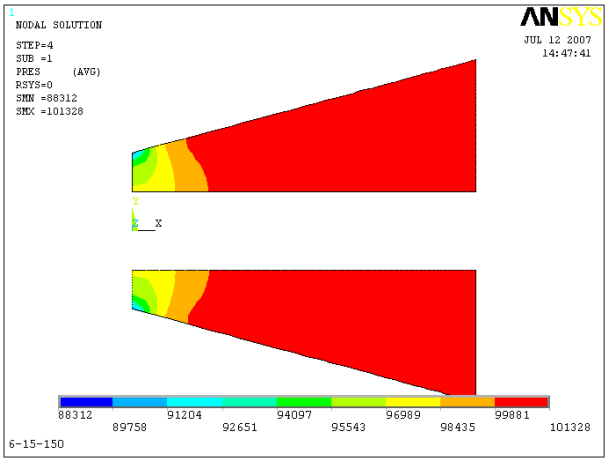

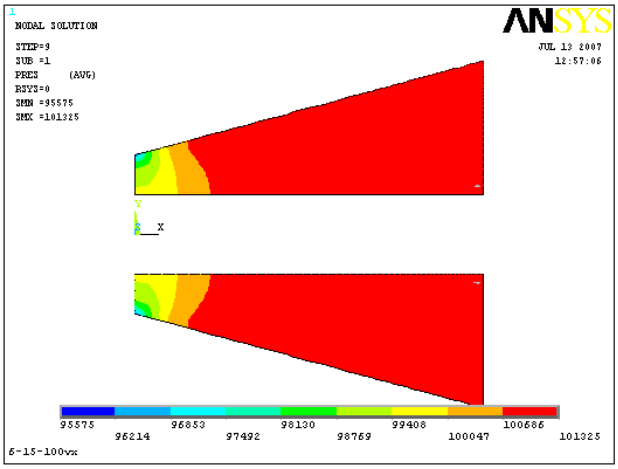

Fig 17Diffuser AR = 6; α = 15 deg.; α = 10deg; Re= 5.5×10^5 ; Re= 7.7×10^5

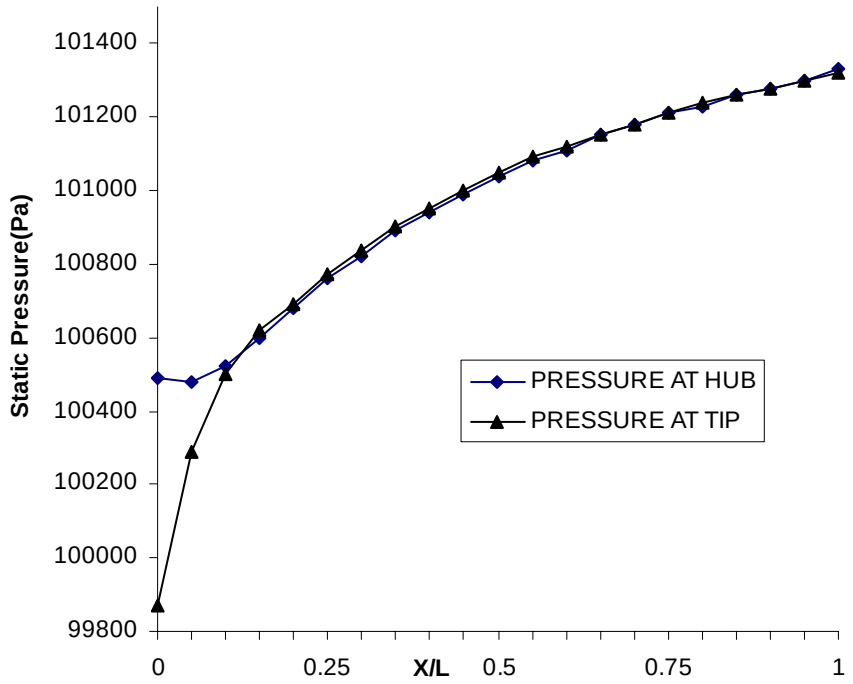

Fig 18 Pressure at Hub and Tip for AR= 2; α = 5; Re=2.5×10^5

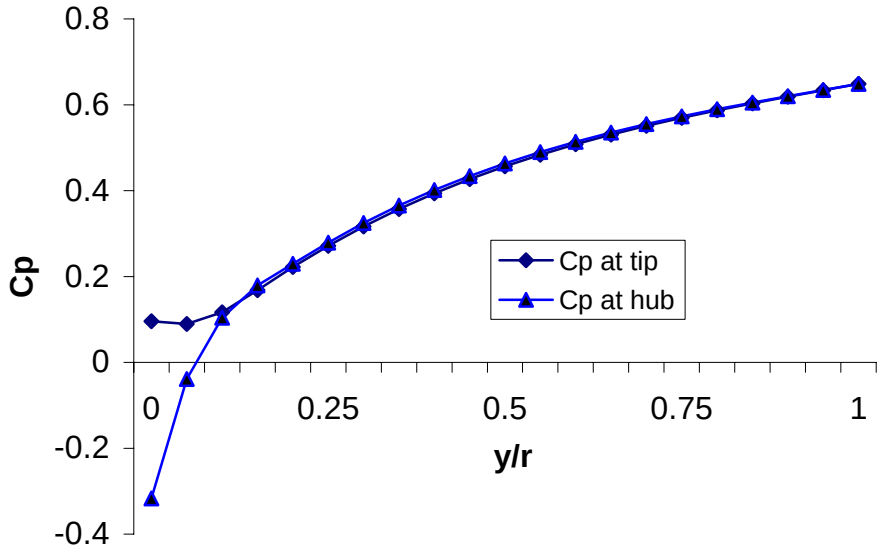

Fig 19 Pressure Recovery Coefficient at Hub and Tip for AR= 2; α = 5; Re=2.5×10^5

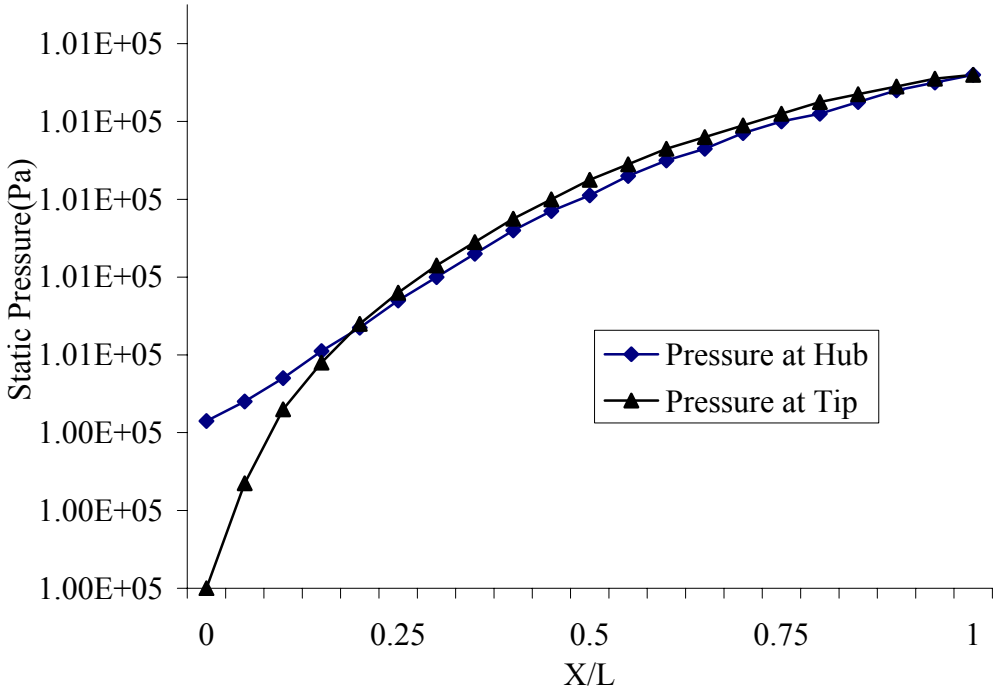

Fig 20 Pressure at Hub and Tip for AR= 2; α = 10; Re=2.5×10^5

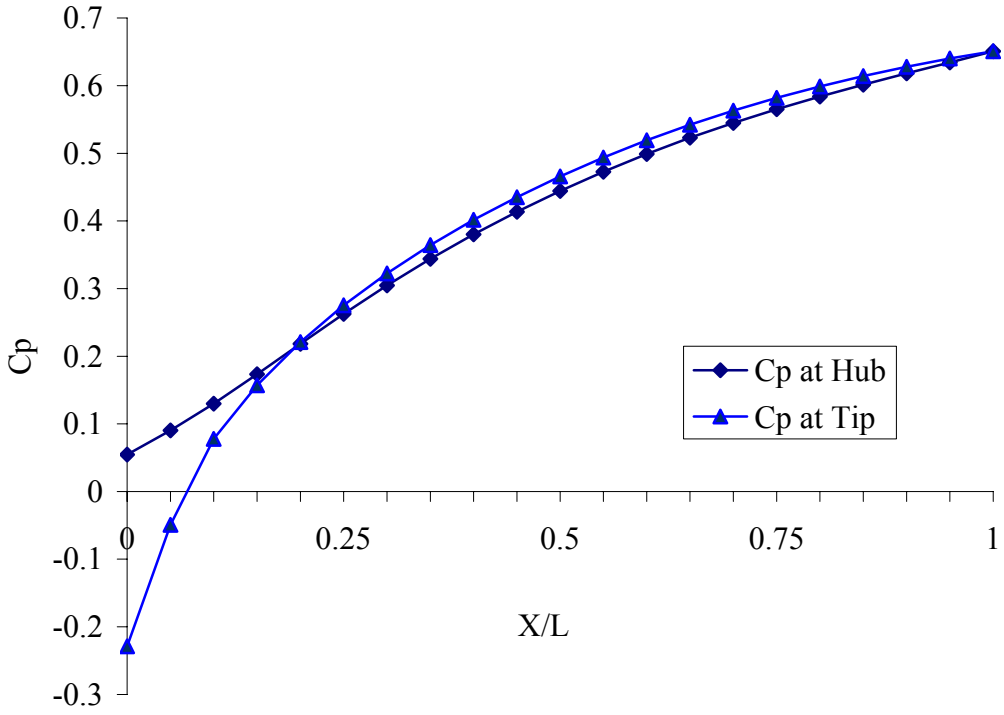

Fig21 Pressure Recovery Coefficient at Hub and Tip for AR= 2; α = 10; Re=2.5×10^5

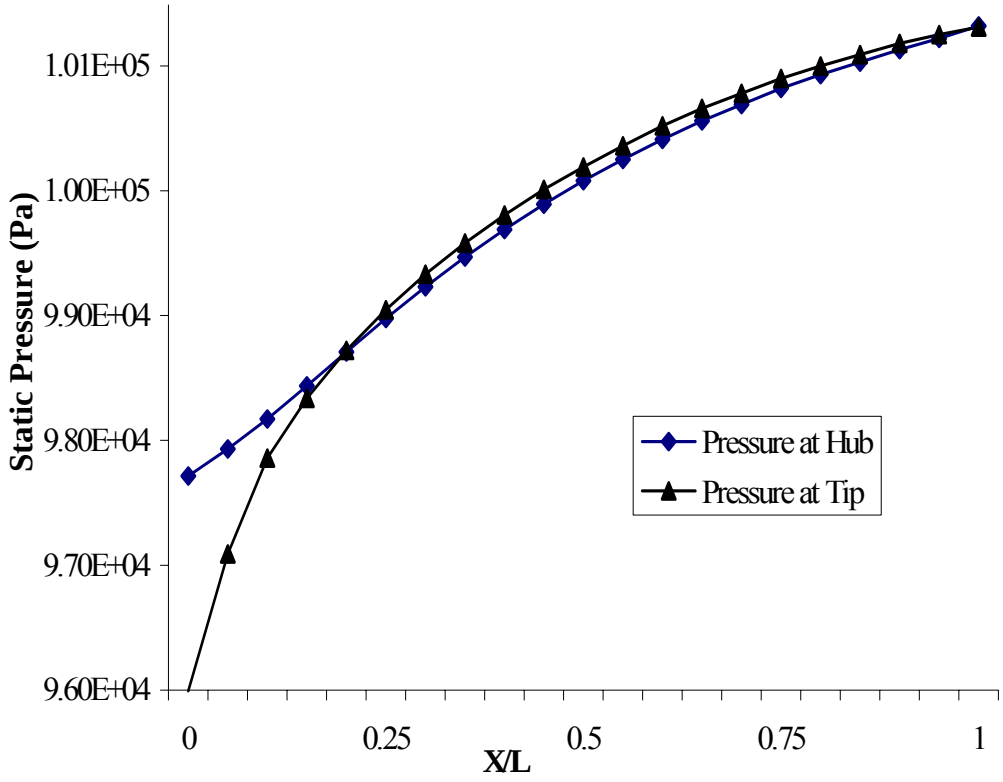

Fig 22 Pressure at Hub and Tip for AR= 2; $\alpha = 10$; $Re=5.5\times10^5$

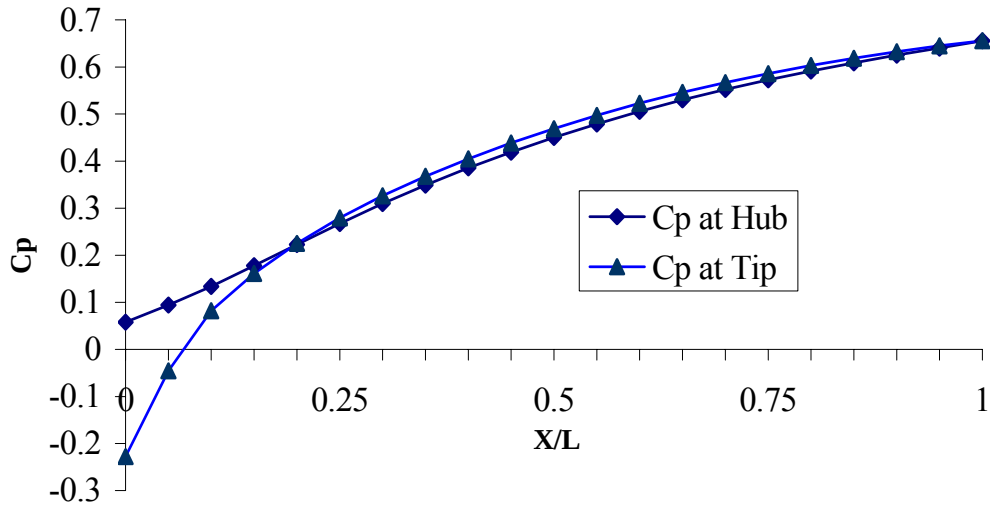

Fig 23 Pressure Recovery Coefficient at Hub and Tip for AR= 2; $\alpha = 10$; $Re=5.5\times10^5$

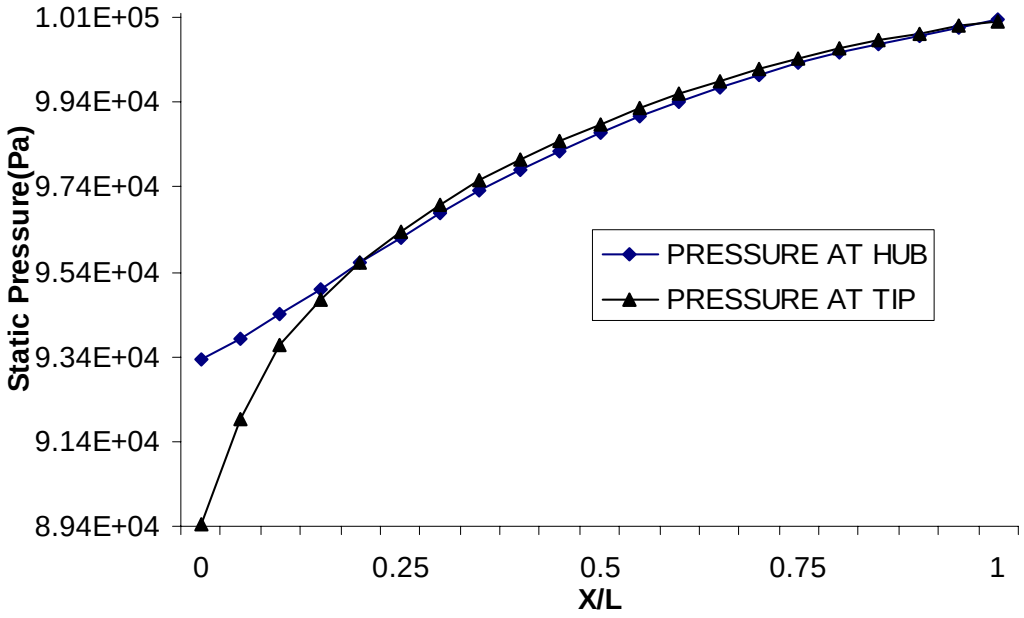

Fig 24 Pressure at Hub and Tip for AR= 2; α = 10; Re=7.5×10^5

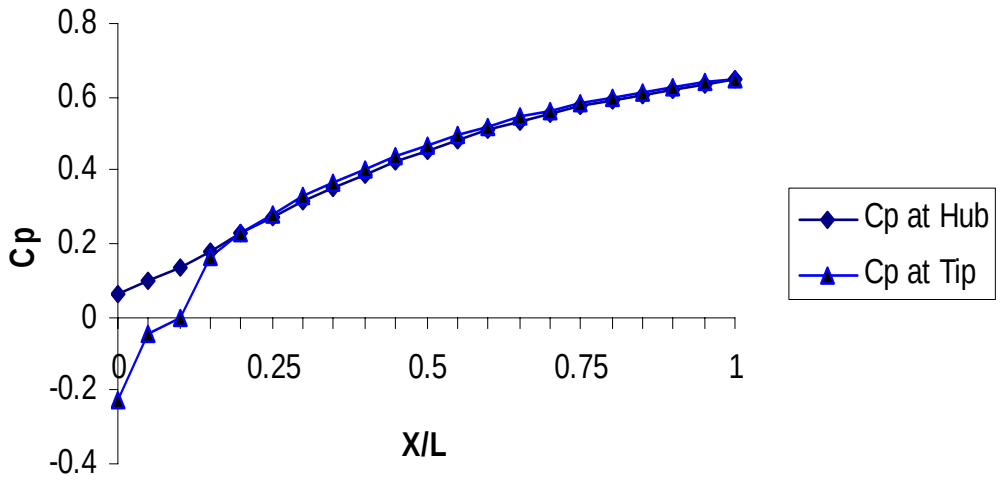

Fig 25 Pressure Recovery Coefficient at Hub and Tip for AR= 2; α = 10; Re=7.5×10^5

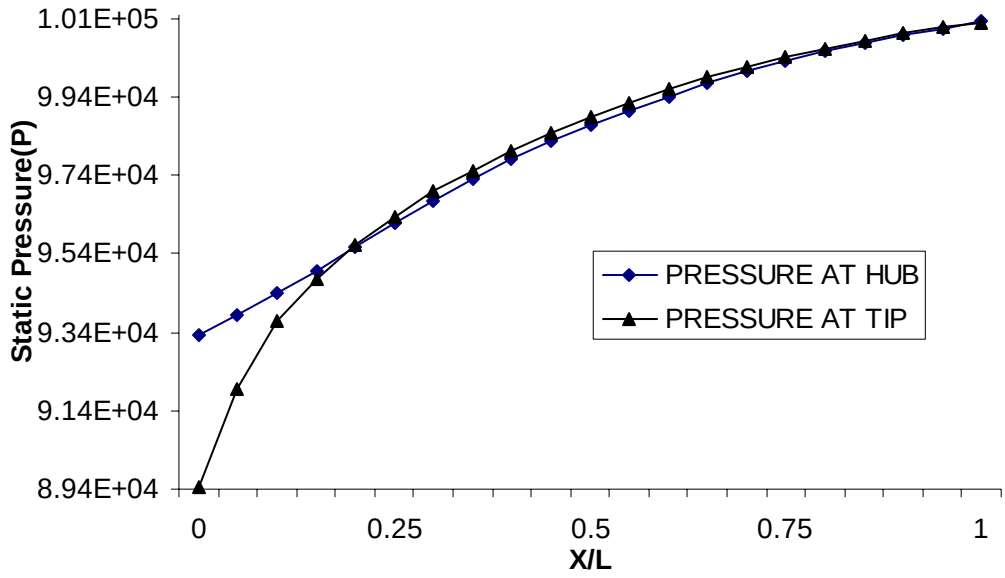

Fig 26 Pressure at Hub and Tip for AR= 2; α = 15; Re=2.5×10^5

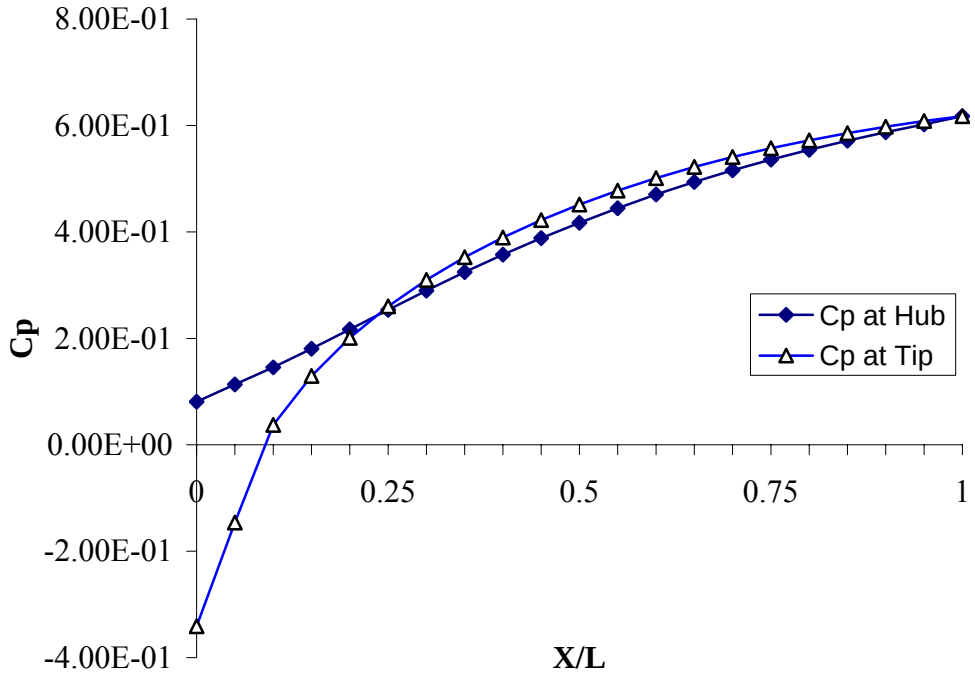

Fig 27 Pressure Recovery Coefficient at Hub and Tip for AR= 2; α = 15; Re=2.5×10^5

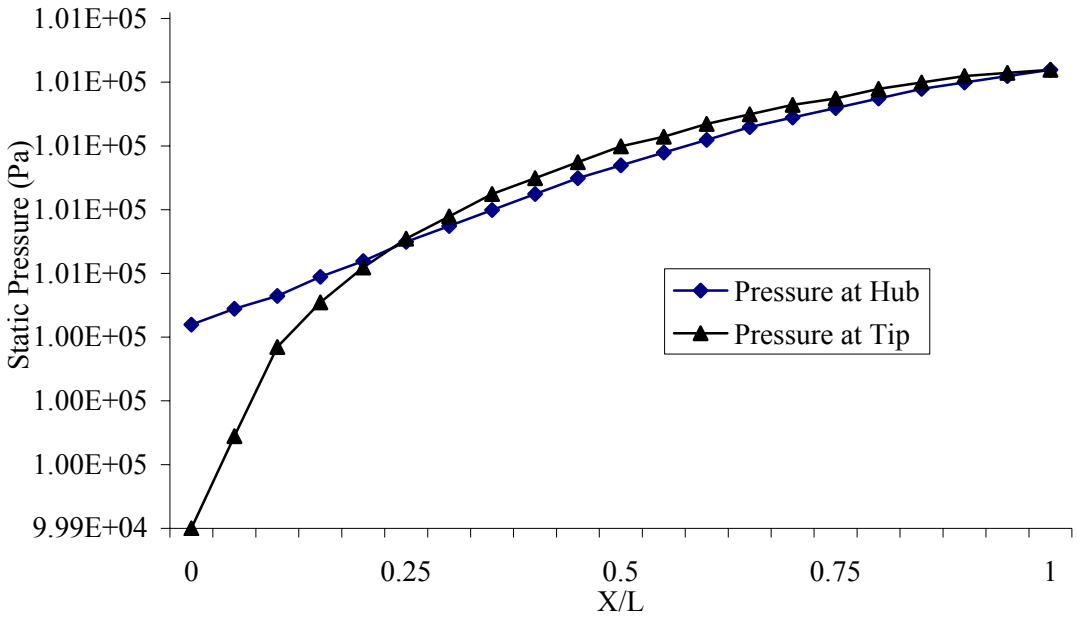

Fig 28 Pressure at Hub and Tip for AR= 2; α = 15; Re=5.5×10^5

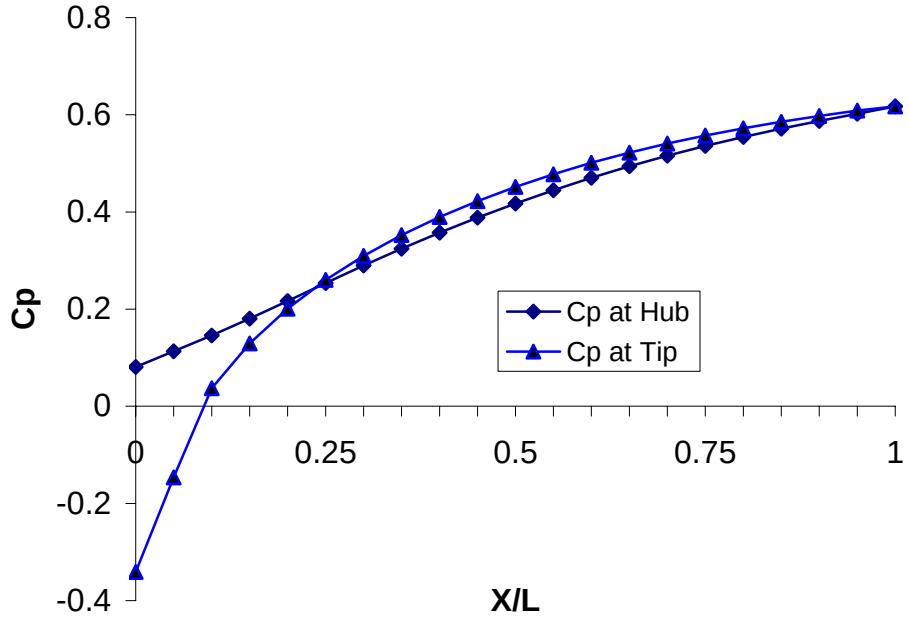

Fig 29 Pressure Recovery Coefficient at Hub and Tip for AR= 2; α = 15; Re=5.5×10^5

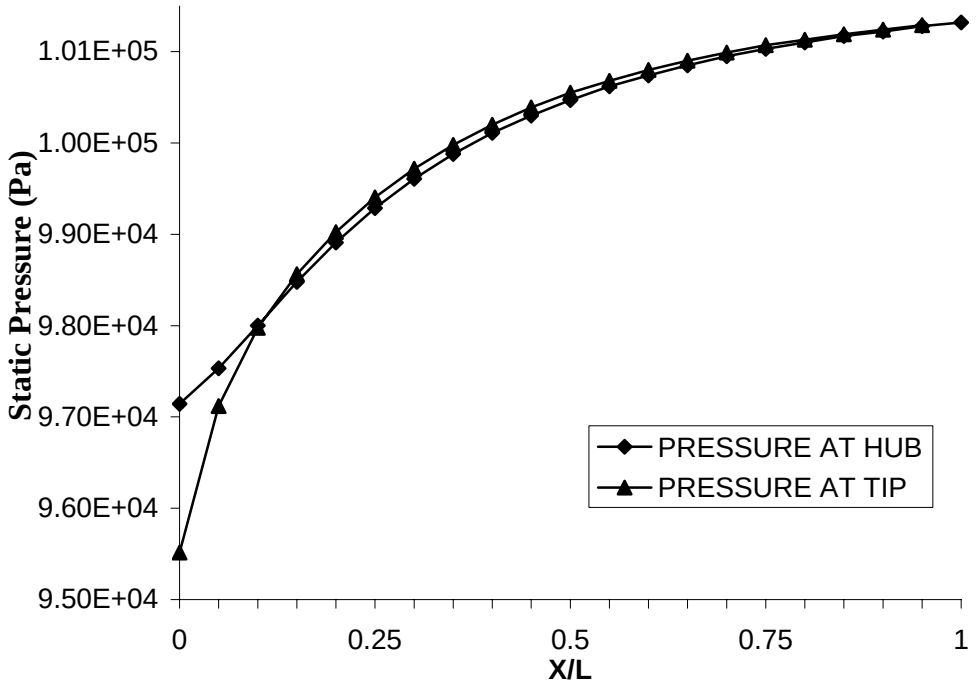

Fig 30 Pressure at Hub and Tip for AR= 3; α = 10; Re=5.5×10^5

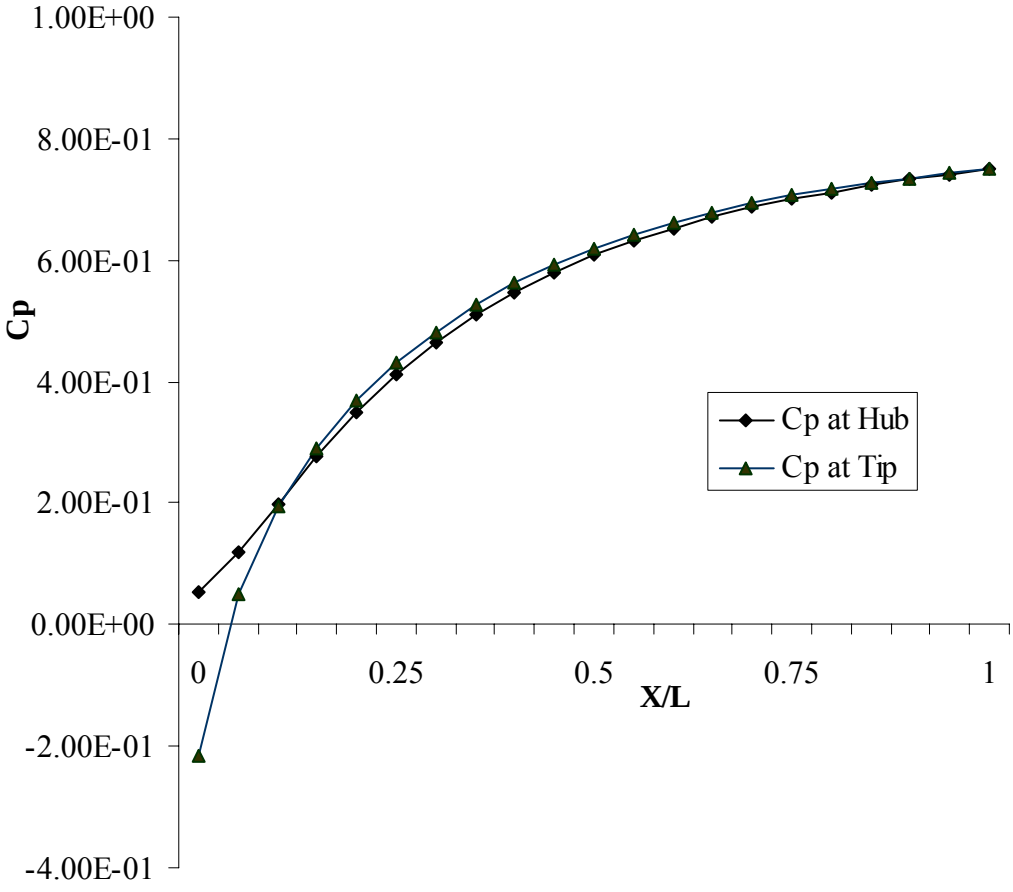

Fig 31 Pressure Recovery Coefficient at Hub and Tip for AR= 3; α = 10; Re=5.5×10^5

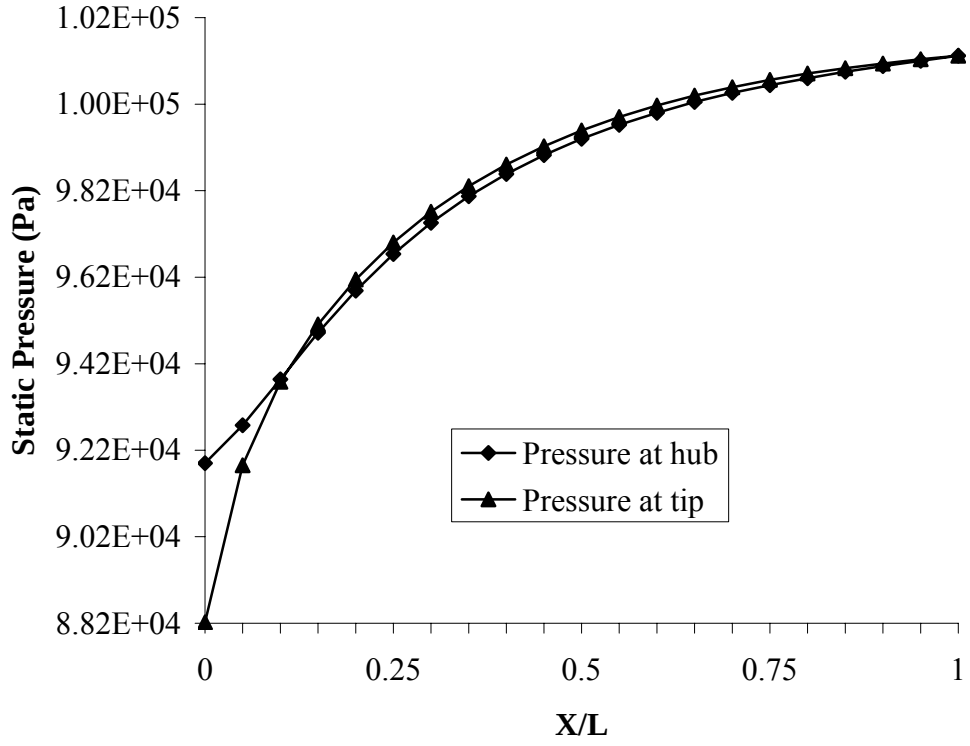

Fig 32 Pressure at Hub and Tip for AR= 3; α = 10; Re=7.5×10^5

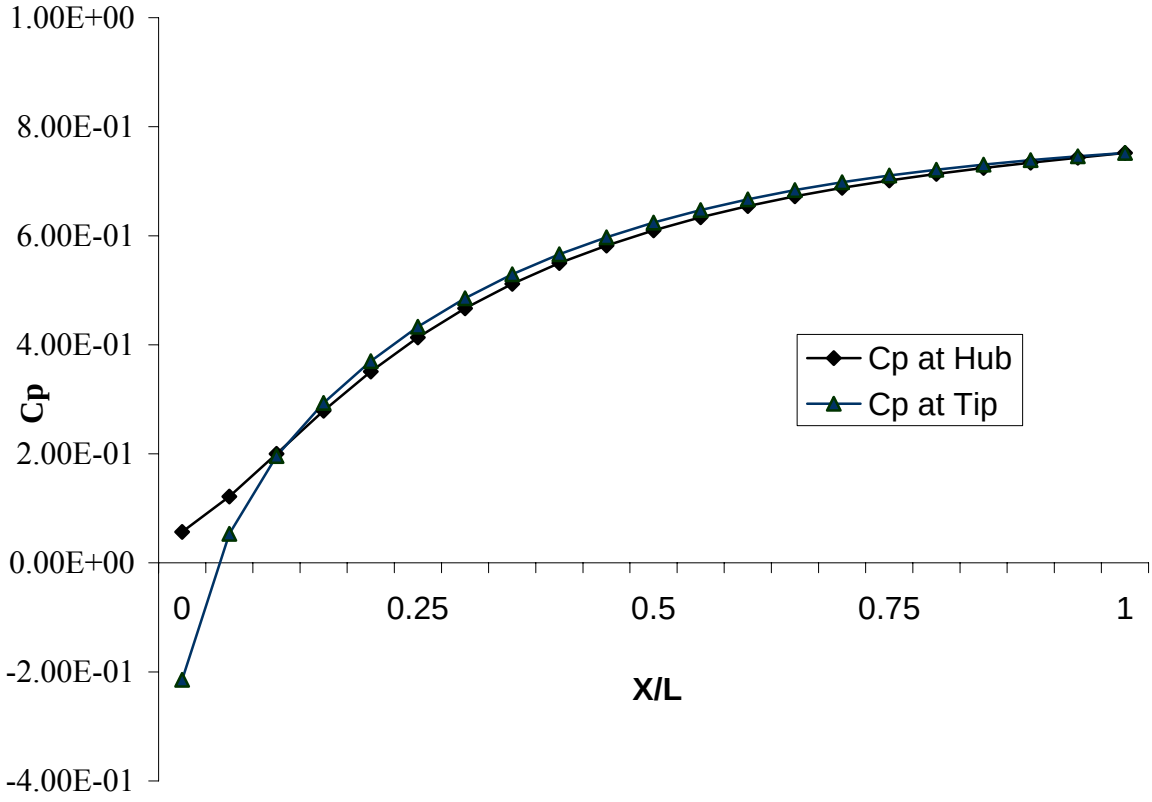

Fig 33 Pressure Recovery Coefficient at Hub and Tip for AR= 3; α = 10; Re=7.5×10^5

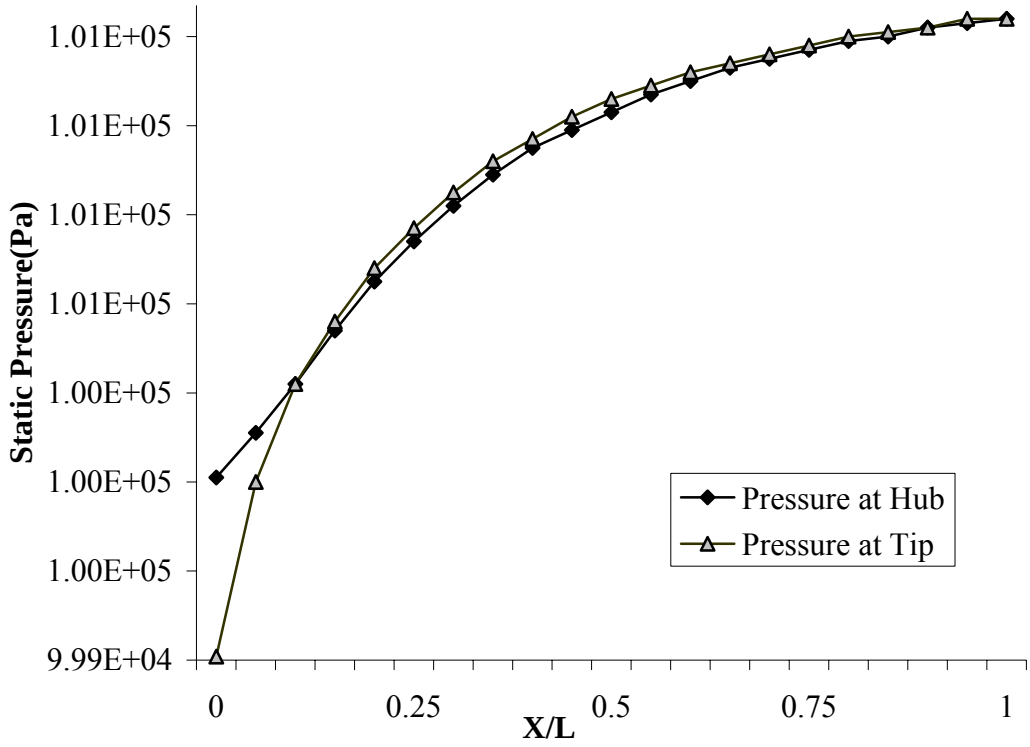

Fig 34 Pressure at Hub and Tip for AR= 3; α = 10; Re=2.5×10^5

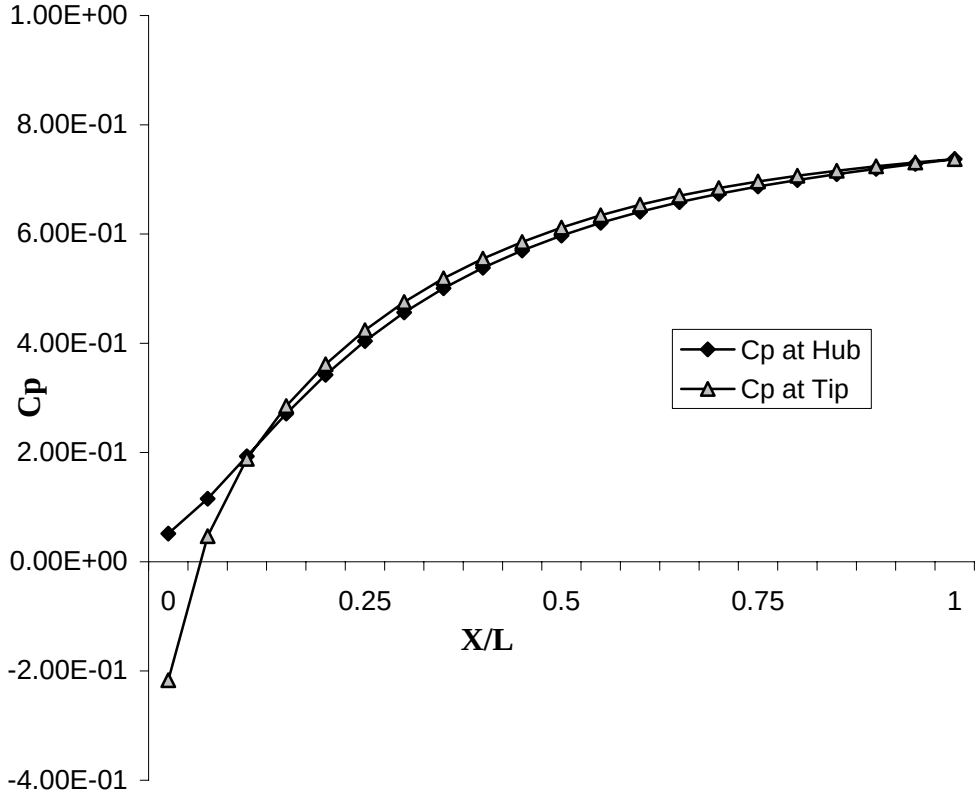

Fig 35 Pressure Recovery Coefficient at Hub and Tip for AR= 3; α = 10; Re=2.5×10^5

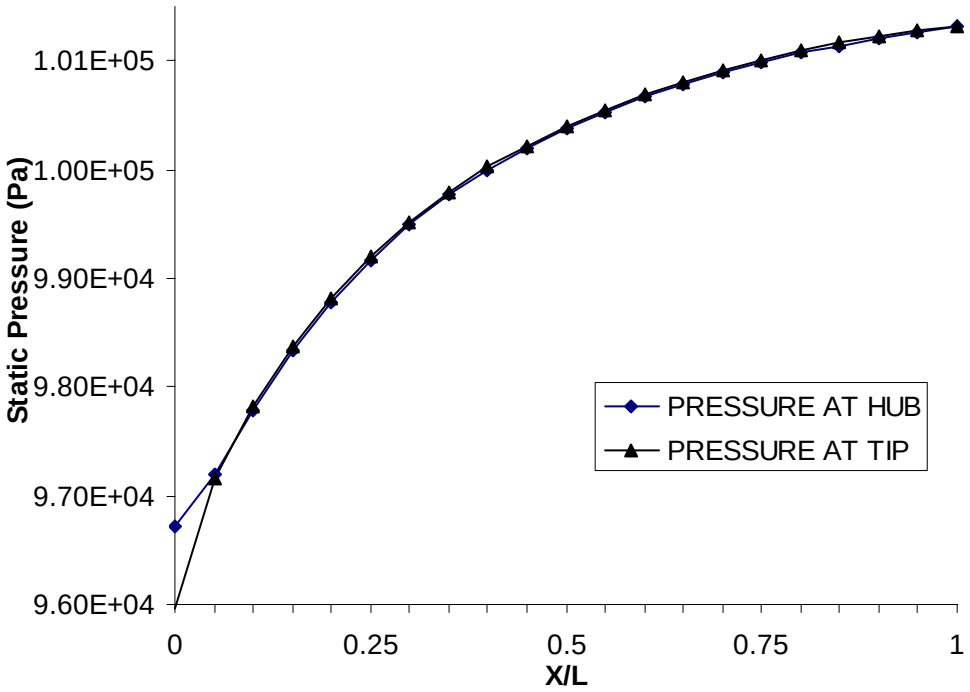

Fig 36 Pressure at Hub and Tip for AR= 3; α = 5; Re=5.5×10^5

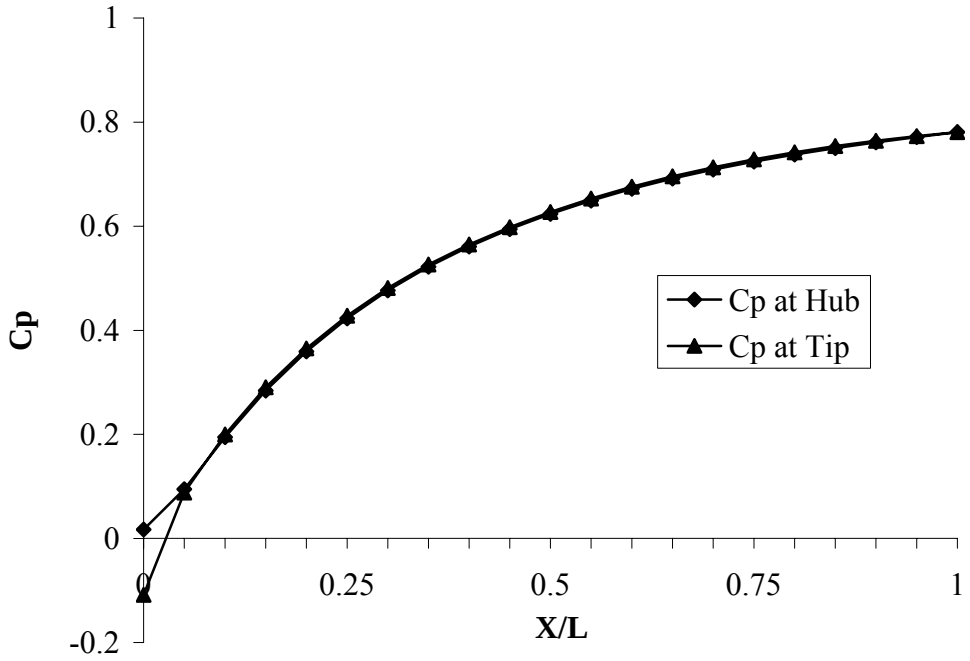

Fig 37 Pressure Recovery Coefficient at Hub and Tip for AR= 3; α = 5; Re=5.5×10^5

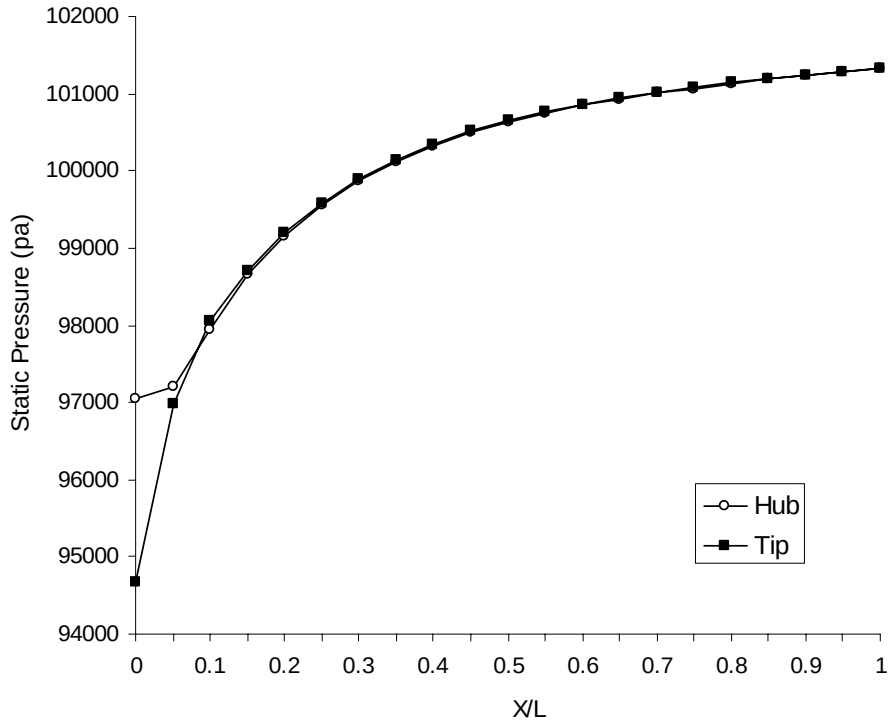

Fig. 38 Static Pressure at Hub and Tip For AR = 4, Angle =5deg; Re=5.5×10^5

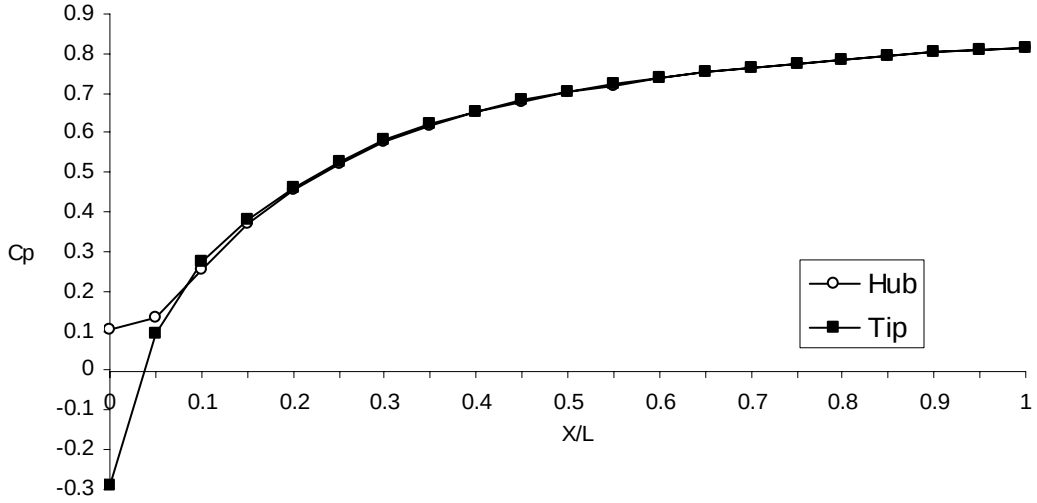

Fig. 39 Static Pressure Recovery at Hub and Tip For AR = 4, Angle =5deg; Re=5.5×10^5

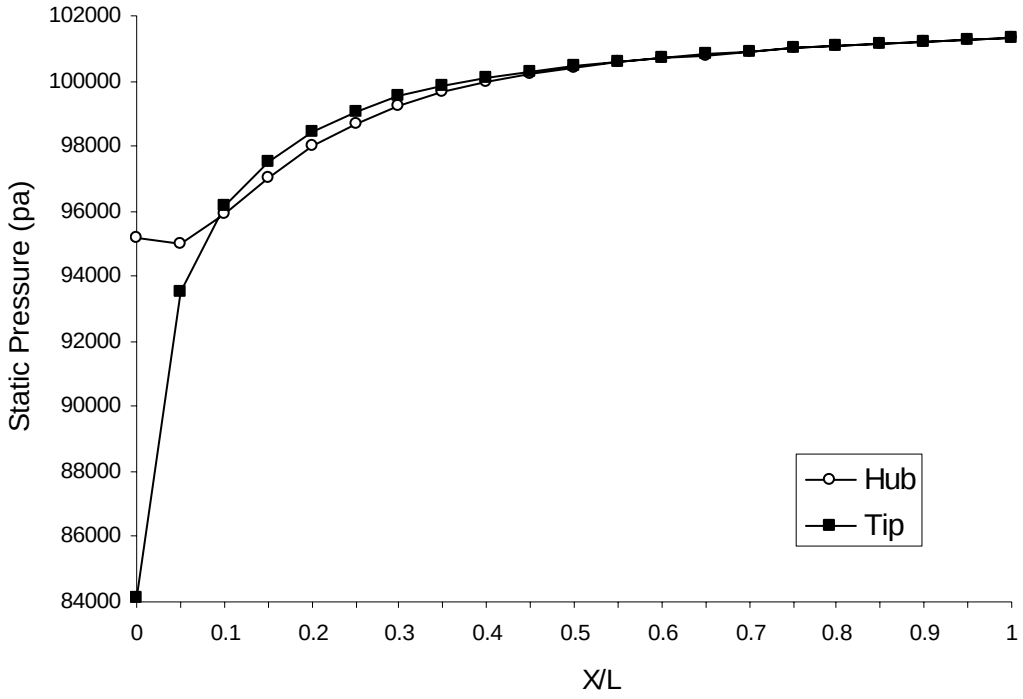

Fig. 40 Static Pressure at Hub and Tip For AR = 4, Angle =5deg; Re=5.5×10^5

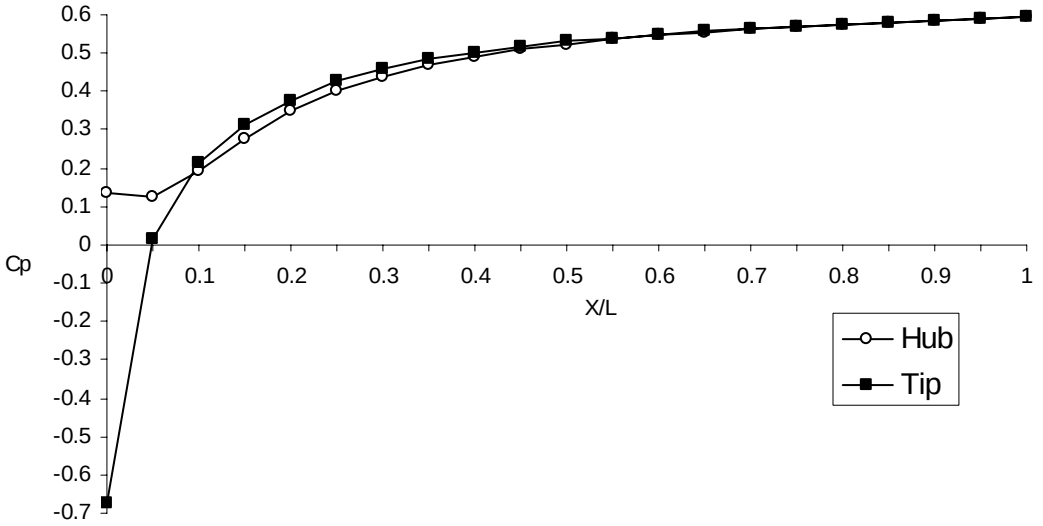

Fig. 41 Static Pressure Recovery at Hub and Tip For AR = 4, Angle =5deg; Re=5.5×10^5

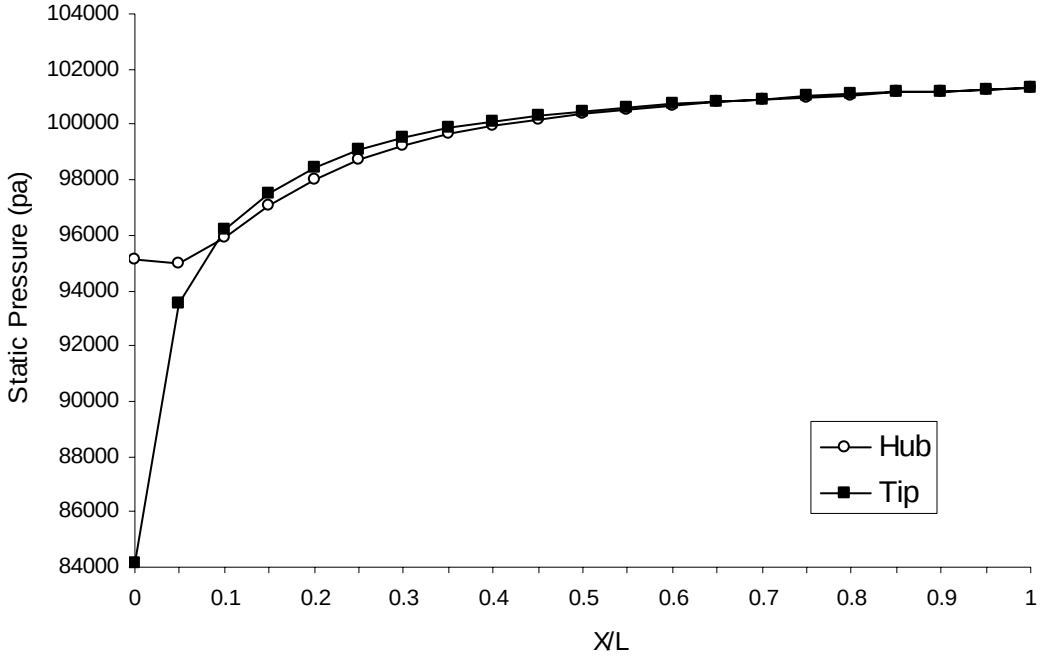

Fig. 42 Static Pressure at Hub and Tip For AR = 4, Angle =10deg; Re=7.5×10^5

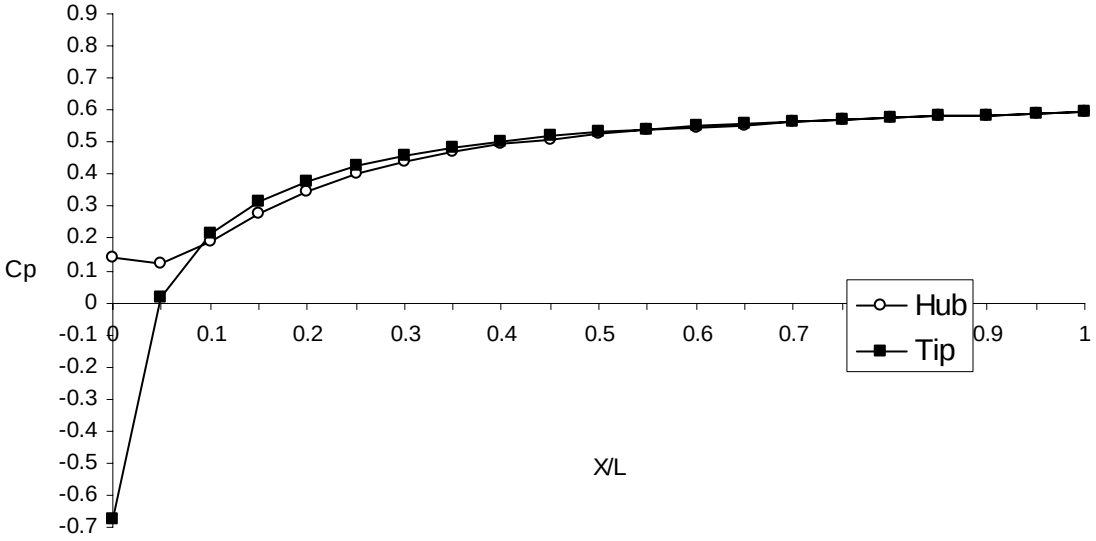

Fig.43 Static Pressure Recovery at Hub and Tip For AR = 4, Angle =10deg; Re=7.5×10^5

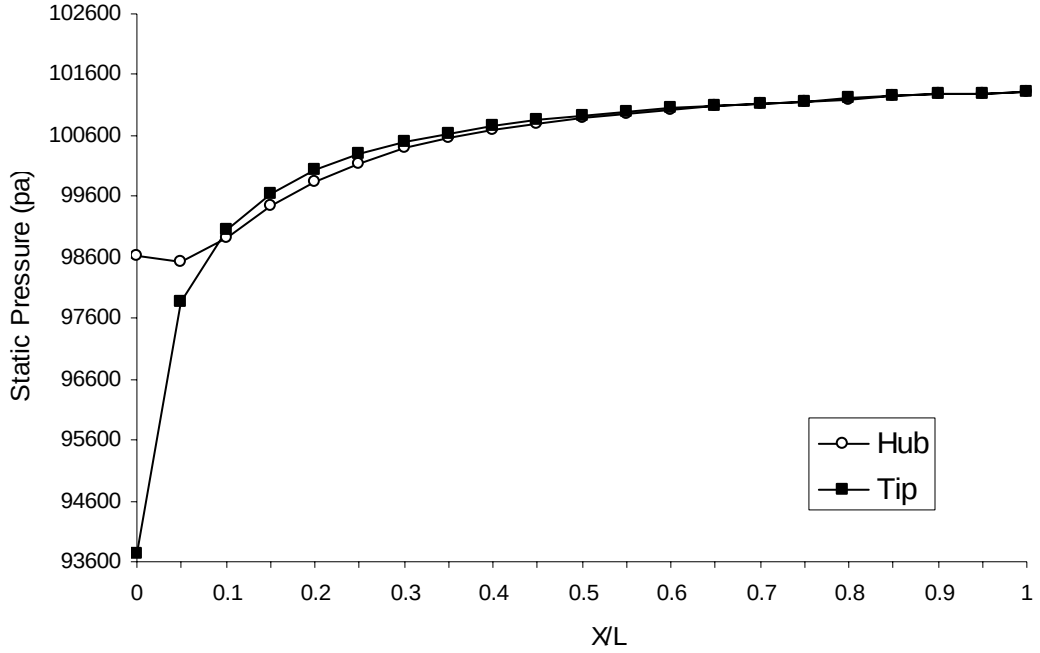

Fig. 44 Static Pressure at Hub and Tip For AR = 4, Angle =10deg; Re=5.5×10^5

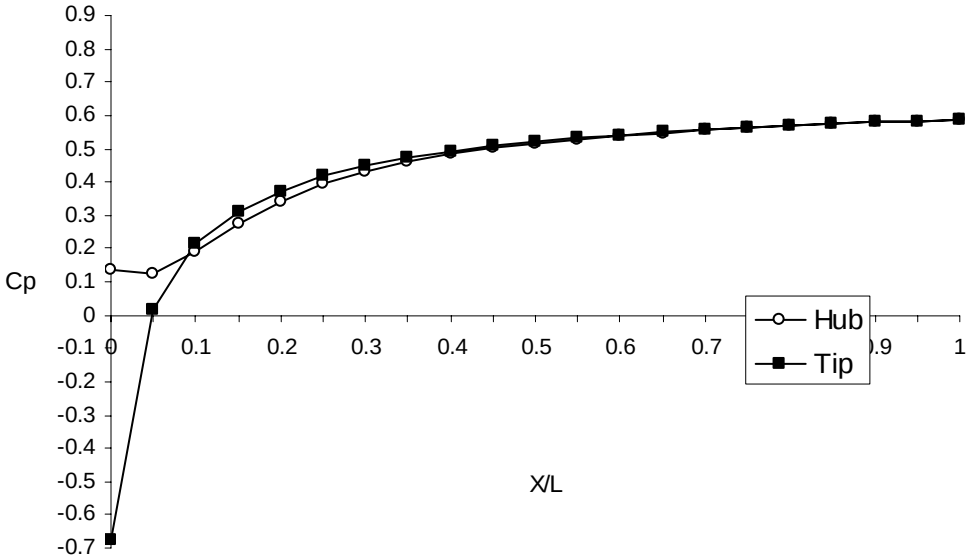

Fig.45 Static Pressure Recovery at Hub and Tip For AR = 4, Angle =10deg; Re=5.5×10^5

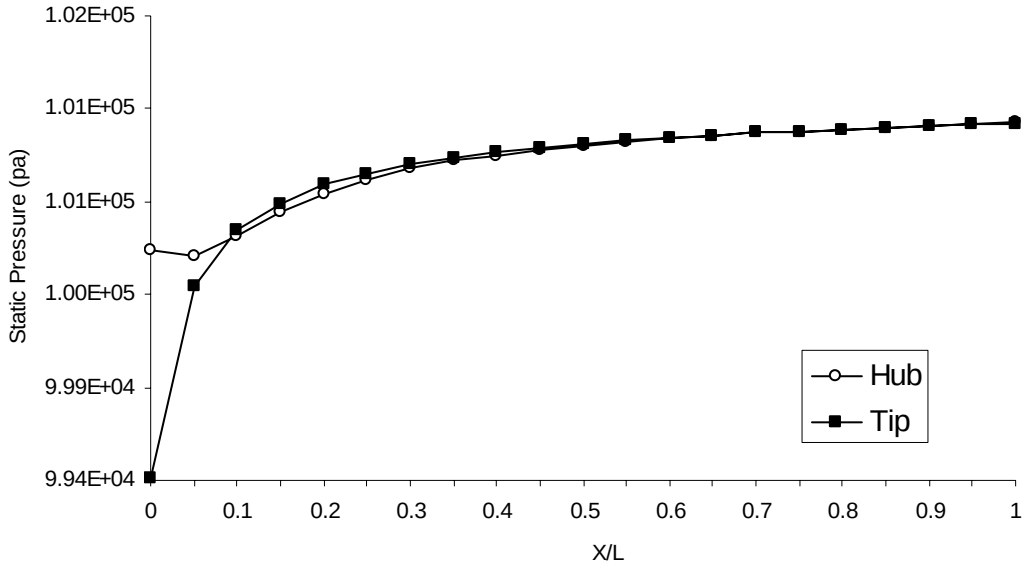

Fig. 46 Static Pressure at Hub and Tip For AR = 4, Angle =10deg; Re=2.5×10^5

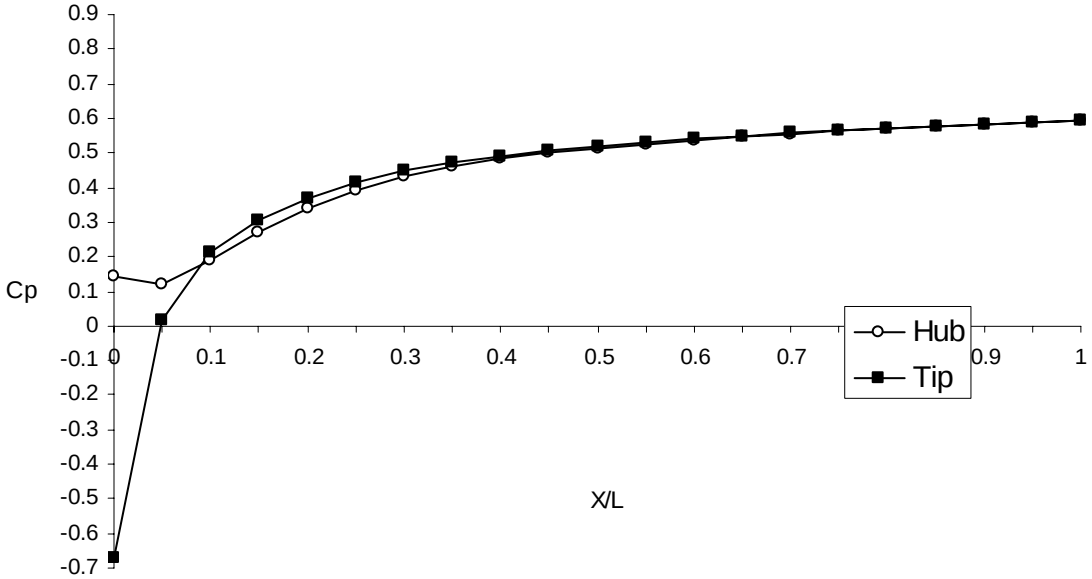

Fig. 47 Static Pressure Recovery at Hub and Tip For AR = 4, Angle =10deg; Re=2.5×10^5

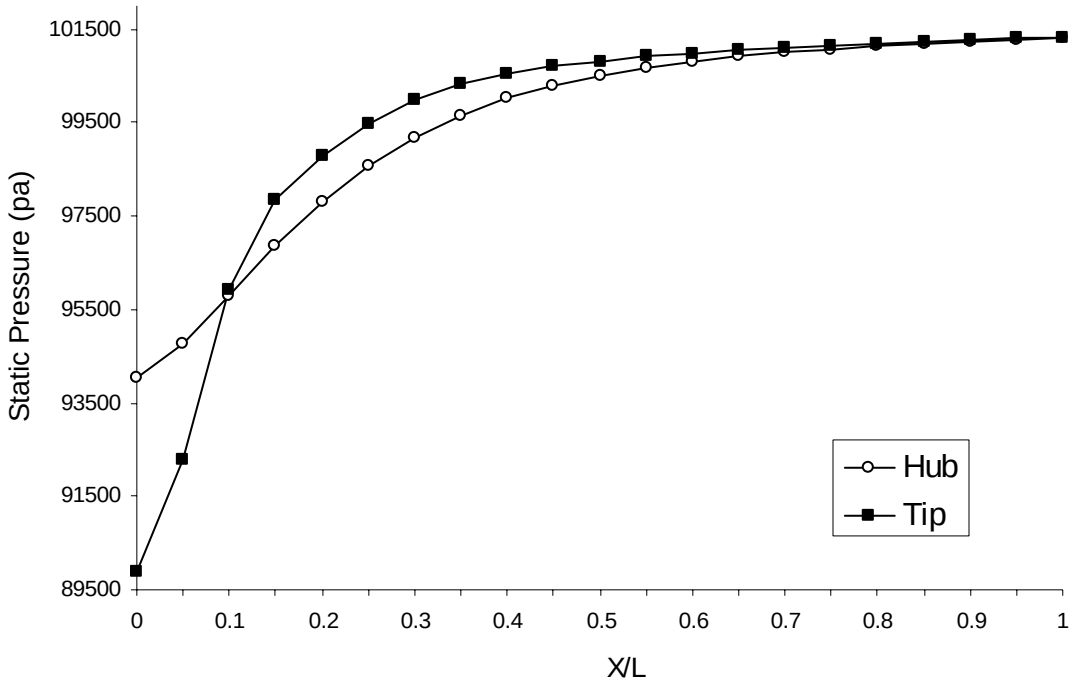

Fig. 48 Static Pressure at Hub and Tip For AR = 4, Angle =15deg; Re=7.5×10^5

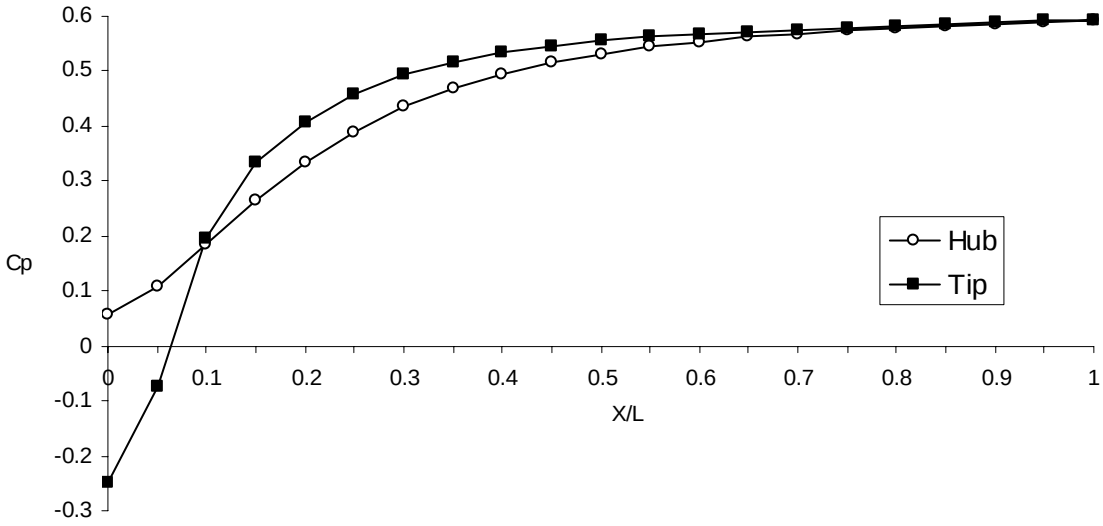

Fig. 49 Static Pressure Recovery at Hub and Tip For AR = 4, Angle =15deg; Re=7.5×10^5

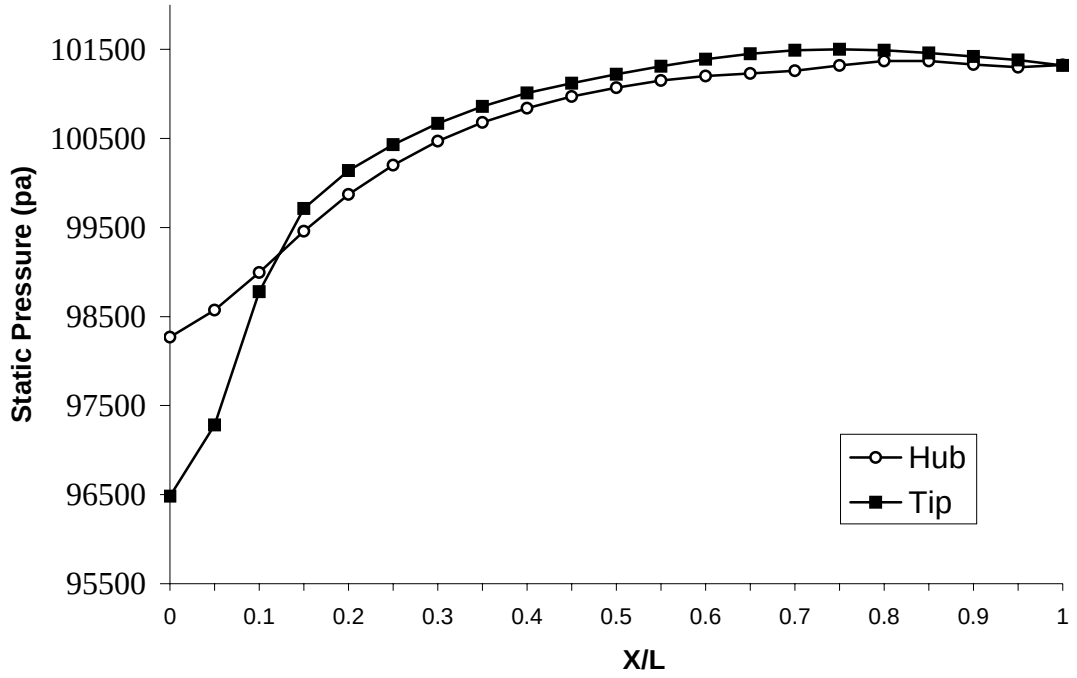

Fig. 50 Static Pressure at Hub and Tip For AR = 4, Angle =15deg; Vx= Re=5.5×10^5

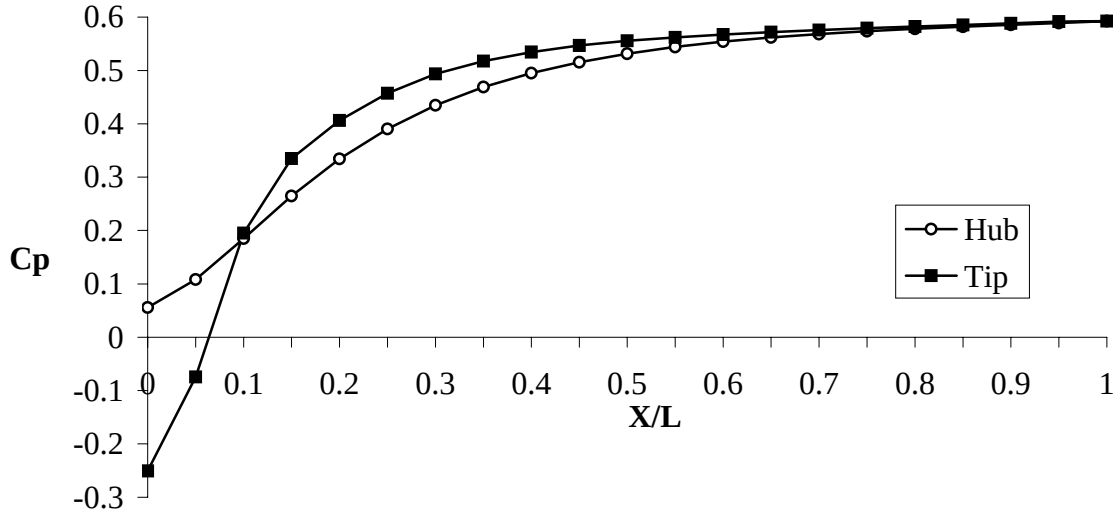

Fig. 51 Static Pressure Recovery at Hub and Tip For AR = 4, Angle =15deg; Re=5.5×10^5

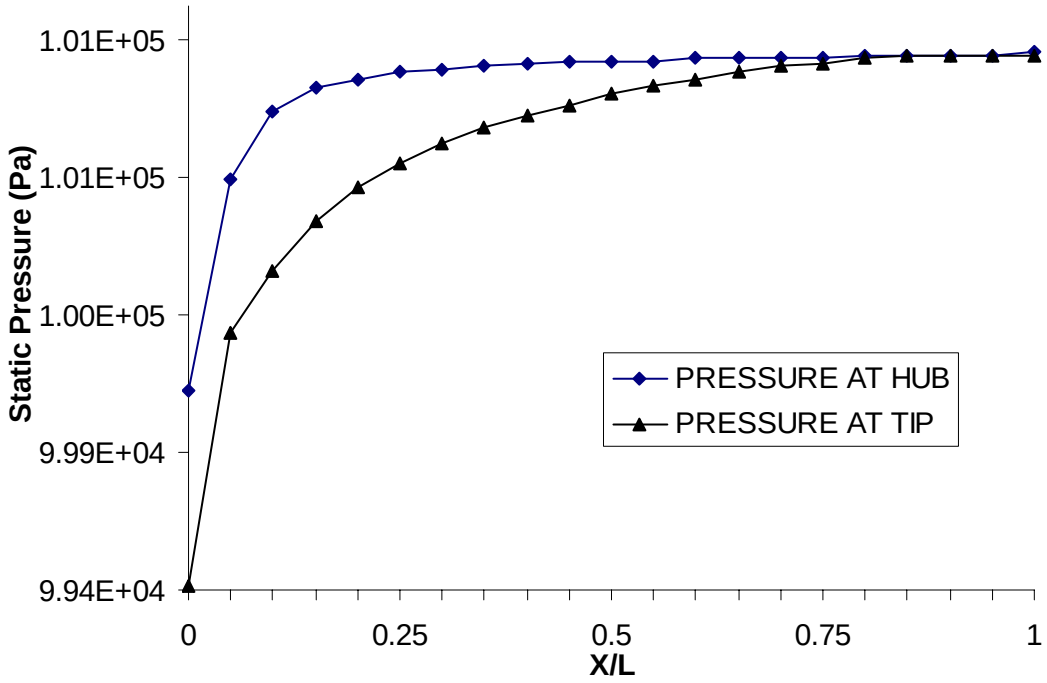

Fig 52 Pressure at Hub and Tip for AR= 5; α = 5; Re=2.5×10^5

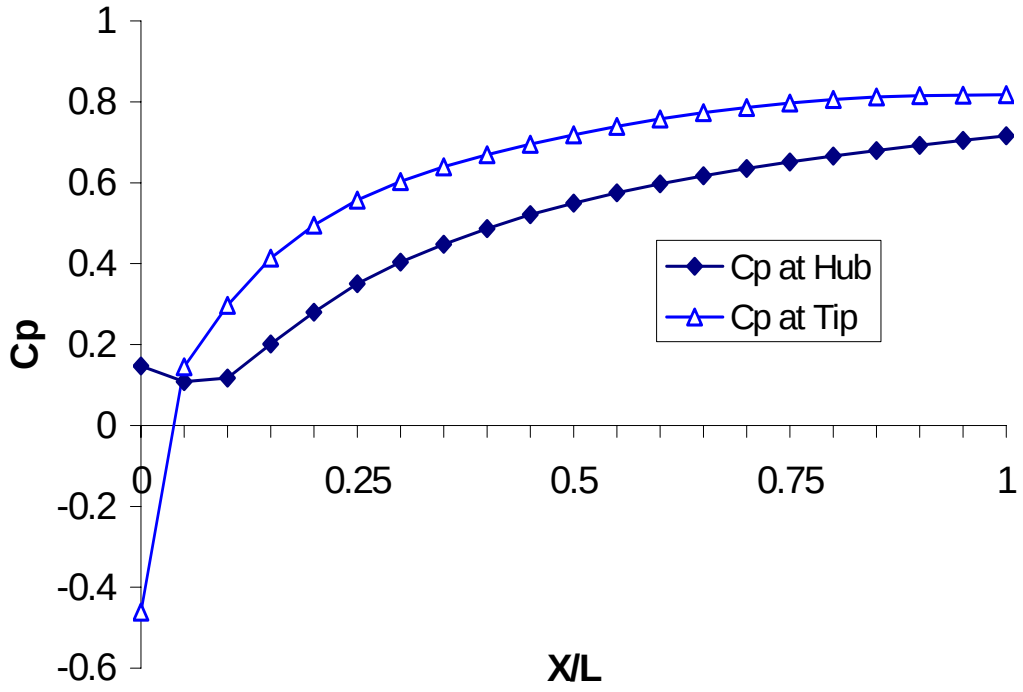

Fig 53 Pressure Recovery Coefficient at Hub and Tip for AR= 5; α = 5; Re=2.5×10^5

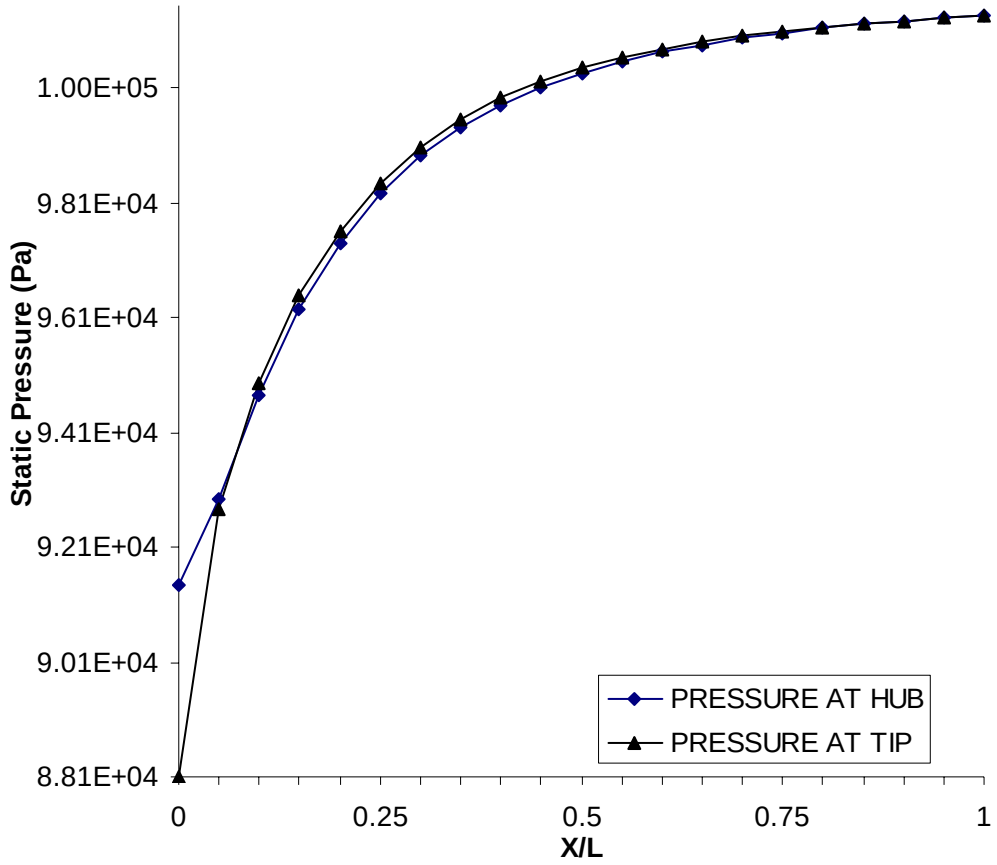

Fig 54 Pressure at Hub and Tip for A R= 5; α = 10; Re=7.5×10^5

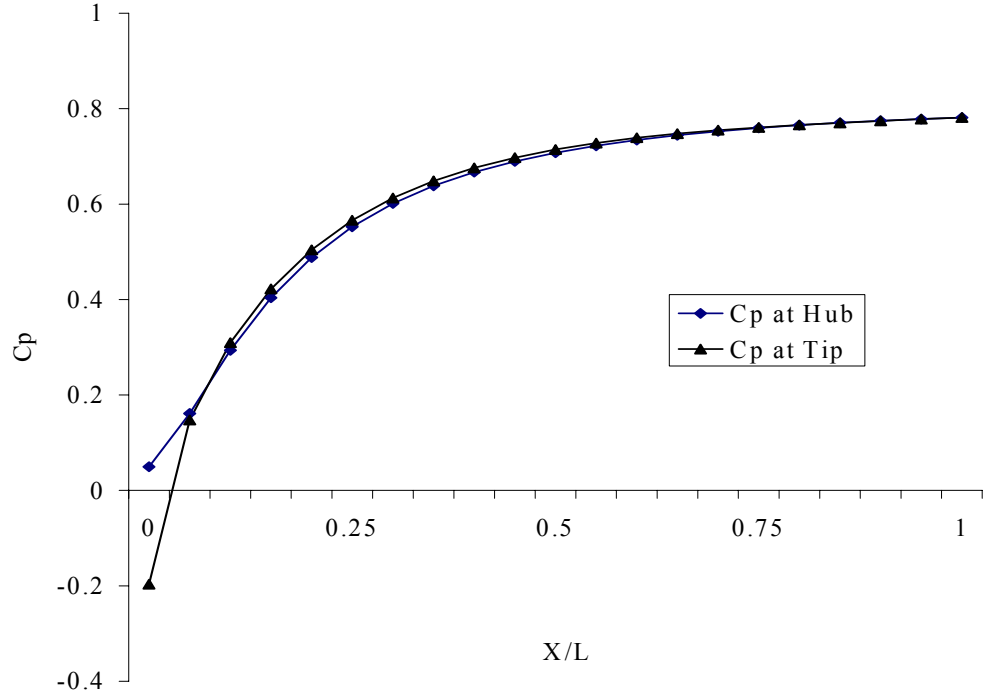

Fig 55 Pressure Recovery Coefficient at Hub and Tip for AR= 5; α =10; Re=7.5×10^5

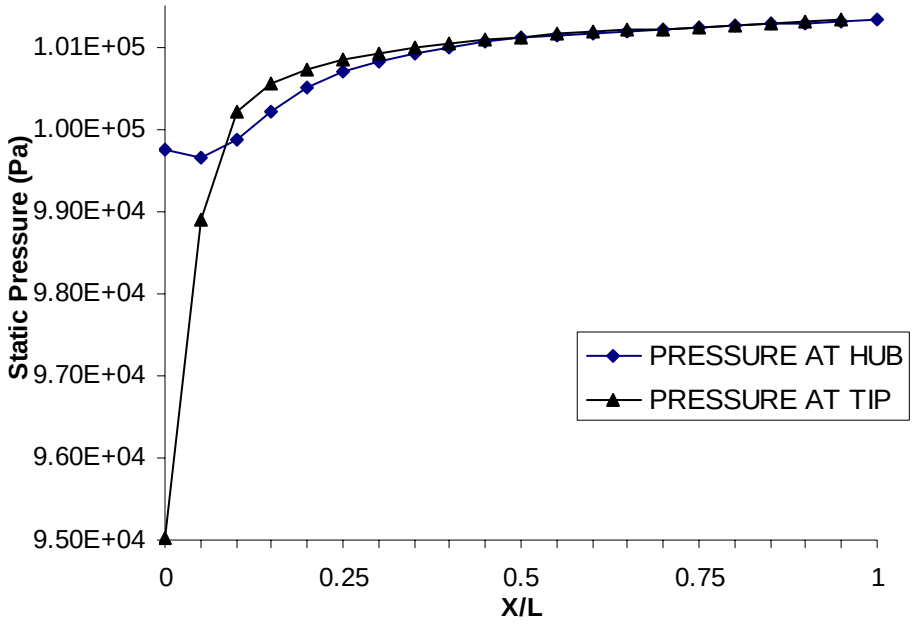

Fig 56 Pressure at Hub and Tip for A R= 5; α = 15; Re=5.5×10^5

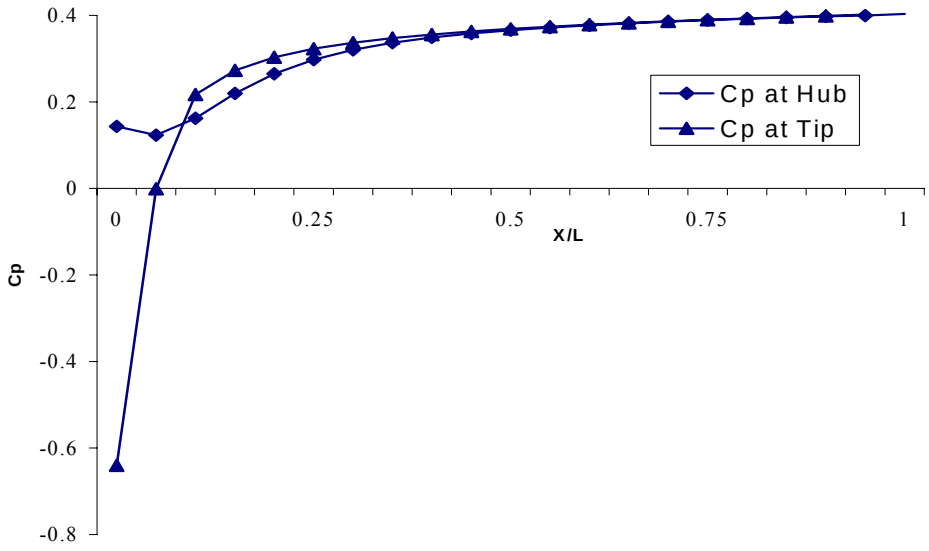

Fig 57 Pressure Recovery Coefficient at Hub and Tip for AR= 5; α =15; Re=5.5×10^5

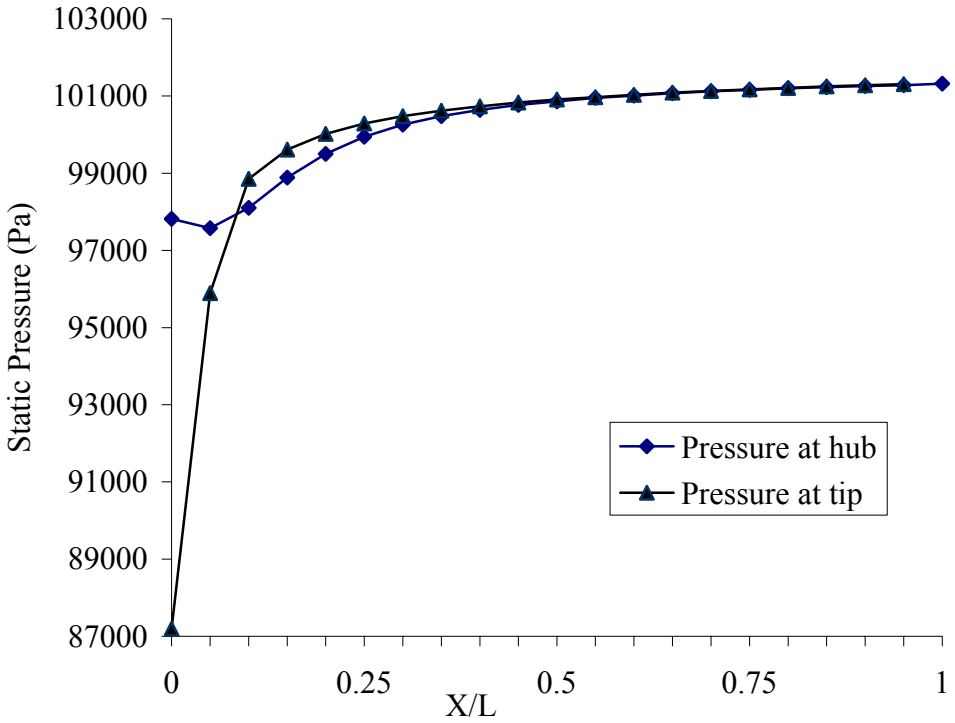

Fig 58 Pressure at Hub and Tip for A R= 5; α = 15; Re=7.5×10^5

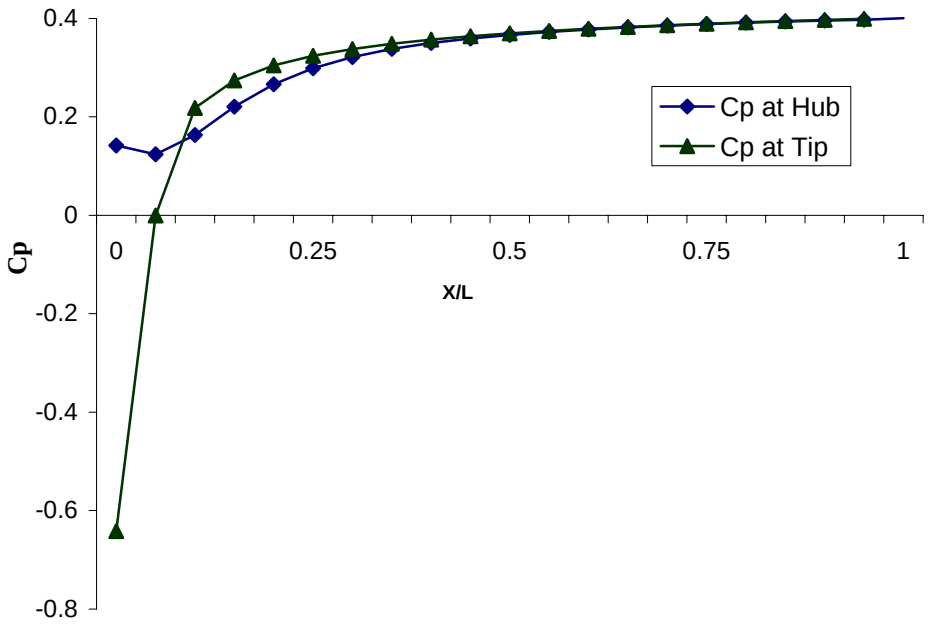

Fig 59 Pressure Recovery Coefficient at Hub and Tip for AR= 5; α =15; Re=7.5×10^5

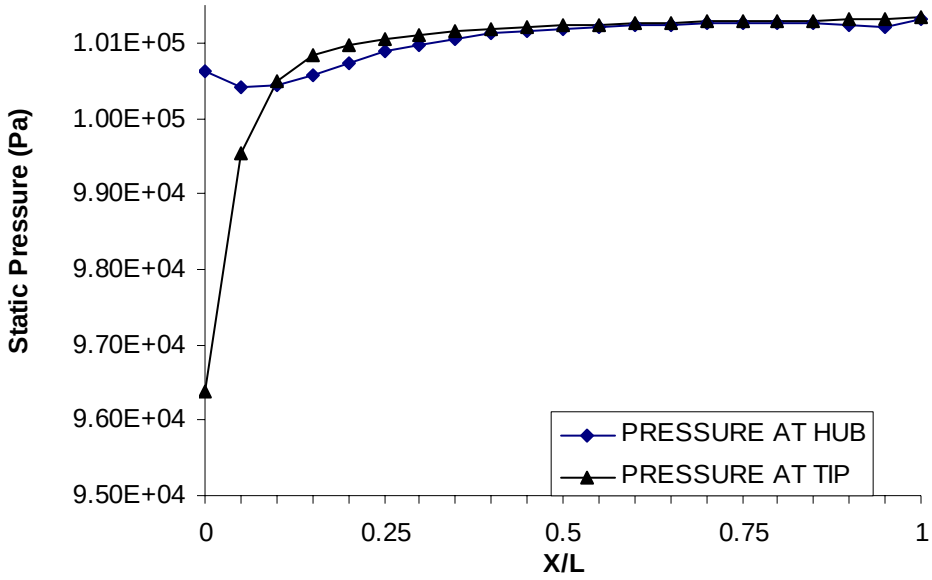

Fig 60 Pressure at Hub and Tip for A R= 5; α = 20; Re=5.5×10^5

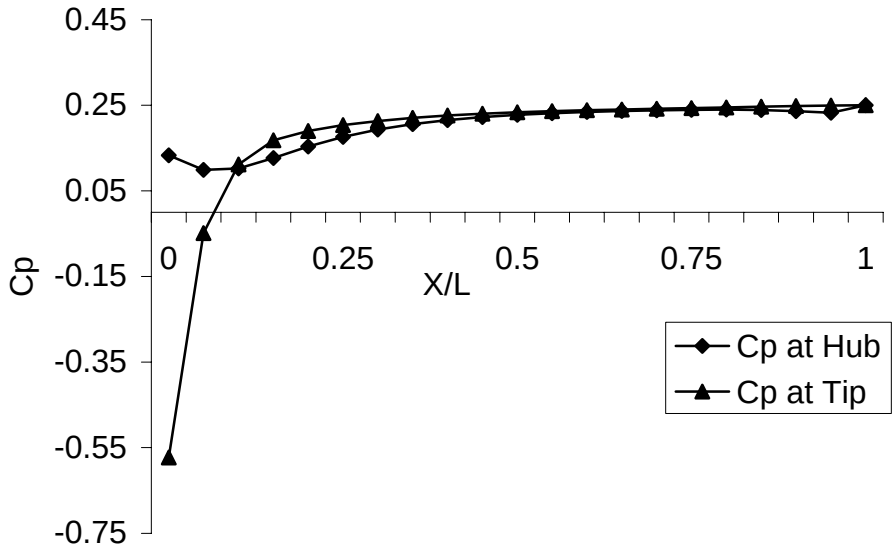

Fig 61 Pressure Recovery Coefficient at Hub and Tip for AR= 5; α =20; Re=5.5×10^5

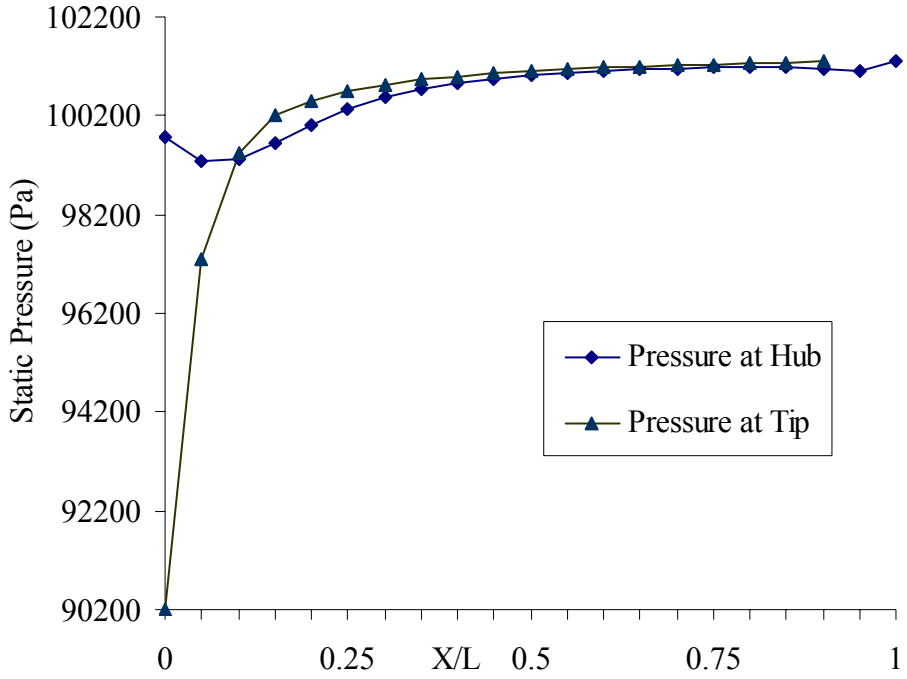

Fig 62 Pressure at Hub and Tip for A R= 5; α = 20; Re=7.5×10^5

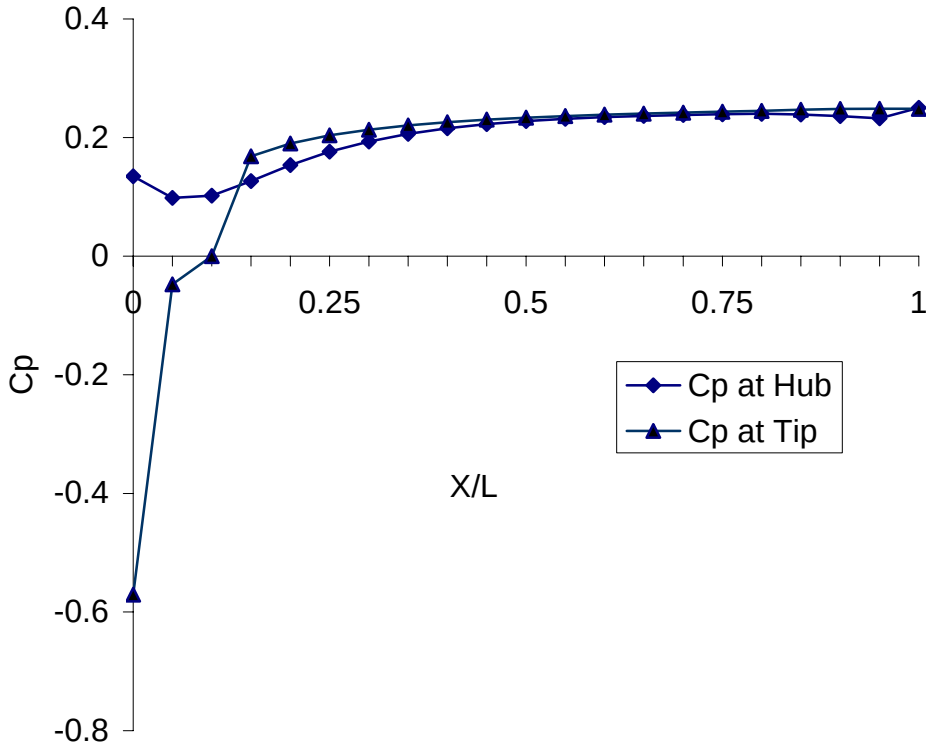

Fig 63 Pressure Recovery Coefficient at Hub and Tip for AR= 5; α =20; Re=7.5×10^5

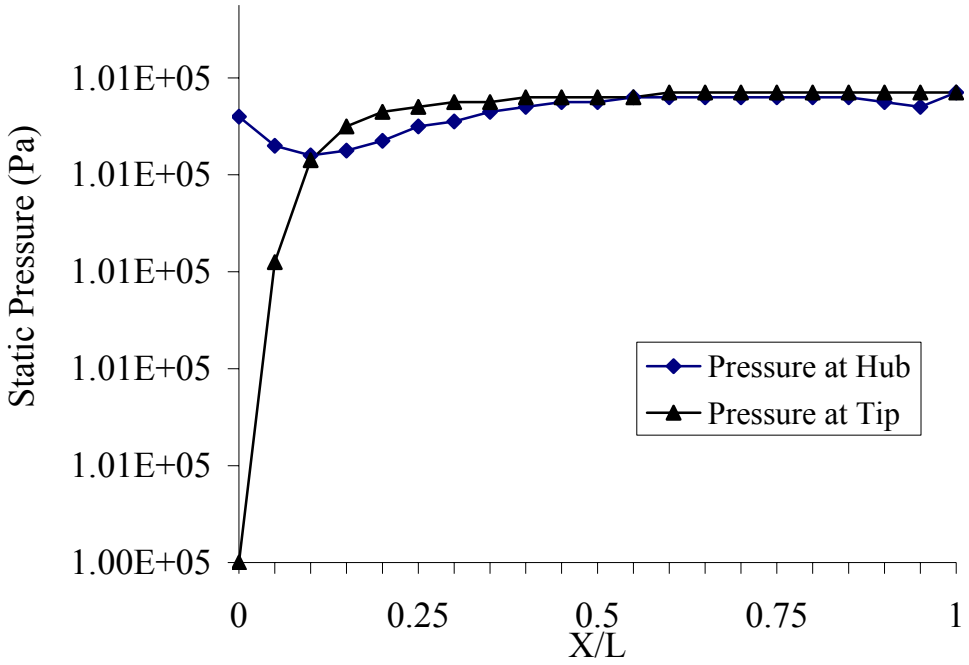

Fig 64 Pressure at Hub and Tip for A R= 5; α = 25; Re=7.5×10^5

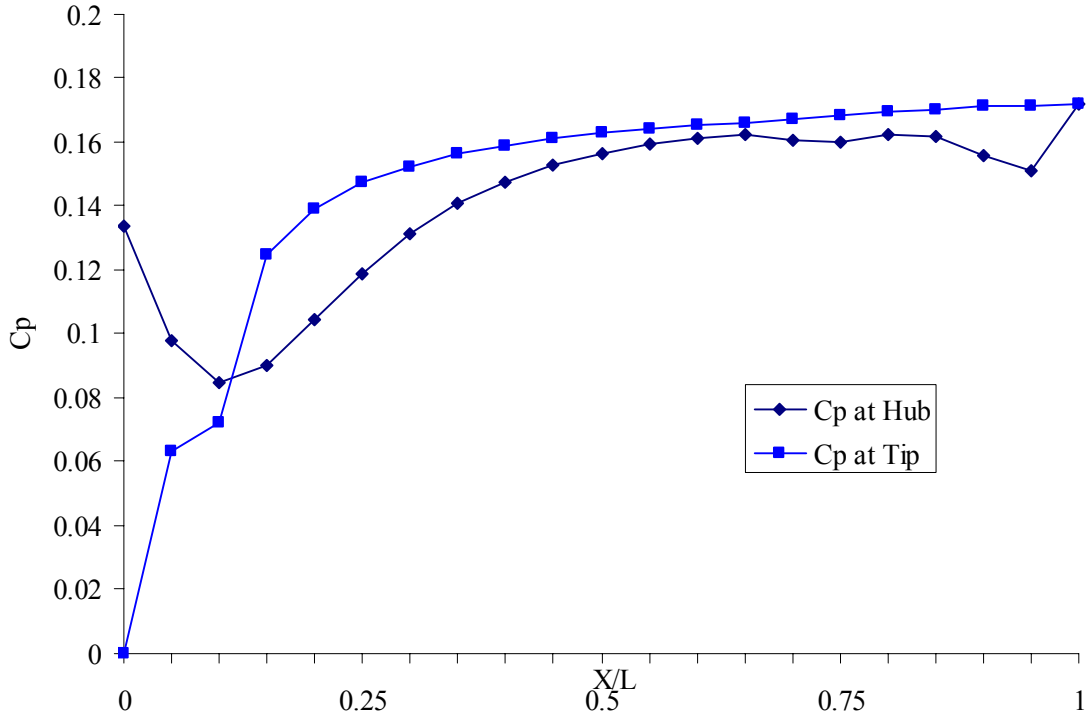

Fig 65 Pressure Recovery Coefficient at Hub and Tip for AR= 5; α =25; Re=7.5×10^5

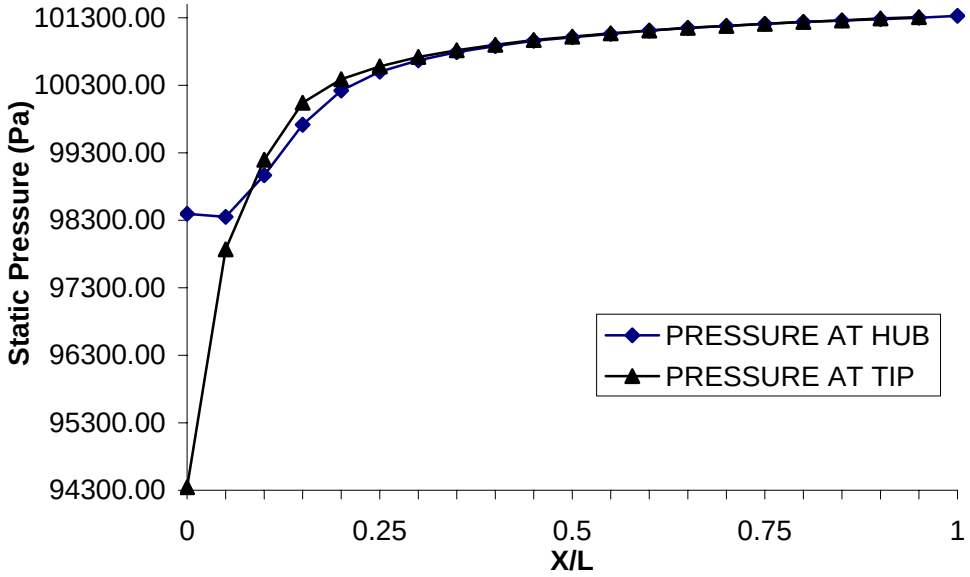

Fig 66 Pressure at Hub and Tip for AR= 6; α = 10; Re=5.5×10^5

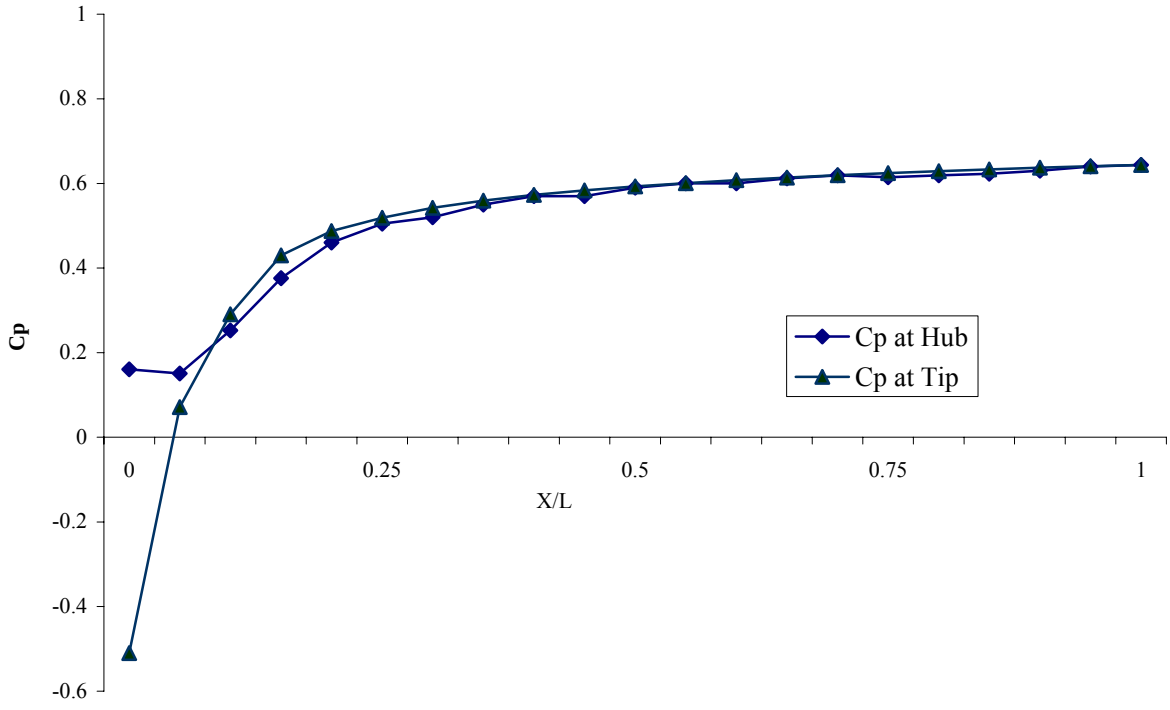

Fig 67 Pressure Recovery Coefficient at Hub and Tip for AR= 6; α = 10; Re=5.5×10^5

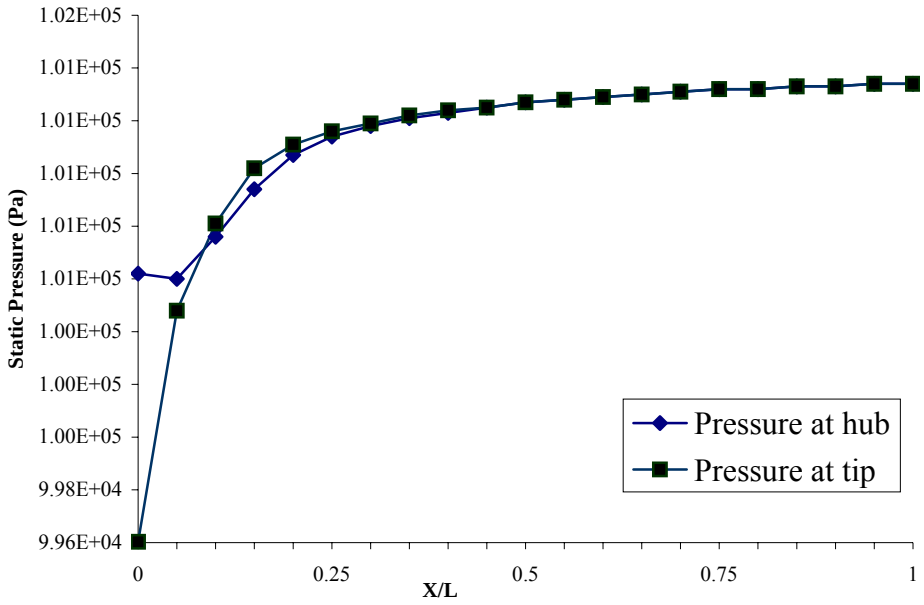

Fig 68 Pressure at Hub and Tip for AR= 6; α = 10; Re=2.5×10^5

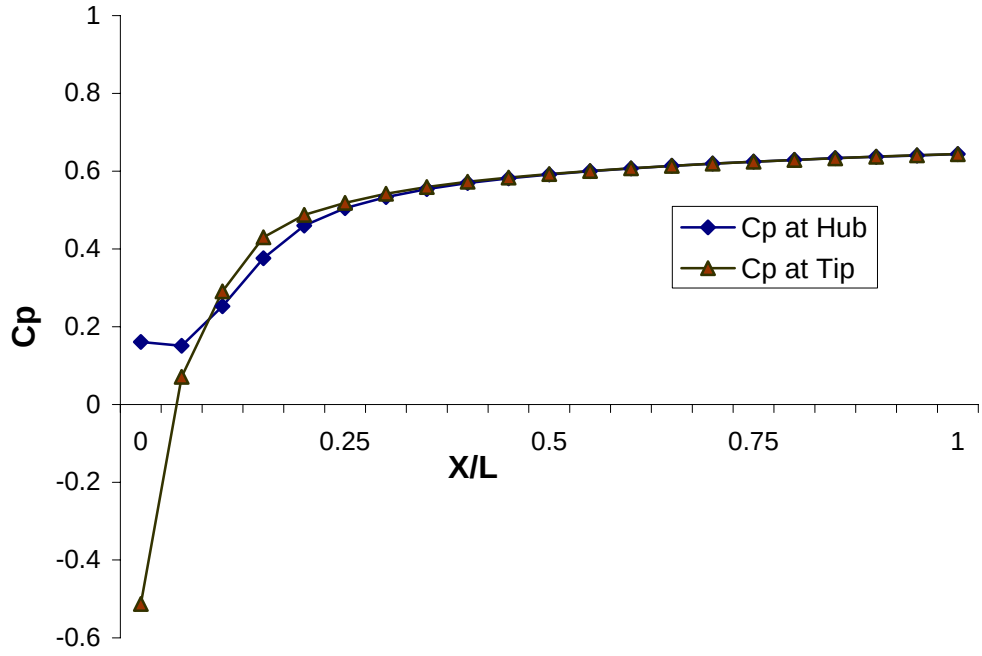

Fig 69 Pressure Recovery Coefficient at Hub and Tip for AR= 6; α = 10; Re=2.5×10^5

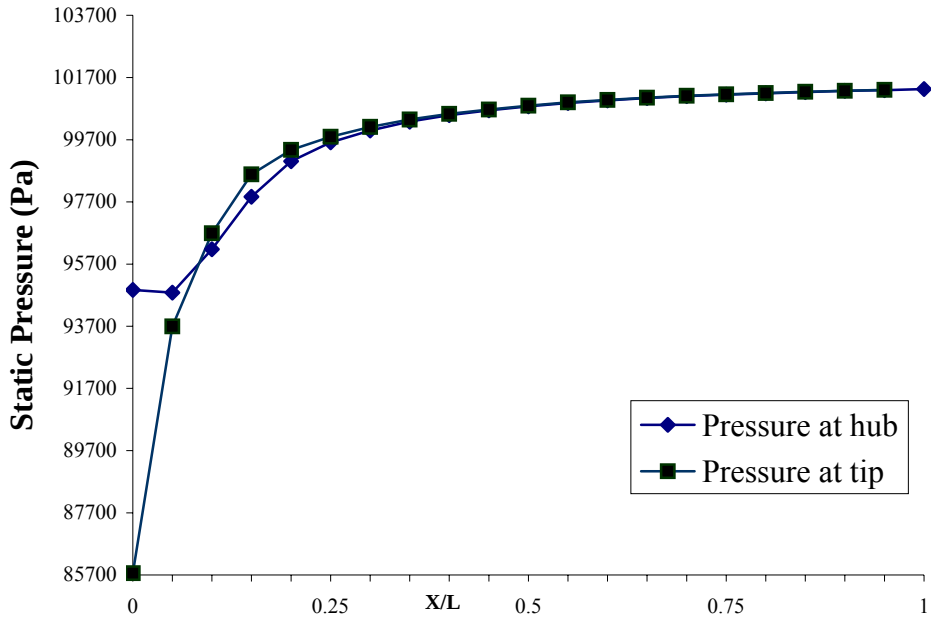

Fig 70 Pressure at Hub and Tip for AR= 6; α = 10; Re=7.5×10^5

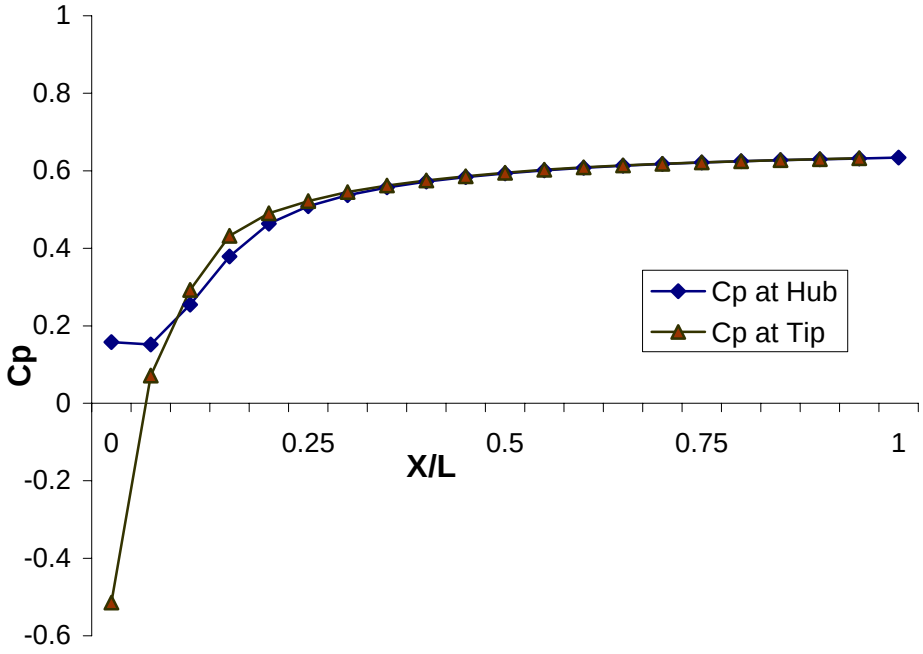

Fig 71 Pressure Recovery Coefficient at Hub and Tip for AR= 6; α = 10; Re=7.5×10^5

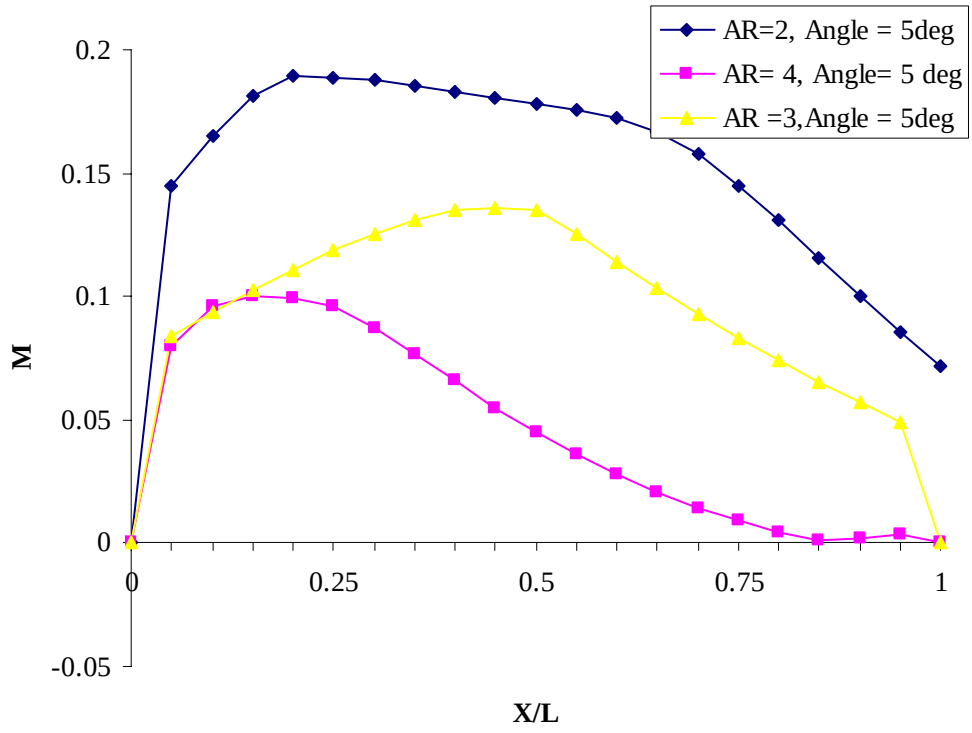

Fig 73 Mach number with varying AR at constant $\alpha = 15^{o}$, Re = 7.7×10^{5}

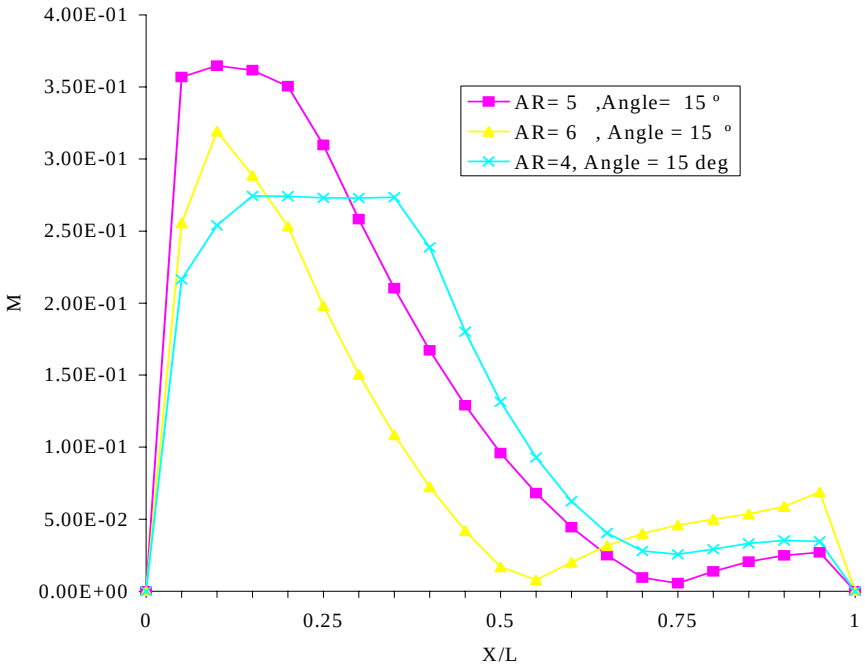

Fig 74 Mach number with varying AR at constant $\alpha = 15^{o}$, Re = 7.7×10^{5}

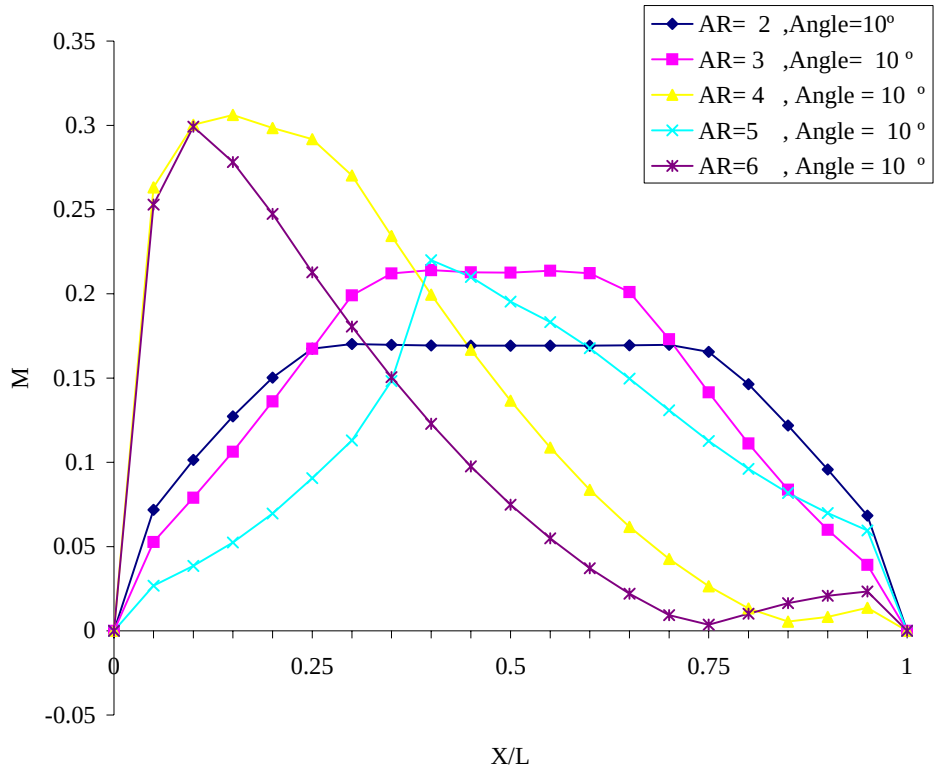

Fig 75 Mach number with varying AR at constant $\alpha = 10º$, Re = 7.7×10^5

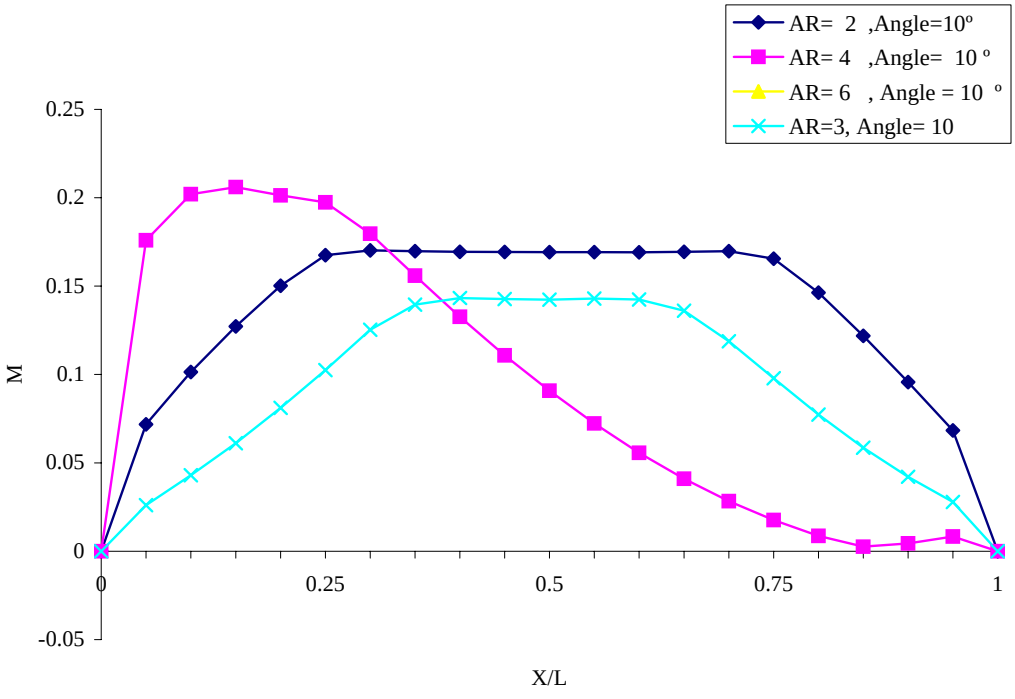

Fig 76 Mach number with varying AR at constant $\alpha = 10º$, Re = 5.15×10^5